

# **Design of Zoom41: An Autonomous Single-Passenger eSTOL Aerial Vehicle**

a project presented to  
The Faculty of the Department of Aerospace Engineering  
San Jose State University

in partial fulfillment of the requirements for the degree  
*Master of Science in Aerospace Engineering*

by

**Shali Nidarsana Subramanian**

August 9, 2019

approved by

Dr, Nikos J. Mourtos  
Faculty Advisor



**San José State**  
UNIVERSITY

## **ABSTRACT**

Air pollution from commuting to work is rising as cities become more crowded. An electric ‘air taxi’—an aerial vehicle that takes advantage of current Li-ion battery capabilities to transport passengers from building rooftops—has been proposed as a solution. Aerospace companies worldwide are investing in this concept, and complex designs with rotary wings and multiple propellers have been proposed. Although vertical takeoff and landing seems to be the best solution for this application, it also presents many difficult design challenges. This paper explores the possibility of a single passenger, fixed-wing, pilotless vehicle, as a simpler option, capable of delivering comparable performance to rotary wing, vertical takeoff designs.

# TABLE OF CONTENTS

ABSTRACT.....	ii
LIST OF TABLES.....	vii
LIST OF FIGURES.....	viii
1.0 INTRODUCTION.....	10
1.1 MOTIVATION.....	10
1.2 LITERATURE REVIEW.....	11
1.2.1 Configuration of STOL and VTOL Vehicle.....	11
1.2.2 Battery Technology.....	12
1.2.3 Electric Motor and Electronics.....	13
1.2.4 Autonomous Technology.....	14
1.2.5 Mature UAM Network Operation.....	15
1.3 PROJECT PROPOSAL.....	16
1.4 METHODOLOGY.....	16
1.5 MISSION REQUIREMENTS.....	17
1.6 OUTLINE.....	17
2.0 WEIGHT SIZING AND WEIGHT SENSITIVITIES.....	20
2.1 MISSION WEIGHT ESTIMATES.....	20
2.1.1 Database for Takeoff Weights and Empty Weights of Similar Airplanes.....	20
2.1.2 Determination of Regression Coefficients A and B.....	21
2.1.3 Determination of Coefficients C and D.....	22
2.1.4 Battery Weight Calculation.....	23
2.2 SENSITIVITIES.....	25
2.2.1 Weight Sensitivity.....	25
2.2.2 Range Sensitivities.....	25
2.3 TRADE STUDIES.....	27
2.4 DISCUSSION, CONCLUSIONS AND RECOMMENDATIONS.....	28
3.0 PERFORMANCE SIZING.....	29
3.1 CALCULATION OF PERFORMANCE CONSTRAINTS.....	29
3.1.1 Takeoff Distance.....	29
3.1.2 Stall Speed.....	30
3.1.3 Landing Distance.....	32

3.1.4	Drag Polar Estimation.....	33
3.1.5	Climb Constraints .....	34
3.1.6	Speed Constraints.....	36
3.1.7	Summary of Constraints .....	37
3.2	PERFORMANCE CONSTRAINTS CALCULATIONS USING AAA .....	39
3.2.1	AAA Stall Speed.....	39
3.2.2	AAA Takeoff Distance .....	39
3.2.3	AAA Landing Distance.....	40
3.2.4	AAA Climb Constraints.....	40
3.2.5	AAA Speed Constraint .....	41
3.3.6	AAA Design Envelope .....	41
3.3	SELECTION OF PROPULSION SYSTEM.....	42
3.3.1	Selection of the Propulsion System Type and the Number of Engines .....	42
3.3.2	Propeller Sizing.....	42
3.5	DISCUSSION, CONCLUSION, AND RECOMMENDATIONS .....	42
4.0	CONFIGURATION DESIGN .....	44
4.1	COMPARATIVE STUDY.....	44
4.2	ZOOM41 CONFIGURATION SELECTION .....	47
4.2.1	Overall Configuration .....	47
4.2.2	Wing Configuration .....	47
4.2.3	Empennage Configuration .....	47
4.2.4	Integration of the Propulsion System.....	47
4.2.5	Landing Gear Arrangement .....	48
4.3	REFERENCES .....	48
5.0	FUSELAGE DESIGN .....	49
5.1	LAYOUT DESIGN OF COCKPIT .....	49
5.2	LAYOUT DESIGN OF FUSELAGE .....	49
5.3	CONCLUSION, DISCUSSION, AND RECOMMENDATIONS .....	53
6.0	WING AND LATERAL CONTROLS DESIGN .....	54
6.1	WING PLANFORM DESIGN.....	54
6.2	SWEEP ANGLE – THICKNESS RATIO .....	55
6.3	AIRFOIL SELECTION .....	57
6.3.1	Reynold’s Number .....	58

6.3.2	Airfoil Properties .....	59
6.4	AERODYNAMIC TWIST AND INCIDENCE ANGLE .....	62
6.5	WING DESIGN EVALUATION .....	62
6.5.1	AAA Wing Geometry Evaluation.....	62
6.5.2	XFLR5 Wing Evaluation .....	62
6.6	LATERAL CONTROL SURFACE SIZING.....	64
6.7	DRAWINGS .....	67
6.8	DISCUSSION, CONCLUSION, AND RECOMMENDATIONS .....	68
7.0	EMPENNAGE DESIGN .....	70
7.1	OVERALL EMPENNAGE DESIGN.....	70
7.2	HORIZONTAL STABILIZER DESIGN.....	71
7.2.1	Horizontal Stabilizer Planform Design.....	71
7.2.2	Elevator Design.....	72
7.3	VERTICAL STABILIZER DESIGN.....	73
7.3.1	Vertical Stabilizer Planform Design .....	73
7.3.2	Rudder Design .....	73
7.4	EMPENNAGE DESIGN EVALUATION.....	73
7.5	DRAWING OF TAIL .....	75
7.6	DISCUSSION AND CONCLUSION.....	75
8.0	LANDING GEAR DESIGN.....	77
8.1	ESTIMATION OF CG LOCATION FOR THE AIRPLANE.....	77
8.1.1	Component Weight Estimation.....	77
8.1.2	Component Center of Gravity.....	78
8.2	LANDING GEAR DESIGN.....	79
8.3	WEIGHT AND BALANCE .....	83
8.3.1	CG Location Drawings .....	83
8.3.2	CG Excursion Diagram.....	84
8.4	DISCUSSION AND CONCLUSION.....	85
9.0	STABILITY AND CONTROLS ANALYSIS .....	86
9.1	STATIC LONGITUDINAL STABILITY .....	86
9.2	STATIC DIRECTIONAL STABILITY .....	87
9.3	REQUIREMENTS CHECK .....	88
9.4	DISCUSSION AND CONCLUSION .....	90

10.0 DRAG POLARS .....	91
10.1 AIRCRAFT ZERO LIFT .....	91
10.2 LOW SPEED DRAG INCREMENTS .....	92
10.3 COMPRESSIBILITY DRAG .....	92
10.4 AIRCRAFT DRAG POLARS .....	94
10.5 DISCUSSION AND CONCLUSION .....	95
REFERENCES .....	96
APPENDIX A: ROSKAM REGRESSION COEFFICIENTS .....	98
APPENDIX B: WEIGHT CALCULATION ASSUMPTIONS .....	99
APPENDIX C: HISTORICAL DATA FOR COMPONENT WEIGHTS .....	101
APPENDIX D: LONGITUDINAL STABILITY CALCULATIONS .....	103
APPENDIX E: DIRECTIONAL STABILITY CALCULATIONS .....	104

## LIST OF TABLES

Table 2.1: Comparison of single-engine electric aircraft	21
Table 2.1: Comparison of single-engine electric aircraft continued	21
Table 2.2: Sensitivity equation criterion	25
Table 2.3: Range sensitivity results	26
Table 4.1: Electric aircraft	45
Table 4.2: Single-engine STOL aircraft	46
Table 6.1: Reynold's number	58
Table 6.2: Flap deflection	66
Table 6.3: Summary of wing parameters	68
Table 7.1: Aircraft database tail area	71
Table 8.1: Estimated empty weight	78
Table 8.2: Aircraft CG location estimate	79
Table 8.3: Updated CG location	85
Table 9.1: Weight and balance	89
Table 10.1: Wetted Area for Zoom41	91
Table 10.2: Drag polars	92
Table 10.3: Wing zero-lift drag coefficient	93
Table 10.4: Wing drag coefficient due to lift	94
Table 10.5: Updated Drag Polars	94
Table B.1: Parameters used to calculate mission weights	99-100
Table D.1: Equation 11.2 Values	103
Table D.2: Munk's method breakdown	103
Table E.1: Directional Stability Parameters	104

## LIST OF FIGURES

Figure 1.1: VTOL Configurations	11
Figure 1.2: Comparison of rechargeable batteries with gasoline	12
Figure 1.3: SAE Levels of Automation	14
Figure 1.4: Munich Case Study	15
Figure 2.1: Weight trends for single engine propeller driven aircraft	22
Figure 2.2: Motor power vs weight for single engine electric aircraft	23
Figure 2.3: Zoom41 mission overview	24
Figure 2.4: Trade studies	27
Figure 3.1: Takeoff distance requirement	30
Figure 3.2: Stall speed requirement for clean wing	31
Figure 3.3: Stall speed requirement for takeoff	32
Figure 3.4: Landing distance requirement	33
Figure 3.6: Predicting equivalent parasite drag	34
Figure 3.7: FAR 23 ROC requirement	35
Figure 3.8: Climb gradient requirement	36
Figure 3.9: Cruise speed requirement	37
Figure 3.10: Constraint summary	38
Figure 3.11: Alternative design point	38
Figure 3.12: AAA stall speed	39
Figure 3.13: AAA takeoff distance	39
Figure 3.14: AAA landing distance	40
Figure 3.15: AAA AEO climb constraint	40
Figure 3.16: AAA cruise speed	41
Figure 3.17: AAA design envelope	41
Figure 5.1: Alpha Electro drawing	50
Figure 5.2: Sketch of fuselage formers	51
Figure 5.3: Seat pitch	51
Figure 5.4: Front-view, top-view, side-view, and isometric view of the fuselage	52
Figure 5.6: Interior arrangement	52
Figure 5.7: Dimensions of current design	53
Figure 6.1: Dihedral guidelines	55
Figure 6.2: Flow separation on varying thickness	56
Figure 6.3: Effect of thickness on Cl and Cd	56
Figure 6.4: Thickness ratio and Mach number	57
Figure 6.5: Profile of NLF 0416	58
Figure 6.6: Theoretical lift-curve	60
Figure 6.7: Theoretical drag polar	60
Figure 6.8: Effect of Re on NLF-0416	61
Figure 6.9: Pressure distribution at $\alpha = 12$ deg	61
Figure 6.10: AAA Wing Geometry	62
Figure 6.11: Wing geometry	62
Figure 6.12: Lift distribution	63
Figure 6.13: XFLR5 wing analysis	64
Figure 6.14: Flap chord and K	66

Figure 6.15: Drawing of wing	67
Figure 6.16: Complete model to date	68
Figure 7.1: Historical data for horizontal stabilizer	71
Figure 7.2: Recommendations of aspect ratio and taper ratio for the tail	72
Figure 7.3: Historical data for the vertical tail from Roskam	73
Figure 7.4: Horizontal stabilizer	74
Figure 7.5: Elevator	74
Figure 7.6: Vertical stabilizer	74
Figure 7.7: Rudder	75
Figure 7.8: Drawing of Zoom41 tail	75
Figure 7.9: Zoom41 model to date	76
Figure 8.1: Coordinate System	78
Figure 8.2: Landing gear tip-over criteria	79
Figure 8.3: Longitudinal tip-over criterion	80
Figure 8.4: Lateral tip-over criterion	80
Figure 8.5: Landing gear ground clearance criterion	81
Figure 8.6: Longitudinal ground clearance	81
Figure 8.7: Lateral ground clearance	82
Figure 8.8: Drawing of landing gear	82
Figure 8.9: Fuselage group CG drawing	83
Figure 8.10: CG of major components	83
Figure 8.11: Excursion Diagram	84
Figure 9.1: Aerodynamic center leg of x-plot	86
Figure 9.2: Static longitudinal stability x-plot	87
Figure 9.3: Directional stability x-plot equation	88
Figure 9.4: Static directional stability	88
Figure 9.5: Updated longitudinal stability	89
Figure 9.6: Updated directional stability	90
Figure 10.1: Wing zero-lift drag coefficient equation	93
Figure 10.2: Wing drag coefficient due to lift equation	93
Figure 10.3: Clean configuration L/D	94
Figure 10.4: L/D for all configurations	95
Figure A.1: Takeoff weight vs empty weight	98
Figure C.1: Historical data	101
Figure C.1: continued	102
Figure C.2: Composite weight data	102

## 1.0 INTRODUCTION

Residents of highly populated urban areas spend significant time commuting to work while contributing to the traffic and air pollution. The Zoom41 will serve as an affordable and green alternative. This chapter will describe the motivation behind this aircraft in more detail, review the current technology and market, and outline the mission specification.

### 1.1 MOTIVATION

Poor air quality is a major global problem that can cause serious illness for those regularly exposed to it. The majority of emissions in the United States are produced by road vehicles. For example, in 2012, 90% of carbon monoxide emissions originated from cars, trucks, and other vehicles burning fossil fuels in urban areas [1]. Although replacing existing fossil-fuel burning vehicles with electric vehicles is a logical conclusion to this problem, it will not solve the problem of overcrowded roads and long commute times experienced by many. Furthermore, traveling even short distances in heavy traffic is a significant contributor to emissions. Replacing ground vehicles with electric air vehicles for short-range travel is another option for the future.

Electric powered aircraft are typically limited by the available battery technology. However, it is predicted that the specific energy is approximately 200 W-h/kg for Li-ion batteries [2]. Reusable batteries are predicted to cut the operating costs of electric aircraft by 15-20% percent [3]. Although batteries are more costly to implement initially, they reduce the impact of harmful pollutants in the environment and are cost-effective in the long run.

There is currently great interest in developing an electric aircraft for short range operation. A short or vertical landing capability is required for such vehicle to take-off from and land on rooftops of buildings. This requirement has proved to be quite a challenge for aerospace engineers. Multiple designs have been proposed with rotary wings and propellers but they tend to be rather complicated in regards to aerodynamics, stability, and control. This paper presents a simpler solution with a

fixed-wing, single-passenger electric aircraft, as an alternate commute option to the fossil fuel burning ground vehicles.

## 1.2 LITERATURE REVIEW

The electric air taxi will serve as a conventional ride-hailing service that provides flights between any available landing pads for a single passenger and their light hand luggage. This section will dive deeper into the issues that accompany this type of mission.

### 1.2.1 Configuration of STOL and VTOL Vehicle

The three configurations used for VTOL mission types are wing type, helicopter type, and ducted type [4]. Wing type configuration can be a rotating wing with fixed engines or a fixed wing with rotating engines for vector thrust maneuvering. A helicopter type will have a motor mounted above, and a ducted type has ducted motors. All three configurations have common problems and increase in complexity if the design calls for multiple motors. The following figure summarizes the issues for common VTOL designs.

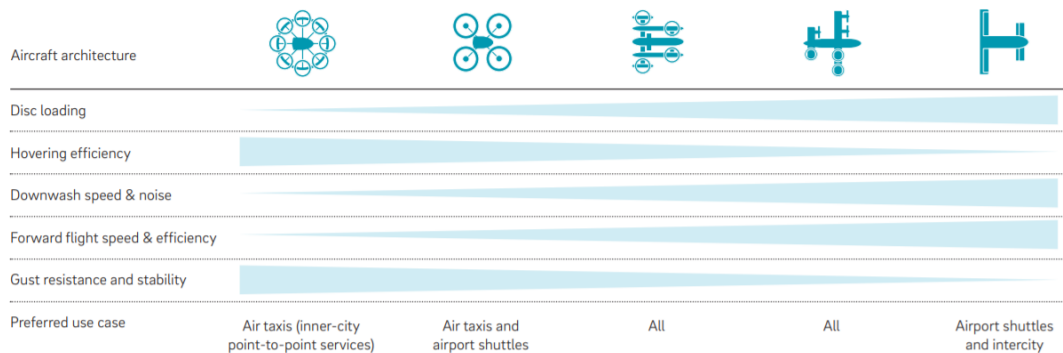


**Figure 1.1: VTOL Configurations [5]**

Type of vehicle will vary based on the type of mission it is required to complete. Disk loading—thrust divided by a representative area such as propeller disk area—provides a method of categorizing various propulsive systems [6]. Higher disk loading translates to more required power for maintaining the rotor speed. Before any of these designs can be implemented, they must obtain certification from the FAA, and ensure the safety requirements are met.

Often the FAA certification process for novel eVTOL configurations is overlooked but is vital to the success of the design. Certification will depend on the vehicles ability to handle catastrophic failure of the active stabilization system controlling the attitude and lift during the vertical and translational phases of flight, power delivery system that supplies power from batteries to the motors, and the batteries themselves [7]. There is a higher consequence for power failure because it often translates to a failure in stability and control as well. The forms for mitigating multiple

high consequence hazards risks can rapidly increase the complexity, weight, and cost of the overall system while simultaneously lengthening the certification process.

Fixed wing STOL configurations are better equipped to handle these critical risks when compared to a VTOL. Less power is required for a STOL aircraft which allows for higher payloads, longer ranges, and smaller aircraft [7]. However, the disadvantage of this configuration is the runway length requirement since space is very limited in large metropolitan areas. In short, VTOL configurations can be advantageous for missions with short travel distances such as intracity point-to-point transportation with limited space TOLAs, while STOL configurations are advantageous for longer range intercity transportation that can take advantage of the higher aerodynamic performance.

### 1.2.2 Battery Technology

Implementing a fully electric propulsive system will provide significant advantages over jet fuel powered aircraft. Using rechargeable batteries can reduce the cost of the flight and make it more accessible. However, batteries are limited by their specific energy density and specific power density. Where specific energy is the amount of energy in a given mass, and similarly power density if the amount of power in a given mass.

Currently, the most promising rechargeable battery technology uses lithium air [8]. Its most optimistic predictions report a potential specific energy density of 2000 Wh/kg and specific power of 0.67 kW/kg [8]. The bar graph below summarizes theoretical and practical specific energy densities of existing batteries.

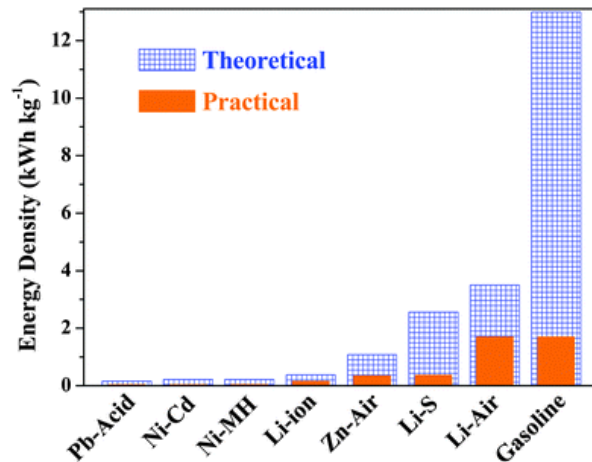
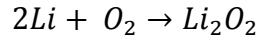


Figure 1.2: Comparison of rechargeable batteries with gasoline [8]

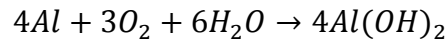
Note that practical energy density estimate for Li-air surpasses its competitors by a significant margin and is close to that of gasoline's energy density.

Four different architectures exist for Li-ion batteries: aprotic, aqueous, all-solid-state, and hybrid [8]. A different electrolyte is used in each architecture, and the non-aqueous systems result in higher potential energy density and rechargeability [8]. The chemical reaction using a non-aqueous electrolyte is shown below.



While it may be true that there is a high potential, the Li-air battery is still in its early stages of development. This battery requires pure oxygen for the reaction and may need filters or storage tanks on board the aircraft. Another consequence of using non-aqueous Li-air batteries is the additional mass gain over the course of the flight due to battery discharge [2]. For larger batteries, the mass gain can be a considerable contribution to the aircraft.

Aluminum air batteries can be another option for aviation applications, which has a specific energy capacity of 1300 Wh/kg and specific power of 0.2 kW/kg [2]. The drawback of Al-air is the major losses in capacity incurred during recharging [2]. It is suggested that the batteries can be recycled instead. The discharge chemical reaction for an Al-air battery is shown below.



This reaction also accumulates oxygen, growing heavier as it discharges, and requires water for the reaction to take place.

A non-metal air battery option is the Lithium-sulfur battery with a specific energy of 500 Wh/kg [2]. Although Li-S specific energy is lower than their metal counterparts, it's significantly higher than the Li-ion battery energy density. Sulfur is used for the cathode, which is abundant, eco-friendly and inexpensive [9]. The solid-state lithium ion conductors show more promise compared to conventional liquid aprotic electrolytes because they are safer to handle, show desirable stability at high voltages, and some can significantly boost energy density [9].

There have been cases where two types of batteries have been used in conjunction for one vehicle. Phinergy's prototype electric car used both a combination of aluminum-air and lithium-ion batteries, where a lithium-ion battery is used for general operation and an aluminum-air battery used for additional range [2]. This concept is being implemented in Eviation's Alice 9-passenger commuter aircraft [2]. Battery technology is evolving rapidly and is already paving the way to fully electric aircraft.

### 1.2.3 Electric Motor and Electronics

Electric motors for aviation applications require continuous operation at cruise power. Lightweight motors with high power densities are ideal for this application. Multiple engine manufacturers such as Siemens, Rolls Royce, Pratt & Whitney, and MagniX are investing in research and development of electric motors [10]. All-electric motors already exist and are put to use for 2-4 passenger

aircraft, for example, the Pipistrel Alpha Electro. A minimum of 500 Wh/kg storage capacity is required from the batteries for electric propulsion [11]. Electrically-propelled aircraft also require electronics to convert, switch, and condition the power generated by the motors [11]. This must be done with minimum losses and associated heat.

### 1.2.4 Autonomous Technology

Autonomous software and hardware are still in development. Technology, regulation and certification barriers must be overcome [12]. Technological barriers include adaptive learning, cyber and physical system security, system perception, and system cognition [8]. Accessible airspace, especially in cities that host busy airports, must be established before this technology can operate at its full potential [12]. Creating safety standards for autonomous aerial vehicles is another hurdle that will slow progress [12]. Ensuring the safety and reliability of a fully autonomous aerial vehicle are vital to realizing this design.

However, it is not necessary to be fully autonomous in the initial stages of design. The transition to a fully autonomous vehicle can be gradual, to give sufficient time to test and validate the new and evolving increasingly autonomous technology. Uber’s Elevate program describes a program which uses pilots in ground stations to control the vehicle using remotes in the early stages of flight testing [13]. This allows statistical proof for FAA certification to be built while increasing the autonomy of the vehicle [13]. Levels of autonomy were outlined by the SAE and are displayed below.

	SAE LEVEL 0	SAE LEVEL 1	SAE LEVEL 2	SAE LEVEL 3	SAE LEVEL 4	SAE LEVEL 5
What does the human in the driver's seat have to do?	You are driving whenever these driver support features are engaged – even if your feet are off the pedals and you are not steering			You are not driving when these automated driving features are engaged – even if you are seated in “the driver’s seat”		
	You must constantly supervise these support features; you must steer, brake or accelerate as needed to maintain safety			When the feature requests, you must drive	These automated driving features will not require you to take over driving	
What do these features do?	These are driver support features			These are automated driving features		
	These features are limited to providing warnings and momentary assistance	These features provide steering OR brake/acceleration support to the driver	These features provide steering AND brake/acceleration support to the driver	These features can drive the vehicle under limited conditions and will not operate unless all required conditions are met	This feature can drive the vehicle under all conditions	
Example Features	<ul style="list-style-type: none"> <li>• automatic emergency braking</li> <li>• blind spot warning</li> <li>• lane departure warning</li> </ul>	<ul style="list-style-type: none"> <li>• lane centering OR</li> <li>• adaptive cruise control</li> </ul>	<ul style="list-style-type: none"> <li>• lane centering AND</li> <li>• adaptive cruise control at the same time</li> </ul>	<ul style="list-style-type: none"> <li>• traffic jam chauffeur</li> </ul>	<ul style="list-style-type: none"> <li>• local driverless taxi</li> <li>• pedals/steering wheel may or may not be installed</li> </ul>	<ul style="list-style-type: none"> <li>• same as level 4, but feature can drive everywhere in all conditions</li> </ul>

Figure 1.3: SAE Levels of Automation [14]

The six levels of automation clearly define the features that are required for a fully autonomous vehicle. Level 5, operating everywhere under all conditions, will present the largest challenge especially in terms of weather. However autonomous VTOLs operate in an open environment except during takeoff and landing. It is possible that autonomy will allow for a safer operation compared to piloted aircraft [13]. Also, autonomous flight control can improve the trajectory flight profiles and minimize required power [13].

### 1.2.5 Mature UAM Network Operation

Development of an Urban Air Mobility (UAM) network, aerial transportation for dense metropolitan areas, is a growing market that is receiving attention worldwide. The ideal vehicle must be the fastest travel option, affordable to the middle-class, safe and easily integrate with transportation options already present in the area. Levels of UAM operation summarized below were defined by Thipphavong et al [15].

- Emergent: Low-tempo, low-density flights along fixed routes
- Early: Higher-tempo, higher-density flights in a network of TOLAs feeding a common location and managed by UAM operators and third-party services
- Mature: High-tempo, high-density flights in a network with multiple hub locations

Market case studies can be conducted using available commuter data, an example for Munich is shown below.

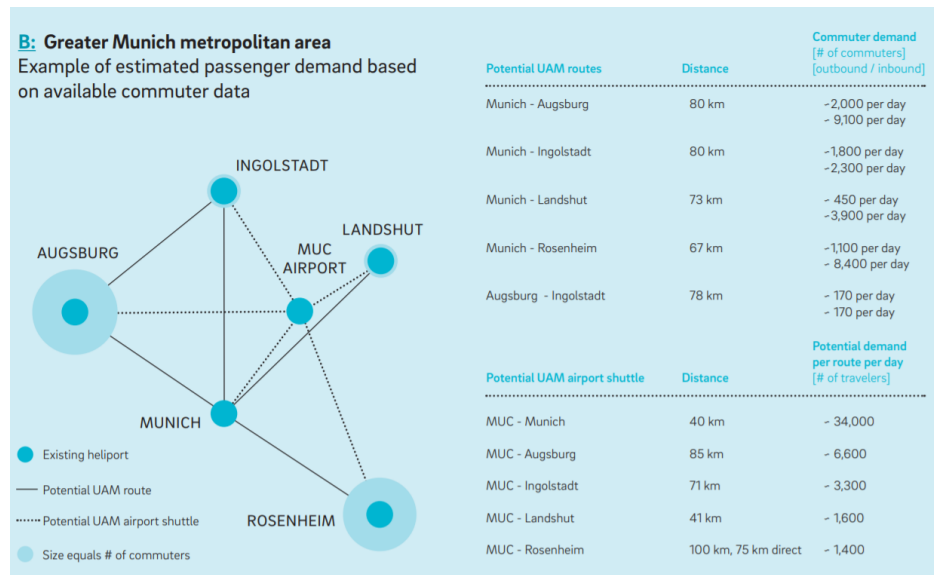


**Figure 1.4: Munich Case Study [5]**

In this case study, the potential demand per route per day can be predicted. The minimum distance for the city of interest can also be determined. This will aid in developing mission specification

for the vehicle design. For Munich, a minimum distance of 100 km would be required for operation and an additional distance for emergency landings.

Helicopters have been proposed previously for this type of mission but were implemented unsuccessfully. Common problems with launching a helicopter type VTOL was high levels of noise, cost of maintenance, and poor safety records [4]. These risks are lowered for current VTOL designs due to their fully electric propulsion systems. Potential hazards for UAM operations that require further investigation include the loss of Command-and-Control link, UAM routes conflicting with existing air traffic, lack of TOLA availability, passenger illness, and ground obstacles such as powerlines [15]. The loss of Command-and-Control link can be due to malfunction of electronic equipment or external hijacking. Either way, a loss of control will lead to critical system failure.

### 1.3 PROJECT PROPOSAL

There is currently great interest in developing an electric aircraft for short range operation. A short or vertical landing distance is required for such vehicle to take-off from and land on rooftops of buildings. This requirement has proved to be quite a challenge for designers. Multiple designs have been proposed with rotary wings and propellers but they tend to be complicated in regards to aerodynamics, stability, and control. This project proposes a simpler solution with a fixed-wing single-passenger eSTOL as an alternate commute option to the fossil fuel burning ground vehicles. Although the STOL will be occupying additional space, it remains as a path with less critical risks compared to the VTOL configuration. Batteries are still in development, so a theoretical energy density that reflects battery technology maturity will be used for calculations necessary for the design. Autonomous technology and UAM network operations will also be assumed to have reached maturity.

Mission specification includes a 240 lb payload (one passenger plus 20 lb carry-on luggage), a range of 80 mi at a cruise speed of 125 mph, and a cruising altitude of 1,500 ft MSL. Most importantly this aircraft must meet the minimum 300 ft takeoff and landing ground run. This will allow the roofs of buildings, small spaces within the city, and helipads to be repurposed to accommodate the unique mission profile.

### 1.4 METHODOLOGY

The design will use multiple methods to account for the features of a fully electric aircraft. Preliminary weight sizing will be completed using the procedure described by Riboldi and Gualdoni. This process begins by compiling a database of single-engine electric aircraft with similar mission requirements. Takeoff weight, empty weight, and motor weight will be estimated using this database. The battery weight estimation will be more involved since the power and energy required varies for each mission phase.

The performance sizing for this normal low-speed FAR 23 airplane will follow Class I preliminary sizing outlined by Roskam. Stall speed must be below the 84 ft/s for clean flaps and below 101 ft/s for flaps up. For takeoff and landing, the aircraft must clear a 50 ft obstacle and reach its cruising altitude in 4 minutes. Multiple trade studies can be conducted to arrive at the final design point. This design point will determine the final takeoff weight, wingspan, and power required. The remaining design and analysis will continue to use the guidelines presented in Roskam. Configuration design will focus on simplicity. The fuselage, wing, tail, and landing gear design will also be completed. The analysis will be conducted to ensure longitudinal, lateral, and directional stability. A CG excursion diagram will be used to visualize the most aft and most forward location during a typical mission. Finally, the lift-to-drag plots for the aircraft at various flight phases will be generated.

## 1.5 MISSION REQUIREMENTS

Below is a list of all the mission requirements of the Zoom41.

- Autonomous electric short takeoff and landing capabilities
- Accommodate for a 240 lb passenger
- Accommodate 20 lb of baggage
- Range of 80 mi
- Cruise speed of 125 mph
- 300 ft landing and takeoff ground distance or less

## 1.6 OUTLINE

Below are the steps to completing preliminary sizing and design.

### **Step 1** Complete weight sizing

#### Step 1.1 Mission weight estimates

##### Step 1.1.1 Compile database for takeoff weight and empty weight

##### Step 1.1.2 Determine regression coefficients

##### Step 1.1.3 Battery weight estimation

###### Step 1.1.3.1 Determine power and energy required for climb phase

###### Step 1.1.3.2 Determine power and energy required for cruise/loiter phase

###### Step 1.1.3.3 Determine power and energy required for takeoff/landing phase

#### Step 1.2 Estimate sensitivities

##### Step 1.2.1 Weight sensitivities

##### Step 1.2.2 Range sensitivities

#### Step 1.3 Weight sizing trade studies

### **Step 2** Complete performance sizing

#### Step 2.1 Calculate performance constraints

##### Step 2.1.1 Takeoff distance

- Step 2.1.2 Stall speed
- Step 2.1.3 Landing distance
- Step 2.1.4 Climb constraints
  - Step 2.1.4.1 Rate-of-climb
  - Step 2.1.4.2 Climb gradient
- Step 2.1.5 Speed constraints
- Step 2.1.6 Compile final performance sizing graph
- Step 2.2 Verify performance constraints using AAA
  - Step 2.2.1 AAA Takeoff distance
  - Step 2.2.2 AAA Stall speed
  - Step 2.2.3 AAA Landing distance
  - Step 2.2.4 AAA Climb constraints
    - Step 2.2.4.1 AAA Rate-of-climb
    - Step 2.2.4.2 AAA Climb gradient
  - Step 2.2.5 AAA Speed constraints
  - Step 2.2.6 AAA Compile final performance sizing graph
- Step 3** Select configuration
  - Step 3.1 Comparative study of airplanes
    - Step 3.1.1 Comparison of weights
    - Step 3.1.2 Comparison of performance
    - Step 3.1.3 Comparison of geometry
  - Step 3.2 Zoom41 Configuration selection
    - Step 3.1 Overall configuration
    - Step 3.2 Wing configuration
    - Step 3.3 Empennage configuration
    - Step 3.4 Propulsion configuration
- Step 4** Complete fuselage design
  - Step 4.1 Layout of cockpit
  - Step 4.2 Layout of fuselage
- Step 5** Complete wing design
  - Step 5.1 Wing planform design
  - Step 5.2 Sweep angle
  - Step 5.3 Thickness ratio
  - Step 5.4 Airfoil selection
  - Step 5.5 Aerodynamic twist
  - Step 5.6 Incidence angle
  - Step 5.7 Wing design evaluation
  - Step 5.8 Lateral Control surface sizing
- Step 6** Complete empennage design
  - Step 6.1 Overall empennage design
  - Step 6.2 Horizontal stabilizer design
    - Step 6.2.1 Planform
    - Step 6.2.2 Elevator

- Step 6.3 Vertical stabilizer design
  - Step 6.2.1 Planform
  - Step 6.2.2 Rudder
- Step 6.4 Empennage design evaluation
- Step 7** Complete landing gear design
  - Step 7.1 Estimation of CG location of airplane
    - Step 7.1.1 Component weight estimation
    - Step 7.1.2 Component center of gravity
  - Step 7.2 Landing gear design
  - Step 7.3 Weight and balance
    - Step 7.3.1 CG location drawing
    - Step 7.3.2 CG Excursion diagram
- Step 8** Estimate drag polar
  - Step 8.1 Aircraft zero lift
  - Step 8.2 Low speed drag increments
  - Step 8.3 Total aircraft drag polar

## **2.0 WEIGHT SIZING AND WEIGHT SENSITIVITIES**

### **2.1 MISSION WEIGHT ESTIMATES**

Weight sizing for the Zoom41 mission relies heavily on the method Riboldi and Gualdoni's article: *An Integrated Approach to the Preliminary Weight Sizing of Small Electric Aircraft* [16]. Their approach consists of compiling a database of similar aircraft and using to obtain regression plots for the variables of interest.

#### **2.1.1 Database for Takeoff Weights and Empty Weights of Similar Airplanes**

Hybrid and more electric aircraft will be not included in this database. Focusing on compiling data from all-electric aircraft will provide the most accurate estimations. The table below displays weight and power data of current electric aircraft designs.

**Table 2.1: Comparison of single-engine electric aircraft**

Aircraft	Alpha Trainer	Alpha Electro	Virus SW	Sinus 912	Taurus Electro G2	Sun Flyer SF2	Solarworld Elektra One
<b>Source</b>	Jane's [17]	Jane's [17]	Jane's [17]	Jane's [17]	Riboldi [16]	Jane's [17]	Jane's [17]
<b>W<sub>TO</sub> (lb)</b>	1,212	1,212	1,322	992	1,212	1,900	661
<b>W<sub>B</sub> (lb)</b>	90	90	99	94	93	N/A	220
<b>W<sub>E</sub> (lb)</b>	615	771	637	626	558	1,460	242
<b>W<sub>M</sub> (lb)</b>	134	134	141	134	24	57	10
<b>P<sub>M</sub> (HP)</b>	80	80	115	80	54	115	21

**Table 2.1: Comparison of single-engine electric aircraft continued**

Aircraft	LAK 17B FES	Antares 20E	Antares 23E	Silent 2 Electro	VoltAir E-Fan 2.0	Yuneec E430
<b>Source</b>	Riboldi [16]	Riboldi [16]	Riboldi [16]	Riboldi [16]	Jane's [17]	Riboldi [16]
<b>W<sub>TO</sub> (lb)</b>	1,213	1455	1874	661	1,278	1,036
<b>W<sub>B</sub> (lb)</b>	75	170	170	79	302	163
<b>W<sub>E</sub> (lb)</b>	542	970	1093	441	1,102	346
<b>W<sub>M</sub> (lb)</b>	15	64	64	42	N/A	42
<b>P<sub>M</sub> (HP)</b>	47	56	56	17	80	54

The electric aircraft in this database have an average takeoff weight of 1,233 lb. Over half the aircraft in this study were designed for 2 passengers. So, the takeoff weight for the Zoom41 will be fixed at approximately 800 lb, which is less than the average from the database. Also, note that these aircraft use batteries with energy densities lower than those that will be used for Zoom41's estimations, which will result in weight savings.

### 2.1.2 Determination of Regression Coefficients A and B

A relationship between the takeoff weight and empty weight is used to determine the regression coefficients A and B [16]. The empty weight of Zoom41 can be reduced by substituting the takeoff weight into equation 2.1.

$$\log(W_{TO}) = A + B \log(W_E) \quad 2.1$$

In Figure 2.1, the empty weight and takeoff weight for the aircraft in Table 3.1 were plotted to observe the statistical correlation between the two parameters.

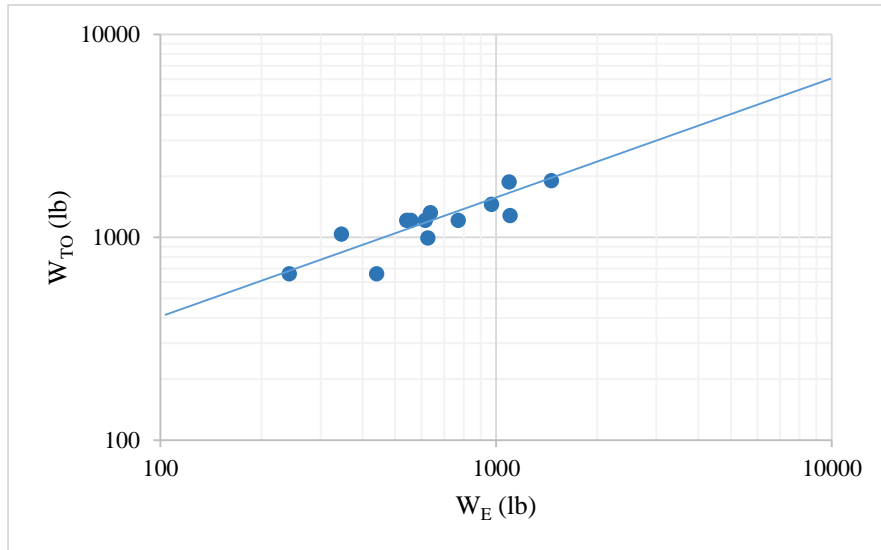


**Figure 2.1: Weight trends for single engine propeller driven aircraft**

Replotting this data to use the logarithmic relationship in [Equation 2.1](#), coefficient A, 1.53, and coefficient B, 0.55, were derived. Empty weight of 319.6 lb was estimated using this method. Regression coefficients are compared with ones found in Roskam in [Appendix A](#).

### 2.1.3 Determination of Coefficients C and D

A semi-logarithmic plot, seen in [Figure 2.2](#), was generated for the motor power versus the motor weight using the data from [Table 2.1](#). The resulting regression line can be used to determine coefficients C and D. Coefficient C for the regression line is 0.97 and coefficient D is 0.01. This is used to define the relationship between motor weight and power of the motor seen in equation 2.2 below [16].

$$\log(W_M) = C + D * P_M \quad 2.2$$

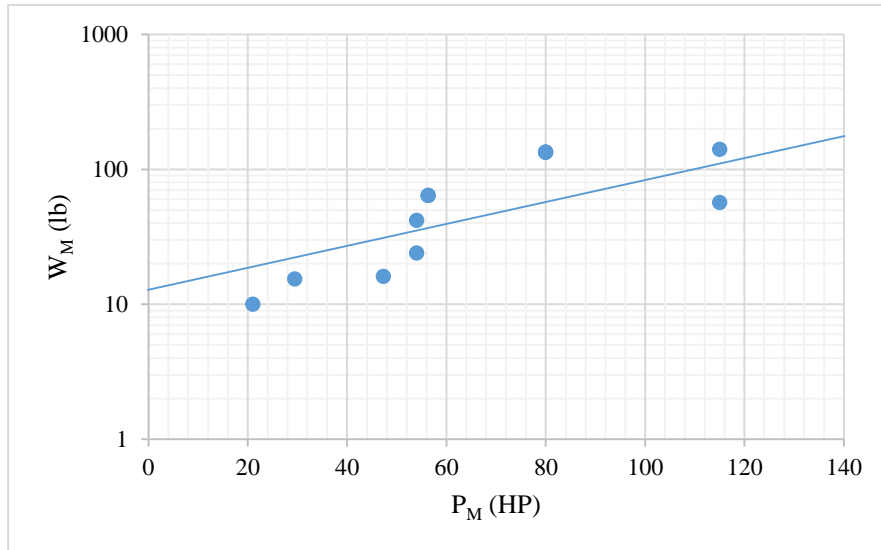


**Figure 2.2: Motor power vs weight for single engine electric aircraft**

Motor power for Zoom41 will be selected within the data’s range, between 20 hp and 115 hp, due to the limited number of data points. An electric motor with a power output of 80 hp will be needed to accommodate for the high cruise speed and low altitude of Zoom41. Motor weight of 70 lb was estimated using this method.

#### 2.1.4 Battery Weight Calculation

The Riboldi and Gualdoni battery weight calculation is a lengthy process with numerous assumptions. [Appendix B](#) details assumptions and notes for the parameters used to calculate the battery weight. The Alpha Electro is used as a reference aircraft for some parameters due to the aircraft’s high-performance characteristics. The general approach uses the maximum power or energy from climb, cruise, or loiter to determine the battery weight. It is designed to travel to the customer, pick up the customer, drop the customer at the destination, and return to the dispatch station as shown in [Figure 2.3](#). For simplification, it was assumed that there will be a passenger aboard during the entire mission.

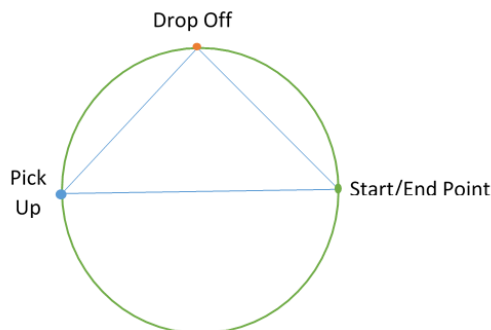


**Figure 2.3: Zoom41 mission overview**

#### 2.1.4.1 Climb Power and Energy Required

Equation 2.3 for power required and equation 2.4 for the energy required for climb were used [16].

$$P_{req} = W_{TO}ROC + \frac{1}{2}\rho V^3 SC_D \quad 2.3$$

$$E = P_{req} t \quad 2.4$$

The estimated takeoff weight of 800 lb was used to calculate the power required. Alpha Electro provided the rate of climb, aspect ratio, and wing area values [18]. Climb velocity was determined by FAR 23 stall speed requirements. Next, drag polar was derived using Figure 3.21a for single-engine propeller-driven aircraft in Roskam, Part 1 [19]. The average density from 0 ft to 1,500 ft MSL was used for climb density. Oswald's efficiency of 0.7 used for a rectangular wing [20]. These assumptions led to a drag coefficient, which was used to get a power required of 49 HP and energy required of 3.7 HPh for the three climb phases.

#### 2.1.4.2 Cruise/Loiter Power and Energy Required

Cruise/loiter power and energy required were calculated similarly to the climb phase with a few exceptions. Everything remained constant apart from the density, velocity, and time. The density at 1,500 ft MSL for cruise and 1,300 ft MSL for loitering were taken. Loiter altitude was determined to be the minimum altitude allowed by the FAA for ZOOM41. A cruise velocity of 125 mph and range of 80 mi, to determine cruise time, was used as specified in the mission requirements. Loiter velocity was calculated by taking 90-percent of cruise velocity as specified in Riboldi. Finally, it was determined 75 HP was required for cruise and 64 HP was required for loitering. Also, the energy required for cruise was 50 HPh and 16 HPh for loitering.

#### 2.1.4.3 Takeoff/Landing and Battery Weight

Battery weight can be determined using Equation 2.5 below [16]. Where the propeller efficiency was estimated at 0.8 [1]. Battery energy was projected for 2026 for future construction of the aircraft and current state-of-the-art value for power density was used [16]. The resulting battery weight was multiplied by a factor of 1.06 to accommodate for takeoff and landing as mentioned in Riboldi [16].

$$W_B = \frac{g}{\eta_p} \max \left\{ \frac{E^{climb} + E^{cruise} + E^{loiter}}{e}, \frac{\max\{P_{req}^{climb} + P_{req}^{cruise} + P_{req}^{loiter}\}}{p} \right\} \quad 2.5$$

A final battery weight of 192 lb was calculated and used to calculate the empty weight of 318 lb. The calculated empty weight and estimated weight from Riboldi are within the 0.5% limit.

## 2.2 SENSITIVITIES

### 2.2.1 Weight Sensitivity

Roskam provides various sensitivity equations, but only the sensitivity of takeoff weight to empty weight can be applied to the ZOOM41. Other equations in Roskam use specific fuel consumption and cannot be utilized for electric aircraft. In [Equation 2.6](#), A and B are regression coefficients different than those derived using Riboldi's regression curves. [Appendix A](#) displays the regression plot used to obtain these coefficients. A positive value of 0.472 was obtained for this weight sensitivity.

$$\frac{\partial W_{TO}}{\partial W_E} = \frac{BW_{TO}}{\log^{-1}\left(\frac{\log(W_{TO})-A}{B}\right)} \quad 2.6$$

### 2.2.2 Range Sensitivities

Range sensitivities for ZOOM41 were determined using Hepperle's article, *Electric Flight – Potential and Limitations* [3]. The following conditions must be met in order to produce valid results.

$$\frac{L}{D} > \frac{R*g}{(1-f_e)*p*\eta_{total}} \quad 2.7$$

$$p > \frac{R*g}{(1-f_e)*\frac{L}{D}*\eta_{total}} \quad 2.8$$

$$f_e > 1 - \frac{R*g}{\frac{L}{D}*p*\eta_{total}} \quad 2.9$$

Total efficiency of 73-percent was assumed using Hepperle's chain efficiency of battery powered motors [3]. SI units are used for equation 2.7 through equation 2.9 as specified in Hepperle [3]. [Table 2.2](#) proves the criterion listed in the equations above were met before proceeding with sensitivity calculations.

**Table 2.2: Sensitivity equation criterion**

Parameter	Units	Left Hand Side		Right Hand Side
L/D	No units	15.40	>	2.93
p	Watt/kg	980	>	185
$f_e$	No units	0.397	<	0.886

The mass growth per distance is given by equation 2.10, which yields a value of 1.7 lb/mi for ZOOM41. Similarly, additional sensitivities with respect to the range are calculated using equation 2.11 through equation 2.14.

$$\frac{\partial m}{\partial R} = \frac{W_{pl}}{\left(1 - f_e - \frac{L}{D} \frac{R * g}{p * \eta_{total}}\right)^2 * p * \eta_{total} * \frac{L}{D}} \quad 2.10$$

$$\frac{\partial R}{\partial f_e} = -\frac{1}{g} * p * \eta_{total} * \frac{L}{D} \quad 2.11$$

$$\frac{\partial R}{\partial m} = -\frac{1}{g} * p * \eta_{total} * \frac{L}{D} * m_B * \frac{1}{m^2} \quad 2.12$$

$$\frac{\partial R}{\partial L/D} = \frac{1}{g} * p * \eta_{total} * (1 - f_e - f_p) \quad 2.13$$

$$\frac{\partial R}{\partial p} = \frac{1}{g} * \frac{L}{D} * \eta_{total} * (1 - f_e - f_p) \quad 2.14$$

To better understand the results of these sensitivities, each one of the parameters was increased by ten-percent to observe its effect on range.

**Table 2.3: Range sensitivity results**

Sensitivity	Value	Units
$\frac{\partial R}{\partial f_e}$	-698	mi
$\frac{\partial R}{\partial f_e} * 10\% f_e$	-71.9	mi
$\frac{\partial R}{\partial p}$	281	mi/HP/lb
$\frac{\partial R}{\partial E} * 10\% p$	43.5	mi
$\frac{\partial R}{\partial L/D}$	10.9	mi
$\frac{\partial R}{\partial L/D} * 10\% \frac{L}{D}$	43.5	mi
$\frac{\partial R}{\partial m}$	-0.2	mi/lb
$\frac{\partial R}{\partial m} * 80lbm$	-95.7	mi

The largest shifts in the range seen in [Table 2.3](#) is due to increasing total or empty weight, which makes sense due to the light weight of the ZOOM41. An increase in battery power density and lift-to-drag ratio have the same positive impact on range. These sensitivities can be used to “trade” one parameter for another in order to meet requirements. For example, if an increase in empty weight is required, then an increase in power density and/or lift-to-drag ratio would be needed to maintain the desired range of the aircraft.

## 2.3 TRADE STUDIES

The range will be studied closely instead of takeoff weight because takeoff weight stays constant throughout the mission. The range is affected by available energy, propulsion system, the mass of the aircraft, and aerodynamic properties of the aircraft [3]. Available energy is represented by the power density, the propulsion system represented by the power, the aerodynamic properties represented by the lift-to-drag ratio, and the mass of the aircraft represented by takeoff weight. Following trade studies were conducted to closely observe how each parameter varies with range. The design point was selected based on the desired range of the aircraft.

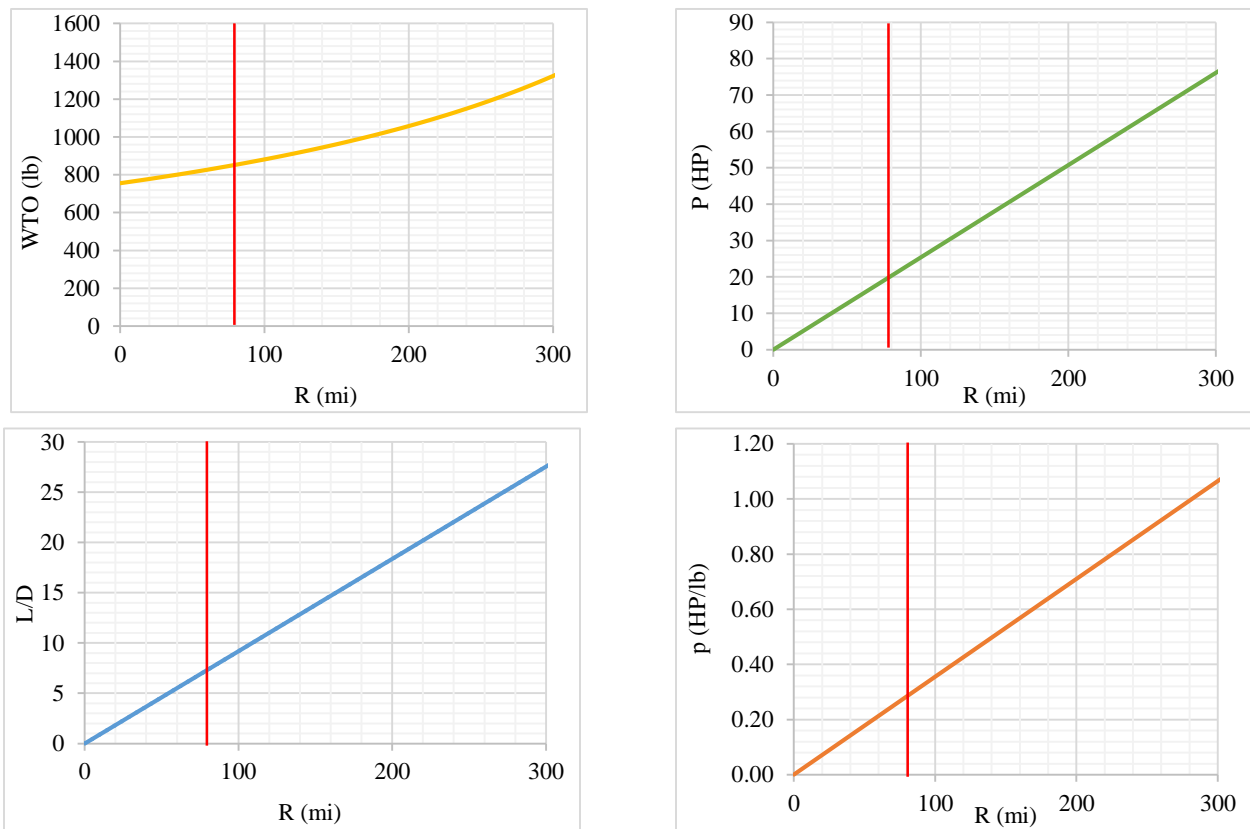


**Figure 2.4: Trade studies. Takeoff weight (yellow), power (green), lift-to-drag ratio (blue), and power density (orange) on the vertical axis with range on the horizontal axis. Red line indicates design point.**

To summarize, if aircraft needs to increase its range, then the aircraft will become heavier, need additional lift, need more power, and batteries with a higher power density. These trade studies will be useful in the following chapter when these parameters will be varied to meet mission or certification requirements.

## 2.4 DISCUSSION, CONCLUSIONS AND RECOMMENDATIONS

Total weight of ZOOM41 was determined using the method outlined in Riboldi's article. Which began with compiling a database of single-engine electric aircraft with similar mission requirements. Then the takeoff weight vs empty weight plot was assembled to determine the regression coefficients, which led to the ZOOM41 total weight of 800 lb and an empty weight of 318 lb. Next, the database was used again to plot motor power vs motor weight. This was used to estimate power of 80 HP and motor weight of 70 lb. The payload weight of 220 was used from mission requirements. Using these weights, an empty weight estimation was made.

The battery weight was calculated by comparing the maximum power and energy required for each phase. Cruise, as expected, required the most power and energy. A battery weight of 192 lb and was used to calculate and compare the empty weight of 318 lb. This estimation for ZOOM41 is reasonable when compared to the existing electric single-engine aircraft.

Weight and range sensitivities were calculated using the aircraft weight. The takeoff weight to empty weight sensitivity was 0.472. The takeoff and empty weight had the greatest negative effect on the range sensitivity as well. Large sensitivities in lightweight aircraft, like the ZOOM41, is expected. Although, if there is a need to increase weight, then the lift-to-drag and/or power density can be used to increase range because these parameters produced a positive effect on range. Trade studies were conducted using these parameters with respect to range. A design point was determined for each parameter by fixing the range required for the ZOOM41 mission.

The significance of trade studies and weight sensitivities in determining a design point is crucial, especially when little information about electric single-engine aircraft is available. These design points are important when proceeding with the design of ZOOM41. Knowing the sensitivity of, for example, the lift-to-drag ratio will prove useful when designing the wing of the aircraft. The repercussions of not meeting requirements are parameterized.

## 3.0 PERFORMANCE SIZING

### 3.1 CALCULATION OF PERFORMANCE CONSTRAINTS

#### 3.1.1 Takeoff Distance

The takeoff ground distance must be within 300 ft at sea-level to meet mission requirements. The takeoff distance for the current design with clean flapped wings can be calculated using equation 3.1 and equation 3.2 [19]. The clean wing takeoff ground distance is 335 ft and takeoff distance is 557 ft, which does not meet the requirements.

$$S_{TOG} = 4.9TOP_{23} + 0.009TOP_{23}^2 \quad 3.1$$

$$S_{TO} = 8.134TOP_{23} + 0.0149TOP_{23}^2 \quad 3.2$$

$$\frac{W}{S} = \frac{TOP_{23} * C_{L,max}}{\frac{W}{P}} \quad 3.3$$

Thus, flaps will be needed during takeoff to meet requirements. The max lift coefficient needed for takeoff can be derived by setting  $S_{TOG}$  to 300 ft and solving for  $TOP_{23}$ . Then plugging  $TOP_{23}$  into equation 3.3 [19]. A  $C_{L,max}$  of 1.2 is required for takeoff ground run under 300 ft. The calculated  $S_{TO}$  is under the 500 ft requirement. [Figure 3.1](#) illustrates the takeoff distance requirement for

varying  $C_{Lmax}$ . If the design point is below or on the curve, then the requirement has been met, and not met if it lies above.

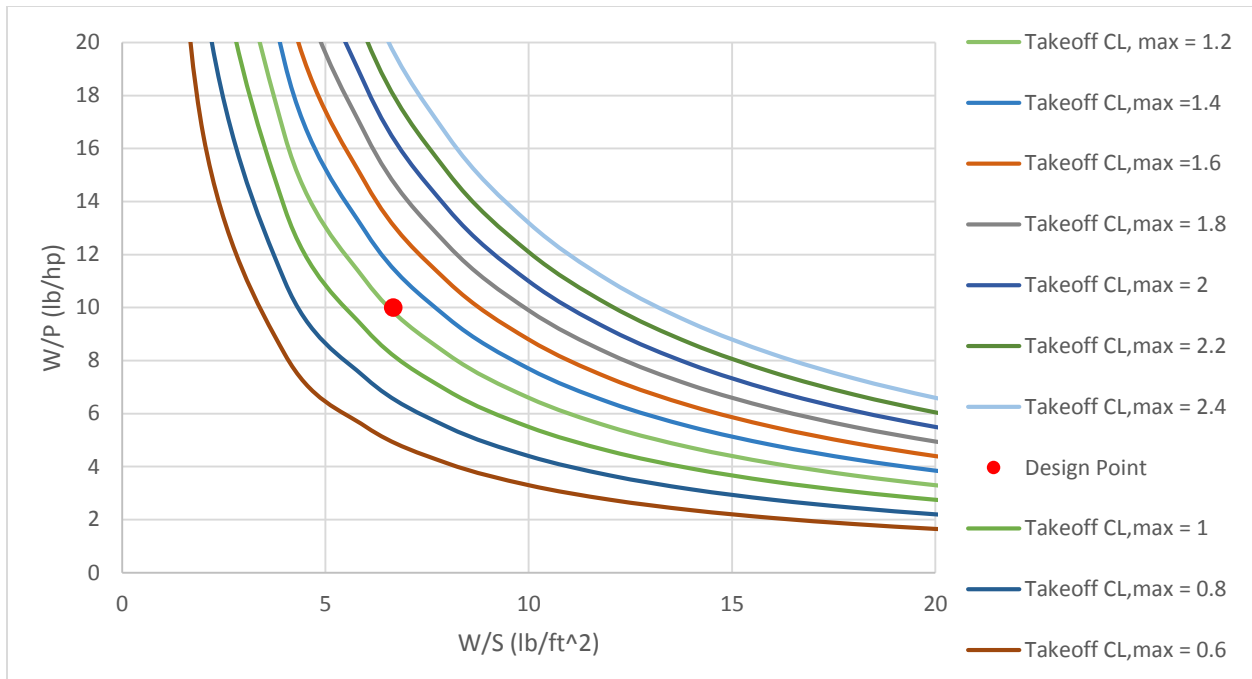


**Figure 3.1: Takeoff distance requirement 300 ft**

The figure illustrates that the requirement for the desired takeoff distance of 300 ft has been met. It can be seen that as the  $C_{Lmax}$  increases, the takeoff distance requirement curves shift up, and allows more room for the design point to move higher.

### 3.1.2 Stall Speed

Stall speed was calculated using the total weight, estimated wing area, density at sea level, and maximum lift coefficient [19]. The sample calculation below shows how the stall speed was found.

$$V_{S,Clean} = \sqrt{\frac{2(W/S)}{\rho C_{Lmax}}} = \sqrt{\frac{2(800 \text{ lb}/120 \text{ ft}^2)}{\left(0.002377 \frac{\text{slug}}{\text{ft}^3}\right) 0.874}} = 80 \text{ ft/s} \quad 3.4$$

$$V_{S,TO} = \sqrt{\frac{2(W/S)}{\rho C_{Lmax}}} = \sqrt{\frac{2(800 \text{ lb}/120 \text{ ft}^2)}{\left(0.002377 \frac{\text{slug}}{\text{ft}^3}\right) 1.2}} = 68 \text{ ft/s} \quad 3.5$$

The calculated stall velocity is below the 84 ft/s FAR 23 requirement for flaps down and below 101 ft/s for flaps up. [Figure 3.2](#) below is a graph of stall speed estimates for varying  $C_{Lmax}$  for a clean wing configuration.

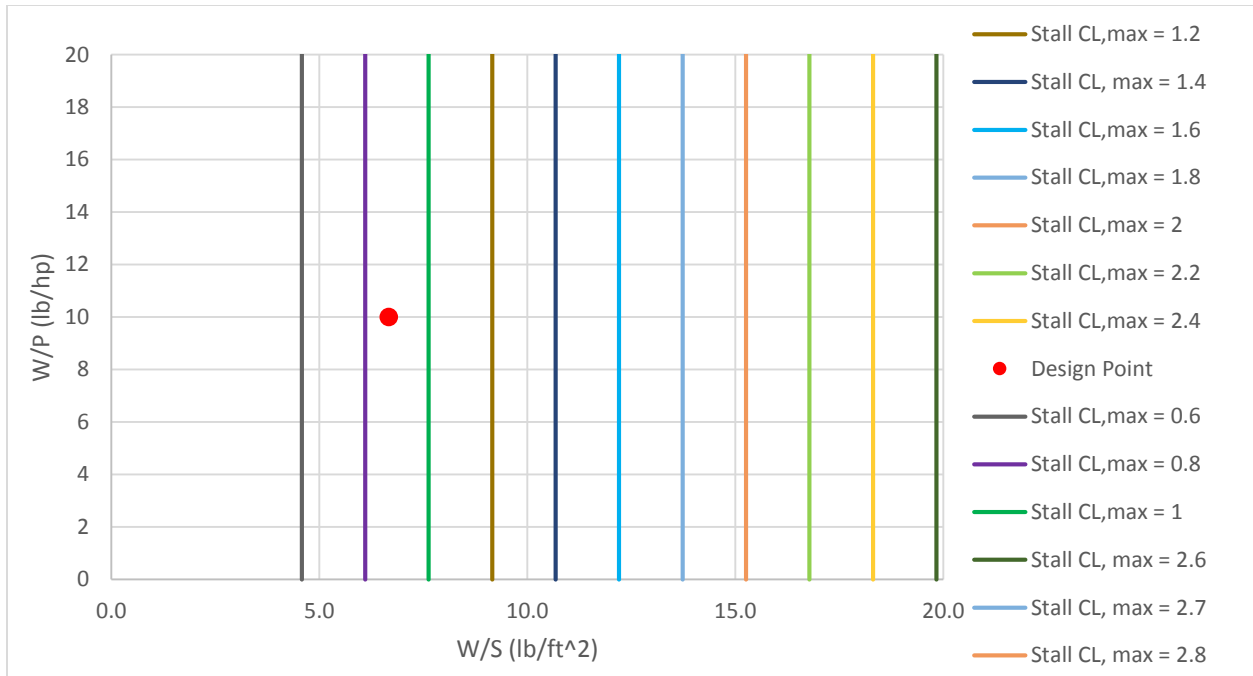


**Figure 3.2: Stall speed requirement for clean wing of 80 ft/s**

If the design point lies on the left side, then the requirement has been met, otherwise it has not been met and will stall. The Zoom41 design point for clean wings meets the stall speed requirement. The next figure illustrates the stall speed requirement for a flapped configuration with a  $C_{L,max}$  of 1.2 for takeoff.

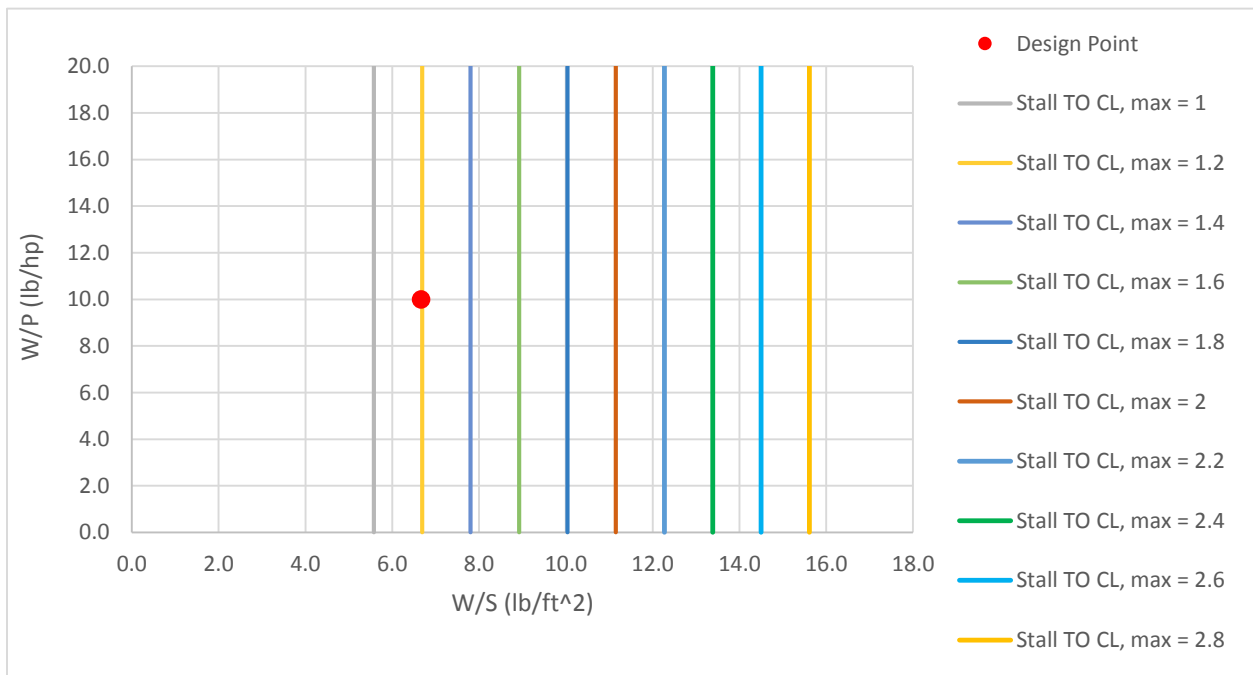


**Figure 3.3: Stall speed requirement for takeoff of 68 ft/s**

Zoom41 will not stall with flaps up during takeoff as [Figure 3.3](#) demonstrates. It is critical to check the stall speed requirement for both configurations because the stall requirement shifts to the left when flaps are up.

### 3.1.3 Landing Distance

The mission requirements specify that the landing ground distance must be below 300 ft and total landing distance below 500ft. The stall speed was found to be 52 ft/s to meet landing distance requirements. Using equation 3.6 and equation 3.7 the landing ground distance was calculated to be 252 ft and a total landing distance of 488 ft [19]. From this, the approach speed can be determined by increasing the stall speed by 30-percent. The approach speed was found to be 68 ft/s [19].

$$S_L = 0.5136V_{SL}^2 \quad 3.6$$

$$S_{LG} = 0.265V_{SL}^2 \quad 3.7$$

Equation 3.8 allowed the landing distance required to be plotted for varying  $C_{L, \max}$  as seen in [Figure 3.4](#) [19].

$$\frac{W}{S} = \frac{V_s \rho C_{L, \max}}{2 * 0.95} \quad 3.8$$

The landing distance requirement is met if the design point lies to the left and not met if it lies to the right. To meet the landing distance requirement a  $C_{L, \max}$  of 2.1 is required. These requirements behave similarly to the stall speed requirements: shifts to the right as the  $C_{L, \max}$  increases.

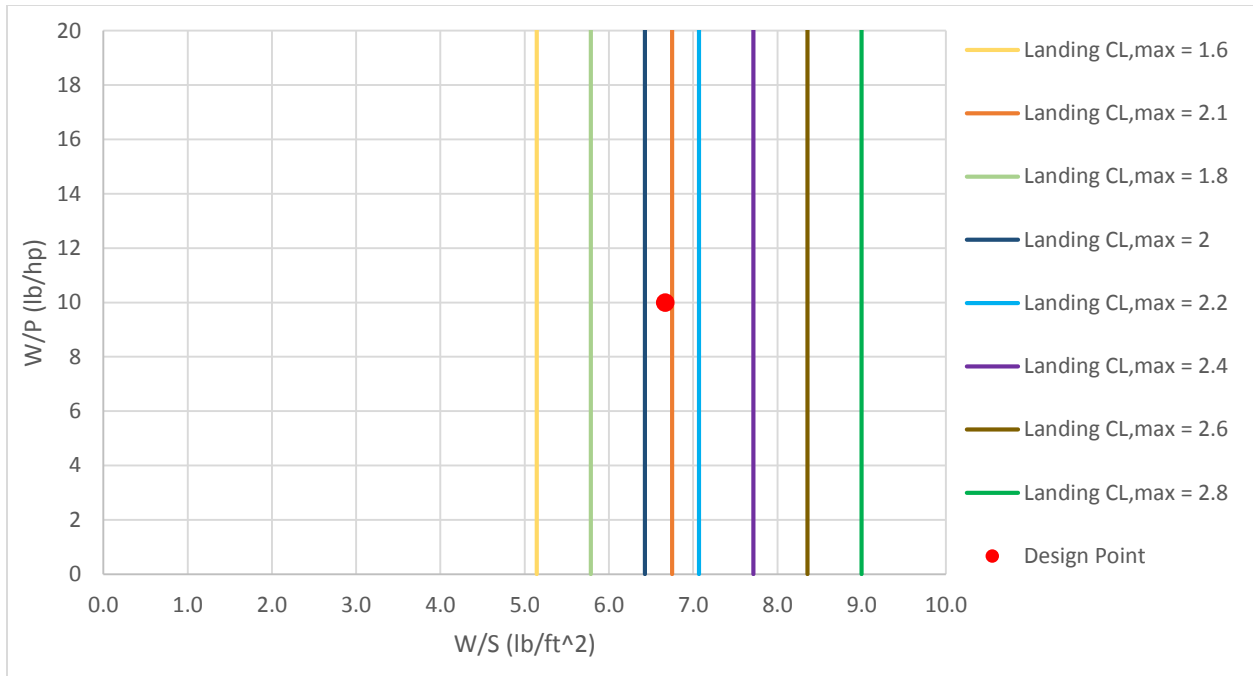


Figure 3.4: Landing distance requirement of 300 ft

### 3.1.4 Drag Polar Estimation

The drag polar was estimated using Roskam's method [19]. First, the wetted area was found using the takeoff weight of 800 lb as seen in Figure 3.5. Due to the lack of historical data, a high equivalent skin friction value was assumed to retrieve the wetted area of 450 ft<sup>2</sup>.

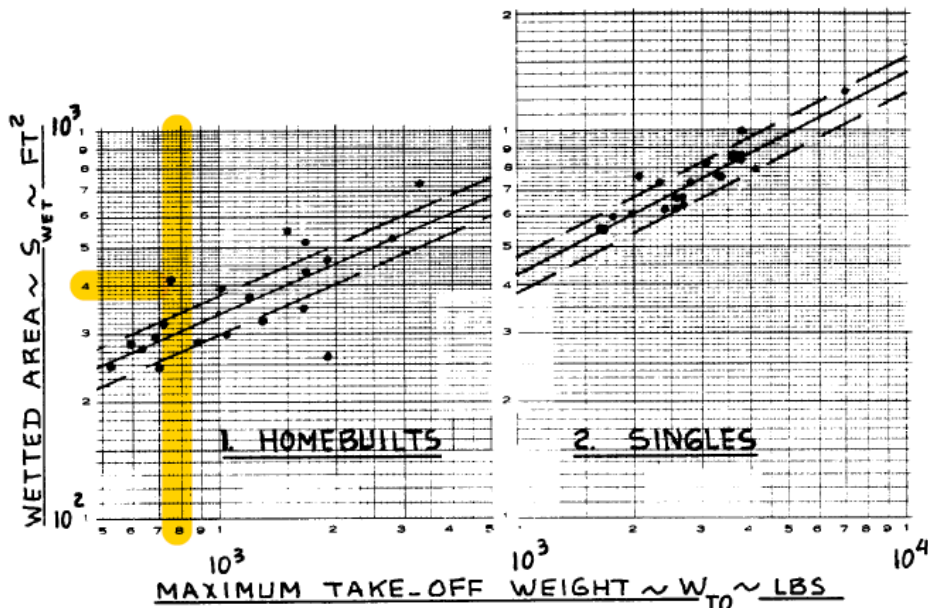


Figure 3.5: Equivalent wetted area

Then by using the wetted area an equivalent parasite area of 3 ft<sup>2</sup> was retrieved as shown below.

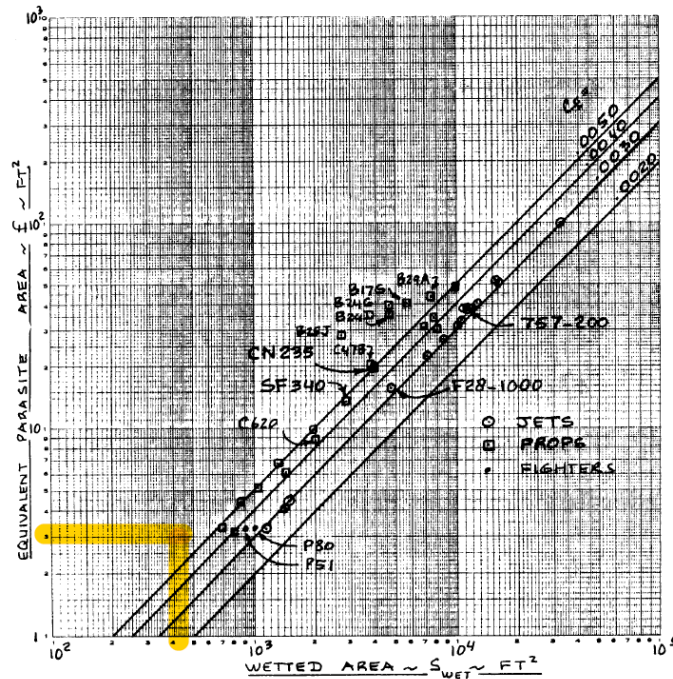


Figure 3.6: Predicting equivalent parasite drag

Again by assuming a higher skin friction value than available. Using equation 3.9, a drag polar of 0.025 was calculated.

$$C_{D0} = \frac{f}{S} = 0.025 \quad 3.9$$

### 3.1.5 Climb Constraints

#### 3.1.5.1 Rate of Climb

The rate-of-climb requirement set by the FAR 23 is 5 fps, and the cruise altitude needs to be reached under 4 minutes. The rate-of-climb for Zoom41 is approximately 20 fps and a time-to-climb of 3 minutes and 41 seconds. Which is close to the rate-of-climb of the Alpha Electro, and was deemed as an achievable rate-of-climb for an electric engine [18]. The climb rate parameter was calculated by dividing the climb rate in fpm by 33,000. This was found to be 0.0370. Using the following equation, the power loading was calculated for a range of wing loadings [19]. This produces the FAR 23.65 AEO takeoff requirement curve shown in [Figure 3.5](#).

$$\frac{W}{P} = \frac{\eta P}{RCP + \left[ \frac{W^{1/2}}{S} \left( \frac{C_L^{3/2}}{C_D} \right) \right]} \quad 3.10$$

If the design point is above the curve then the climb requirement is not met, but if it lies below then the requirement is met. Thus, the rate-of-climb requirement is not critical for the Zoom41, because the design point is well below the curve. Also, the nearly horizontal nature of the curve suggests that the wing and power loading does not affect this requirement compared to other requirements.

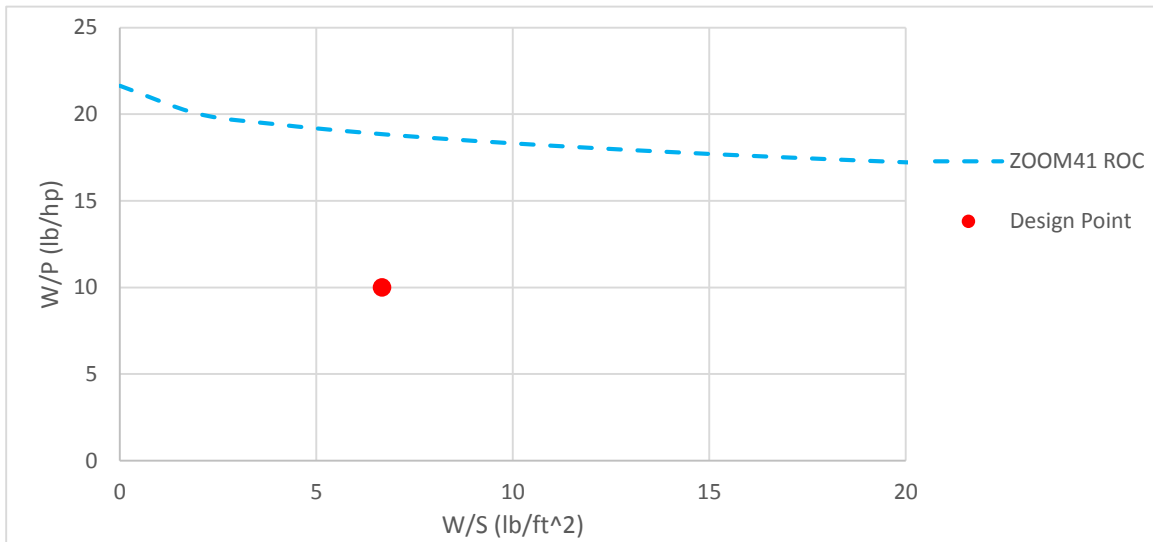


**Figure 3.7: FAR 23 ROC requirement of 5 ft/s**

### 3.1.5.2 Climb Gradient

The FAR 23 climb gradient requirements can be described with equation 3.11 where the CGRP is the climb gradient rate parameter [19]. Setting equation 3.11 equal to equation 3.12 and solving for power loading results equation 3.13 [19].

$$CGRP = \frac{18.97\eta_p\sigma^{1/2}}{(W/p)(W/S)^{1/2}} \quad 3.11$$

$$CGRP = \frac{ROC + L/D^{-1}}{C_L^{1/2}} \quad 3.12$$

$$\frac{W}{P} = \frac{18.97\eta_p\sigma^{1/2}}{\frac{ROC + L/D^{-1}}{C_L^{1/2}} W/S^{1/2}} \quad 3.13$$

Equation 3.13 was used to plot the climb gradient requirement for varying lift coefficients and illustrated in [Figure 3.5](#) [19]. The climb requirement is met if the design point is below the curve, and not met if it is above the curve. Curves shift up as the  $C_{Lmax}$  increases. This parameter is met by the Zoom41 design and is a non-critical requirement.

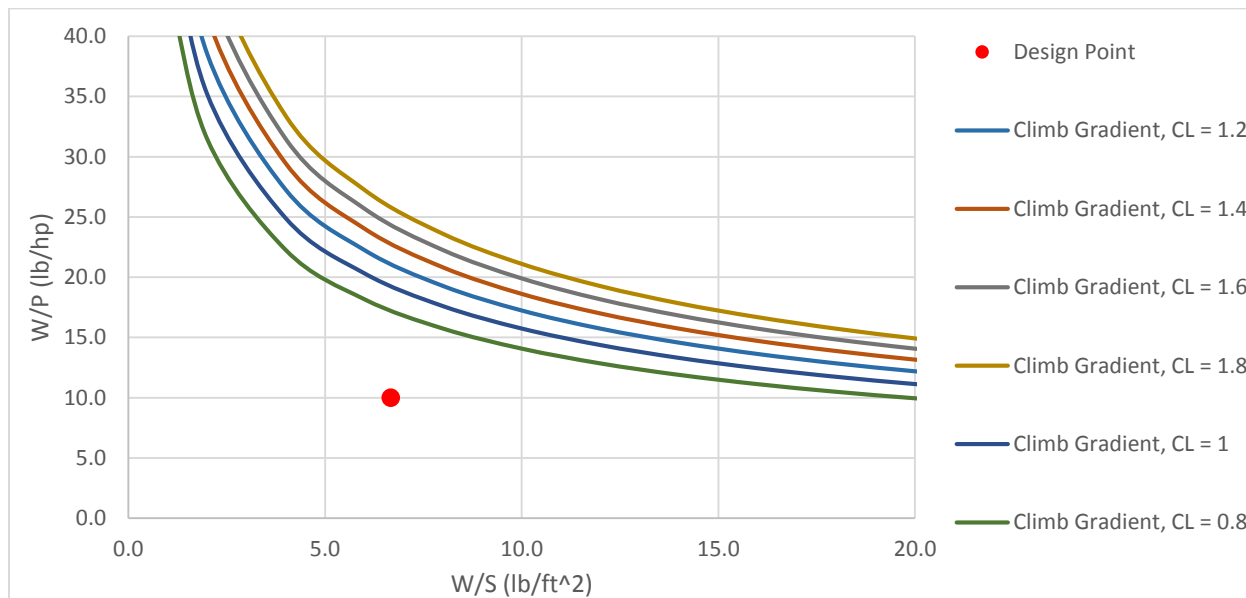


**Figure 3.8: Climb gradient requirement**

### 3.1.6 Speed Constraints

Cruise speed is proportional to the power index. Equation 3.14 describes the relationship between the power index, wing loading, and power loading [19]. This equation was used to plot the cruise speed requirement for multiple power indices during cruise, takeoff, and loiter. The dashed lines represent the desired speed for each phase.

$$I_P = \left( \frac{W/S}{(W/P)\sigma} \right)^{1/3} \quad 3.14$$

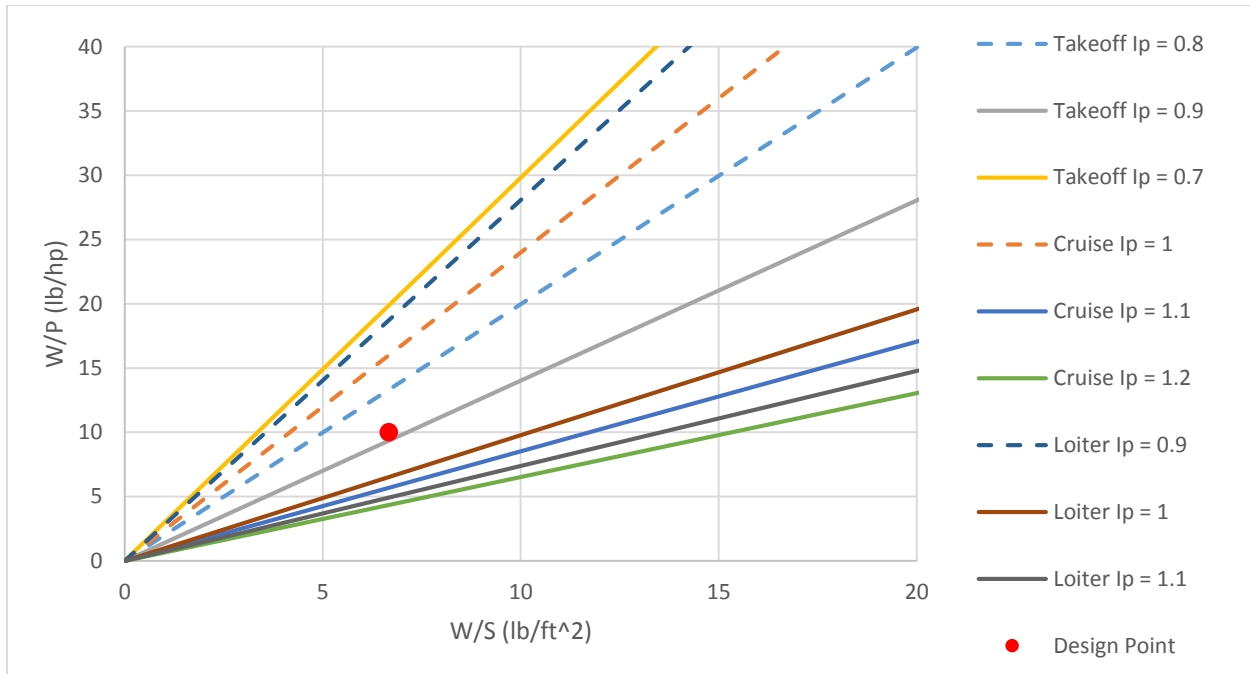


**Figure 3.9: Cruise speed requirement**

Cruise speed requirement is met if the design point is below the curve, and not met if it lies above. Curve shifts down as the power index increases. This was expected because an aircraft would need more power and less weight if it needs to fly faster.

### 3.1.7 Summary of Constraints

The following figure summarizes the constraint curves used to verify the design point of Zoom41. The critical requirements are takeoff distance and takeoff stall. This design point allows Zoom41 to meet requirements with a power of 80 HP, wing area of 120 ft<sup>2</sup>, and a weight of 800 lb as determined in *Chapter 2*. This point lies at a wing loading of 6.7 lb/ft<sup>2</sup> and a power loading of 10 lb/HP. Which results in a clean  $C_{Lmax}$  of 0.874, takeoff  $C_{Lmax}$  of 1.2, and landing  $C_{Lmax}$  of 2.1. An aspect ratio of 18 and a wingspan of 46.5 ft derived using the design point.

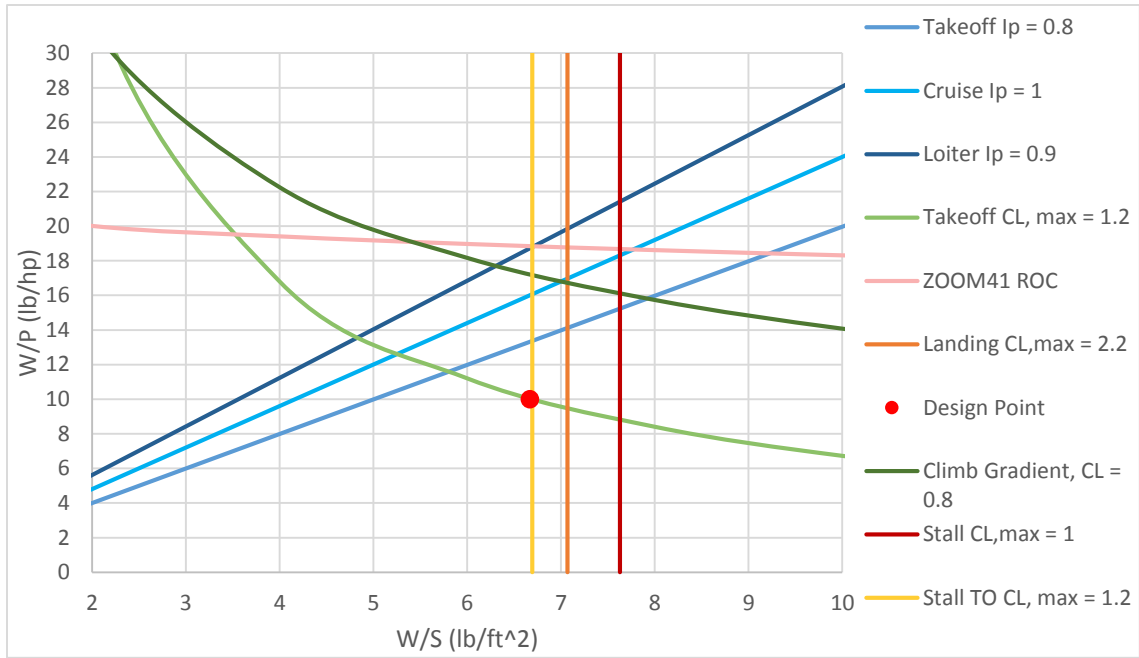


**Figure 3.10: Constraint summary**

An alternative design point, shown in [Figure 3.11](#), was considered. It would increase the wing area to 160 ft<sup>2</sup> and weight to 925 lbs. This would increase parasitic and lift-induced drag. Also, increasing the cost of the aircraft, because a heavier aircraft will entail additional material cost. Therefore, this design point was rejected.

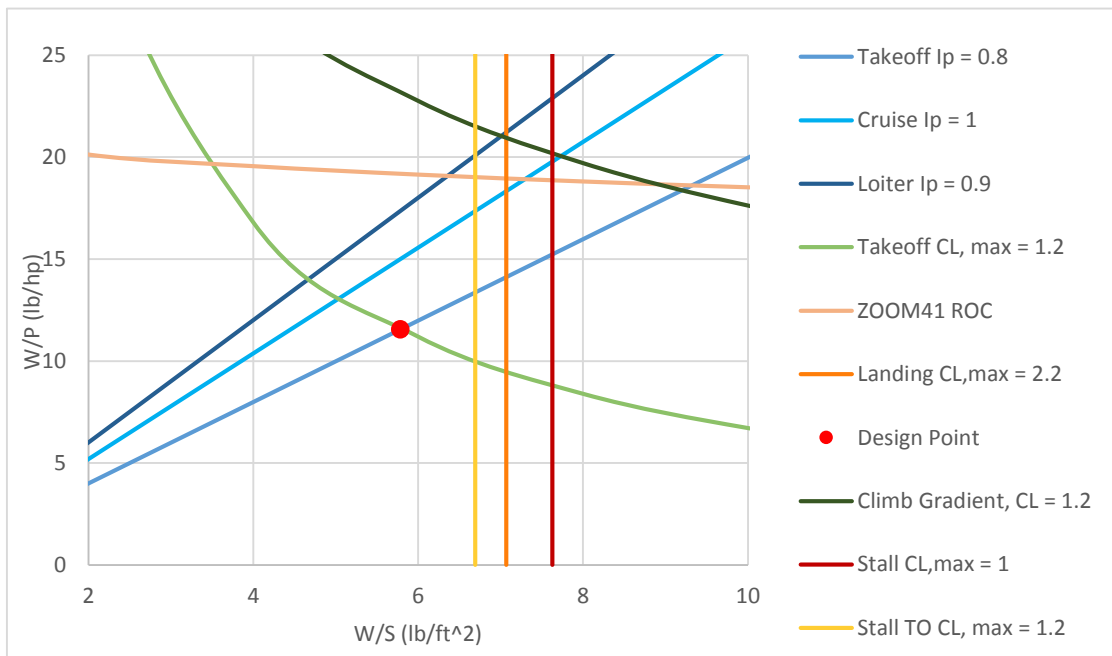


**Figure 3.11: Alternative design point**

# 3.2 PERFORMANCE CONSTRAINTS CALCULATIONS USING AAA

## 3.2.1 AAA Stall Speed

Only the stall speed for clean wings and stall speed for flaps were plotted because there are no options in AAA to vary  $C_{Lmax}$  for this parameter.

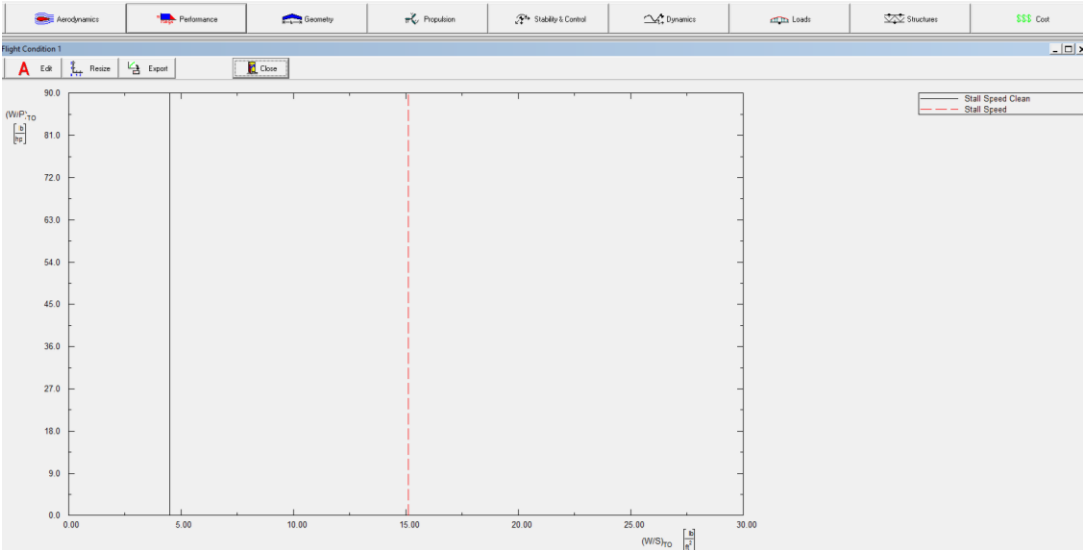


Figure 3.12: AAA stall speed

## 3.2.2 AAA Takeoff Distance

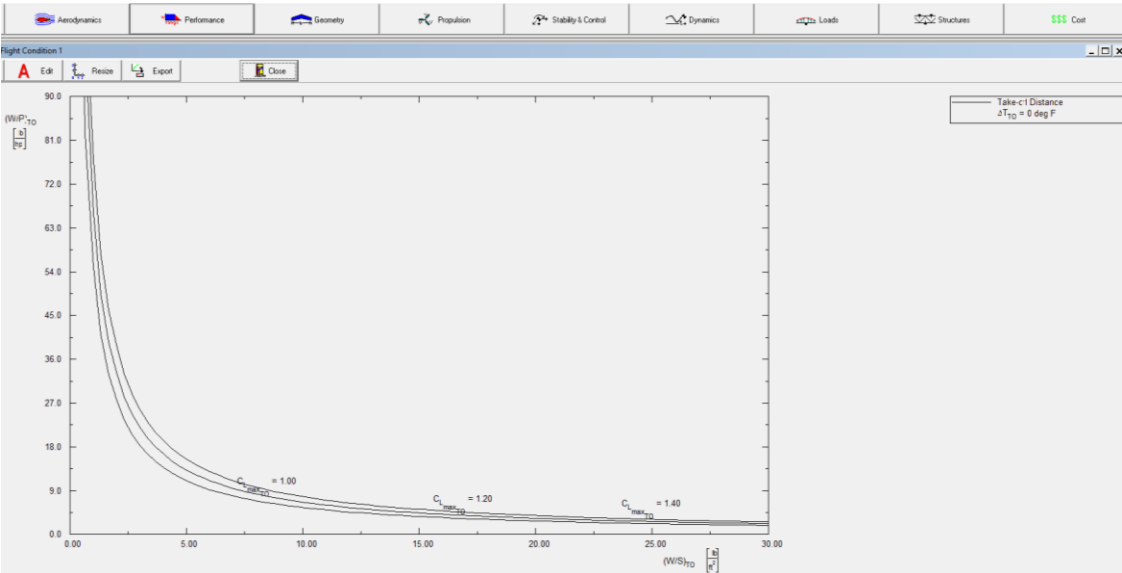


Figure 3.13: AAA takeoff distance

### 3.2.3 AAA Landing Distance

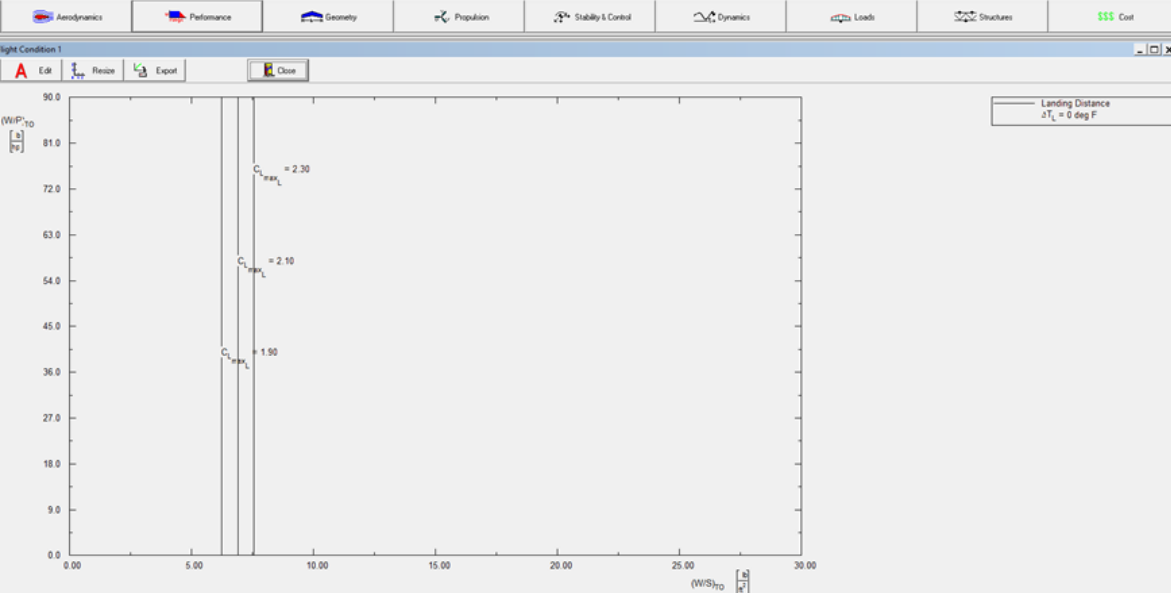


Figure 3.14: AAA landing distance

### 3.2.4 AAA Climb Constraints

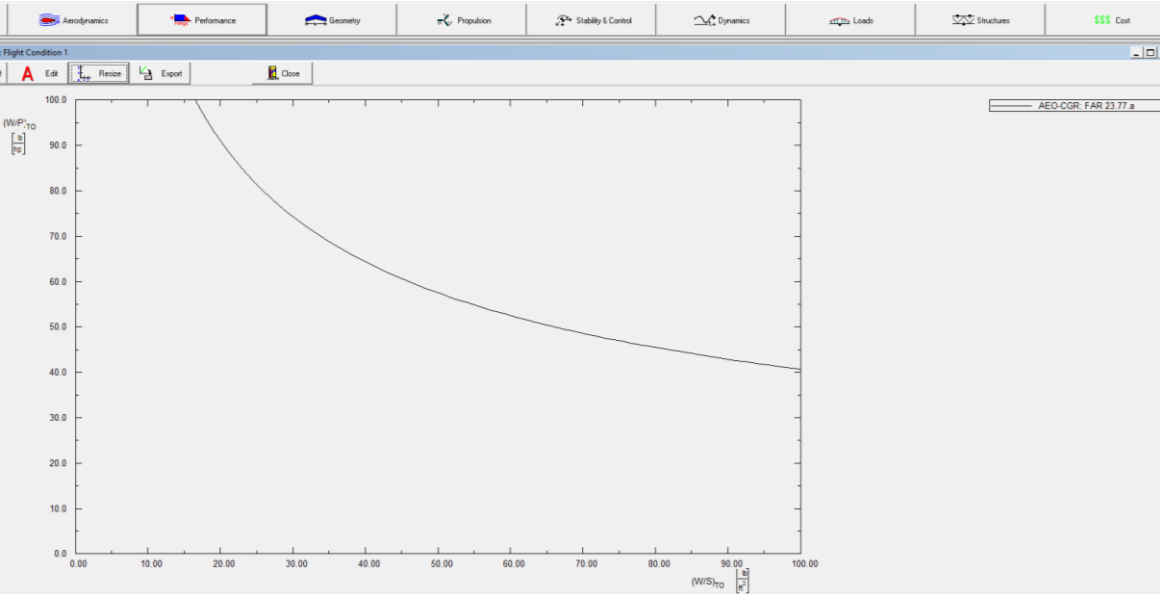


Figure 3.15: AAA AEO climb constraint

### 3.2.5 AAA Speed Constraint

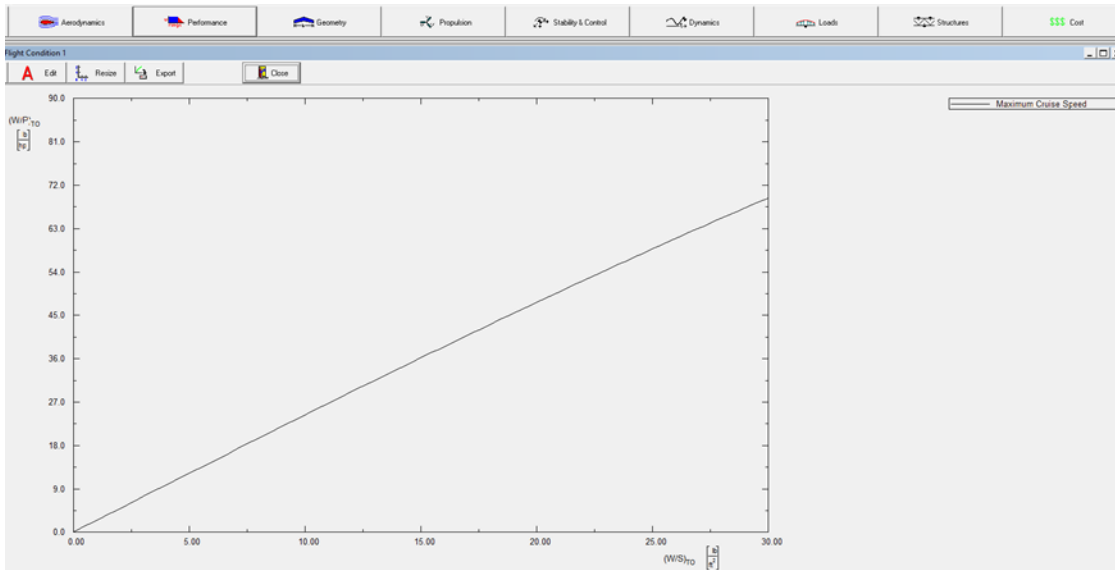


Figure 3.16: AAA cruise speed

### 3.3.6 AAA Design Envelope

The design point selected using manual calculations matches the AAA design envelope shown in Figure 3.17.

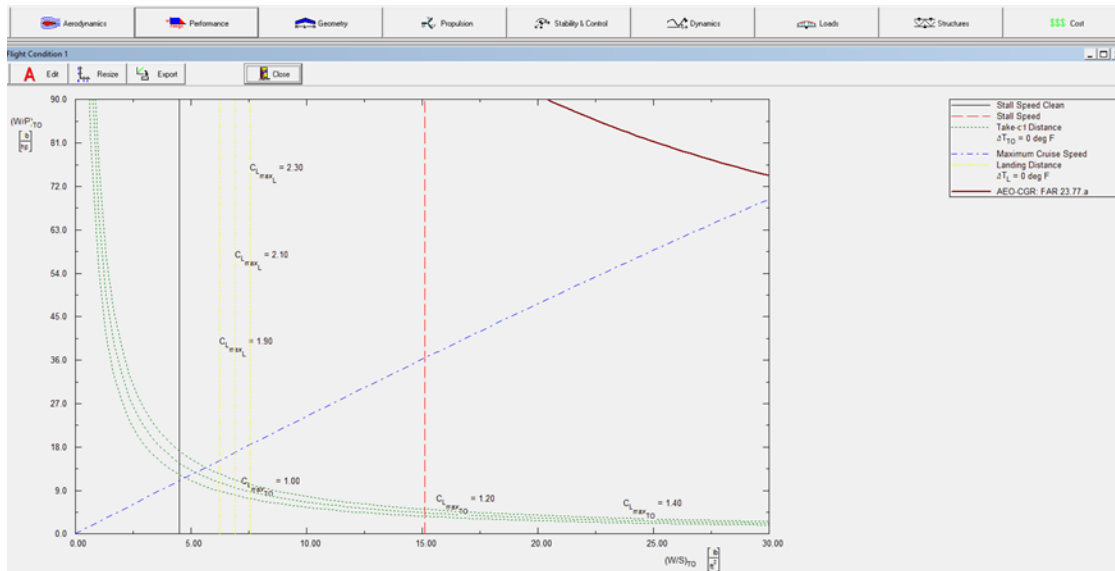


Figure 3.17: AAA design envelope

## 3.3 SELECTION OF PROPULSION SYSTEM

### 3.3.1 Selection of the Propulsion System Type and the Number of Engines

As specified in the mission requirements the Zoom41 will utilize a single electric propeller-driven engine for its propulsion system. The engine will be powered by Li-ion batteries. This is a reasonable selection because it's a low-altitude and low-speed aircraft with a Mach number less than 0.2. The design envelope requires an 80 HP engine. Revisiting the aircraft database compiled in *Chapter 2* ensures that this is a possible power output for a single electrically powered engine.

### 3.3.2 Propeller Sizing

A wooden propeller reinforced with composite fiber will be selected for cost-effectiveness. Another benefit is the lighter weight of the wooden-composite combination compared to an all-metal propeller. The propellers pitch will be fixed for simplicity. For propeller sizing, Table 5.2 in Roskam was used to narrow down the number of blades and diameter required. A fixed-pitch 2-blade propeller with 5.5 ft diameter was selected. The pitch-to-diameter ratio determines the climb, speed, and acceleration performance. A value of less than 0.5 allows an excellent climb and acceleration, but low top speed [21]. A value between 0.5 and 0.8 is optimal for a good climb, speed, and acceleration [21]. A value higher than 0.8 results in poor acceleration and climb, but excellent top speed. Thus, a pitch of 52 in. was selected, which gives a 0.8 pitch-to-diameter ratio. Next, the rpm required for a cruise speed of 125 mph using an 80 HP engine was estimated using a propeller sizing calculator [22]. The propeller will need to operate at 3000 rpm.

## 3.5 DISCUSSION, CONCLUSION, AND RECOMMENDATIONS

The constraints were calculated using equations from Roskam and plotted on power versus wing loading graph. The takeoff distance of 500 ft was specified by mission requirements, and was used to determine the takeoff  $C_{Lmax}$  of 1.2. Next, the takeoff and clean wing  $C_{Lmax}$  were used to determine the stall speed for both conditions. The stall speed for a clean wing is at 80 ft/s and 68 ft/s with flaps, both meet the FAR 23 stall requirement. Then, the landing distance of 500 ft was used to solve for the landing  $C_{Lmax}$  of 2.1. FAR 23 requires a climb rate of 5 fps and a minimum climb gradient for aircraft in the normal category. Zoom41 has a climb rate of 20 fps and meets the climb gradient requirement with clean wings. Finally, the speed constraints were plotted according to the desired climb, cruise, and loiter speeds. These curves determine the design envelope that the Zoom41 was sized to. They were cross-checked with the results from the AAA program and showed little variation. The critical requirements for Zoom41 are the takeoff stall speed and takeoff distance. Another design point was considered but was rejected due to the increase in drag and weight of the design. The final design point with a power loading of 10 lb/HP and wing loading of 6.7 lb/ft<sup>2</sup> was selected.

The propulsion system was selected as specified in the mission requirements. Zoom41 will be equipped with one 80 HP electric engine powered by Lithium-ion batteries. The propeller will be 5.5 ft in diameter, 52 in pitch, and operated at 3000 rpm.

It would be beneficial to look into designing an engine that is optimized for Zoom41's mission. A variable pitch propeller designed to synergize with this engine will also provide the highest efficiency for future prototypes. Alternative batteries, such as the lithium-oxygen battery, that have a higher energy density and made from sustainable materials should be considered. Although the lithium-oxygen batteries have poor recharge capability, it is worth reinvestigating this option in the future when technological advances have been made.

## **4.0 CONFIGURATION DESIGN**

### **4.1 COMPARATIVE STUDY**

In this section, single-engine aircraft are used to study geometries, weights, and mission performance. The two tables below show these values for electric aircraft and non-electric STOL aircraft. The critical mission requirements, especially the short takeoff and landing distance, will be used to decide the configuration of Zoom41. The five electric airplanes shown below have similar missions designed to be a replacement for trainer aircraft but have desirable characteristics also required for the Zoom41. An average of 94 lb of battery weight and takeoff run is 466 ft.

**Table 4.1: Electric aircraft**

Aircraft	Alpha Electro	Virus SW	Sinus 912	Taurus Electro G2	Sun Flyer SF2
Source	Jane's [17] Pipistrel [23]	Jane's [17] Pipistrel [23]	Jane's [17] Pipistrel [23]	Pipistrel [23]	Jane's [17]
<b>Weights:</b>					
Mission Takeoff Gross Weight (lb)	1,212	1,322	992	1,212	1,900
Battery Weight (lb)	90	99	94	92.59	N/A
Empty Weight (lb)	771	637	626	558	1,460
<b>Design Mission Performance:</b>					
Takeoff Run (ft)	460	525	289	590	N/A
Takeoff Field Length (ft)	739	1,050	486	870	N/A
Rate of Climb (ft/min)	1,348	1,049	1,280	610.23	1,050
Service Ceiling (ft)	18,000	19,000	28,875	12,795	N/A
Max Speed (mph)	138	170.89	137	80.77	159
Cruise Speed (mph)	124	164	87.46	74.56	84
Range (mi)	93	738	978.66	varies	294
Landing Run (ft)	885	460	430	varies	N/A
Landing Field Length (ft)	1,510	755	885	varies	N/A
<b>Geometry:</b>					
Wing Area (ft <sup>2</sup> )	100	102.4	132	132.72	129
Wing Span (ft)	34.52	35.15	49.11	49.11	38
Wing Chord (ft)	N/A	N/A	N/A	N/A	N/A
Wing Aspect Ratio	11.9	12.1	18.3	18.6	11.2
Overall Length (ft)	21.33	21.17	21.33	23.85	21.5
Overall Height (ft)	6.75	6.75	5.98	4.63	6.75

All the electric aircraft in this sample have a T-tail, tricycle landing gear, and seats two. Both the Virus and Sinus have cowls on the wheels of the landing gear intended to reduce the drag. The Pipistrel's designs have a high-wing configuration, while the Sun Flyer has a mid-wing. Sun Flyer 2, Alpha Electro, Virus, and Sinus all have a tractor motor mounted on the nose. Meanwhile, the Taurus has a motor mounted on its T-tail.

The SF2 is the heaviest aircraft in the sample with a takeoff gross weight of 1,900 lb, and the Sinus the lightest with a gross weight under 1000 lb. However these aircraft in [Table 4.1](#) were designed to carry two passengers, so it can be assumed the weight of Zoom41 should be lighter in comparison. The battery weight is consistent, with an average of 93 lb, and can be used as a benchmark.

Takeoff run and speed are significant parameters that indicate the performance of the aircraft. Takeoff run ranges from 289 ft to 590 ft, which is similar to the 300 ft requirement set for Zoom41. The fastest aircraft is the Virus, with a cruise speed of 164 mph, significantly larger than the average cruise speed of 106 mph.

**Table 4.2: Single-engine STOL aircraft**

Aircraft	Zlin Z 242	AirLony Skylane	Zenith STOL CH 701	FLS Sprint 160	Maule MXT-7-180
<b>Source</b>	Jane's [17]	Jane's [17] Skylane [24]	Jane's [17] Zenith [25]	Jane's [17]	Jane's [17]
<b>Weights:</b>					
Mission Takeoff Gross Weight lb	2,138	992	1,100	2,050	2,500
Fuel Weight lb	N/A	133	120	180	438
Empty Weight lb	1,642	546	580	1,375	1,528
<b>Design Mission Performance:</b>					
Takeoff Run ft	689	278.9	50	660	300
Takeoff Field Length ft	1,477	721.8	N/A	N/A	703
Rate of Climb ft/min	1,082	1,574	1,100	1,000	1,000
Service Ceiling ft	15,740	18,044	15,000	10,000	4,570
Max Speed mph	146	150	95	161	N/A
Cruise Speed mph	141	130	85	145	138
Range mi	307	1,025	350	575	949
Landing Run ft	870	328	80	N/A	N/A
Landing Field Length ft	1,695	918.6	N/A	N/A	500
<b>Geometry:</b>					
Wing Area ft <sup>2</sup>	149.2	113.8	122	120	165.6
Wing Span ft	30.6	29.4	27	30.7	32.9
Wing Chord ft	4.9	5.9	4.8	4.6	5.3
Wing Aspect Ratio	6.3	N/A	N/A	7.9	6.5
Overall Length ft	22.8	21.8	20.9	22	23.7
Overall Height ft	9.7	6.5	8.6	7.8	8.3

The five aircraft, Zlin, Skylane, Zenith, Sprint, and Maule that can be seen in [Table 4.2](#) have similar configurations. All are land-based aircraft with a conventional wing and tail, most likely for simplicity of design. Three of the presented aircraft have a high wing supported by struts, which typically reduces the wing weight, and shortens the nose landing gear. An interesting feature of the Zlin and Skylane is the cowl, intended to reduce drag, on each wheel of the landing gear. The propeller-driven engines are buried in the nose to reduce drag, which suggests that they are all tractor engines instead of pusher engines.

Maule is the heaviest at 2,500 lb and can carry up to 4 passengers and the pilot. Lightest of the five is the Skylane with a takeoff weight of 992 lb, and the Zenith has a similar weight. The discrepancies in the weights are due to the minimal number of passengers these aircraft were designed to transport and a mostly aluminum structure.

Maule, Skylane, and Zenith have a takeoff run under 300 ft, which is also the ideal distance for Zoom41. The Skylane, with 1,574 fpm, has the largest rate of climb when compared to the other four aircraft. In this study, cruise speed is between 85 mph and 145 mph with the Sprint taking the lead at 145 mph in this performance category. The lightest aircraft, Skylane, also has the largest range in this study. Although the weight and performance vary significantly between the five

aircraft, the geometries are nearly identical with the exception of wing area. Maule and Zlin have the largest wing areas, Skylane has the smallest wing area, while Sprint and Zenith have similar wing areas.

Features used for both electric and STOL aircraft will be used to select the configuration of Zoom41. In both categories of planes, the majority have a high wing configuration, tricycle landing gear, and tractor engine/motor. It's understood that the single electric motor can provide sufficient power for a comparable speed to an engine that burns fossil fuel. A significant difference is in the wing geometry, the electric aircraft typically has a smaller wing area, but a larger wingspan and aspect ratio compared to the fossil fuel burning STOL aircraft.

## 4.2 ZOOM41 CONFIGURATION SELECTION

### 4.2.1 Overall Configuration

Zoom41 will be a land-based single-seat monoplane aircraft. The design configuration focuses on simplicity and will have a T-tail, high wing, fixed tricycle landing gear, and a buried electric motor. This selection is further explained in the following sections.

### 4.2.2 Wing Configuration

A high wing supported with negligible sweep will be used to provide a simple, lightweight, and stable aircraft solution. It will also allow the passenger to board and unload quickly. This is safer than the other wing configurations because the damage and fire risks are lower during a forced landing. Although it limits visibility in most aircraft, the Zoom41 is autonomous and will not require a 360-degree view to operate. However, there is a possibility of the aircraft being too stable in roll, which must be considered in the stability and controls analysis.

### 4.2.3 Empennage Configuration

A T-tail design will allow the tail to avoid prop wash from the engine and downwash from the wing. It will provide reliable spin recovery due to the rudder clearance. Also, a T-tail configuration for a single-engine propeller aircraft will cause a pitch up moment due to prop wash hitting the vertical stabilizer. This may aid in balancing the pitch down moment from the high wing configuration. V-tail was considered but was not used because it is more difficult to manufacture and maintain.

### 4.2.4 Integration of the Propulsion System

A single propeller-driven tractor electric motor will be used for the propulsive system, buried in the nose of the fuselage for a more aerodynamic configuration. A buried tractor will also protect the engine from any environmental hazards during flight. However, a malfunction in the engine

can put the passenger in danger, but the Zoom41 will use a firewall to minimize damages caused by catastrophic engine failure.

A tractor has a higher noise level inside the cabin compared to a pusher, but an electric engine will dampen the noise produced and be more environmentally friendly. A hybrid propulsion system was considered, to aid with the multiple takeoffs and landings, but was not implemented due to the complexity it would add to the design.

#### 4.2.5 Landing Gear Arrangement

Fuselage-mounted fixed tricycle landing gear with one tire on each strut will be implemented. Cowls on the landing gear wheels will be considered for a more aerodynamic design. Although a non-retractable gear will add drag and require a heavy nose gear, the benefit of added stability, a level fuselage, and a reduced drag during initial takeoff outweighs the negative characteristics. Retractable landing gear was not used because it also increases the acquisition and maintenance cost.

### 4.3 REFERENCES

- [1] Jane's by IHS Markit. (n.d.). Retrieved from <https://janes-ihc-com.libaccess.sjlibrary.org/>
- [2] Pipistrel-aircraft.com. (2019). *Pipistrel – Pipistrel official web page*. [online] Available at: <https://www.pipistrel-aircraft.com/>
- [3] SKYLANE - pilots operating handbook EN SE-VUB version 2.3. (n.d.). Retrieved September 11, 2018, from [http://www.kopingsfk.se/wp-content/uploads/2016/06/SKYLANE-pilots-operating-handbook\\_EN-SE-VUB-version-2.3.pdf](http://www.kopingsfk.se/wp-content/uploads/2016/06/SKYLANE-pilots-operating-handbook_EN-SE-VUB-version-2.3.pdf)
- [4] STOL CH 701 Performance and Specifications: Real Short Take Off and Landing performance. (n.d.). Retrieved September 11, 2018, from <http://www.zenithair.com/stolch701/7-perf.html>

## **5.0 FUSELAGE DESIGN**

In *Chapter 5: Fuselage Design*, the fuselage, and its components will be modeled. Cockpit and fuselage layout will be designed. Similar aircraft are compared to aid in the dimensioning of the fuselage. A 3-view of the final fuselage design and its major features will be presented.

### **5.1 LAYOUT DESIGN OF COCKPIT**

The Zoom41 is an autonomous aircraft and will not need a pilot nor a cockpit. However, there will be a compartment behind the passenger for the batteries, navigation system and other electronics to be stored. These electronics will be easily accessed through the panel located on the side of the aircraft.

### **5.2 LAYOUT DESIGN OF FUSELAGE**

The fuselage design is a combination of the designs previously used for single-passenger aircraft. Pipistrel's Alpha Electro was a major influence for Zoom41's design. A drawing of the Alpha Electro, a two-passenger aircraft, is shown below. Note that the dimensions are in millimeters. The fuselage width is 3.7 ft and height is 7 ft when including the landing gear. Length of the fuselage is 21 ft.

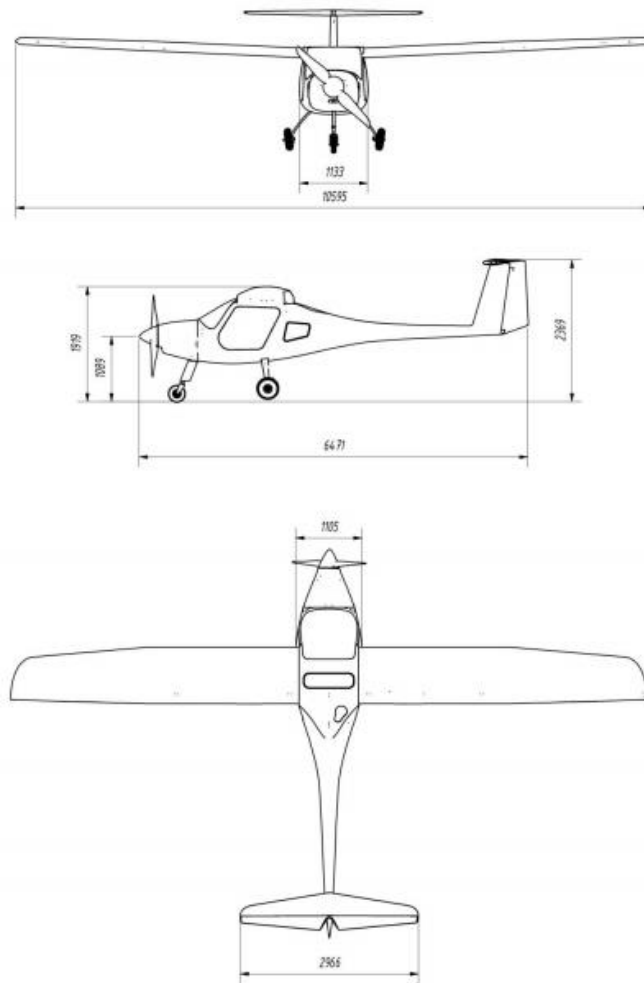


**Figure 5.1: Alpha Electro drawing [18]**

Zoom41 will include a compact and comfortable seating arrangement for the passenger with room to stow luggage underneath the seat. A firewall will be installed to protect the passenger in case of engine failure. Circular formers were used to achieve the profile of the fuselage as shown by the sketch in [Figure 5.2](#). Largest section of the fuselage, the passenger compartment, will have a radius of 3 ft. It was determined that a fuselage diameter smaller than the Alpha Electro will suffice because the Zoom41 will only carry one passenger.

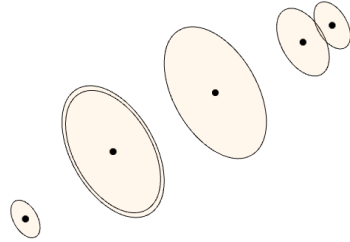


**Figure 5.2: Sketch of fuselage formers**

The typical passenger seat pitch is less than 2.5 ft and 1.46 ft seat width according to the information presented in [Figure 5.3](#). In order to make the Zoom41 comfortable for all passengers, the length of the compartment will be 3.5 ft with a seat width of 1.8 ft.

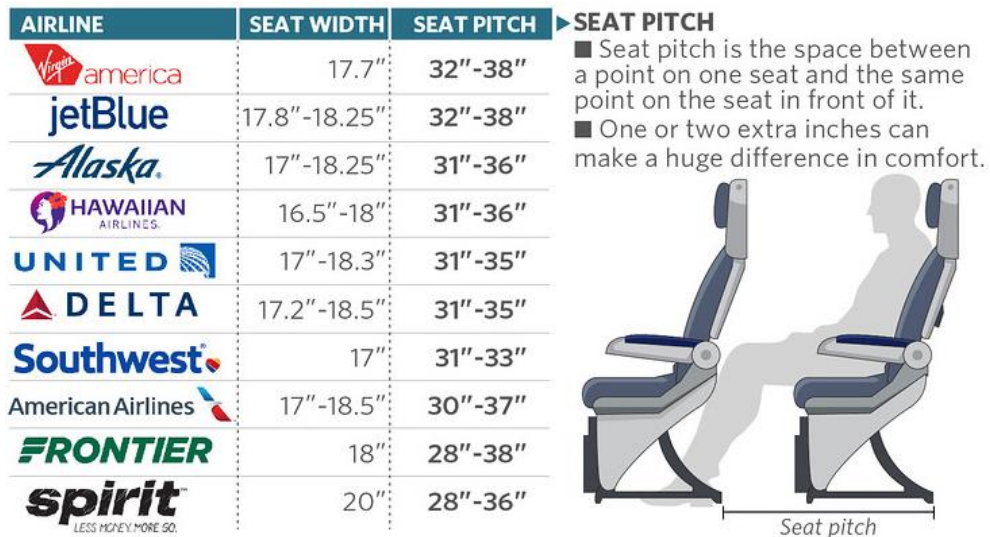


**Figure 5.3: Seat pitch [26]**

Additional length for the tail was allowed to avoid downwash from the wing and propeller. Alpha Electro's tail is 11 ft away from the end of the fuselage. Allowing an arbitrary 3.5 ft in front and behind the passenger compartment for the engine and electronics puts the total length of the Zoom41 at 21 ft, which matches the length of Alpha Electro. Below are multiple views of the current design.



**Figure 5.4: Front-view, top-view, side-view, and isometric view of the fuselage**



**Figure 5.5: Front and back view of the fuselage**

In the following cutaway of the aircraft shown in [Figure 5.6](#), the passenger seating, engine placement, and electronics compartments can be seen. There is room under the seat for the passenger to stow a piece of small carryon luggage. The cargo volume of 1.1 ft<sup>3</sup> was calculated and meets the requirements described in the mission specification.

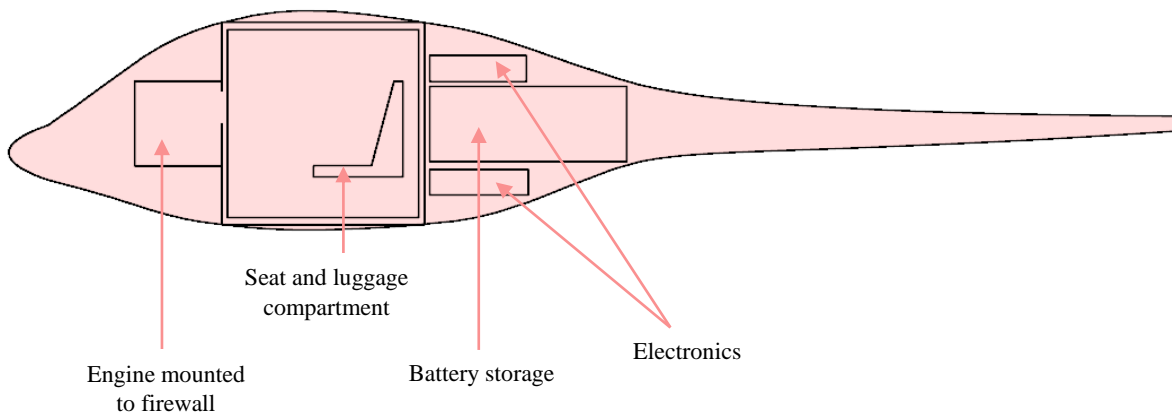


**Figure 5.6: Interior arrangement**

### 5.3 CONCLUSION, DISCUSSION, AND RECOMMENDATIONS

Zoom41’s fuselage design offers the passenger both comfort and safety. Passenger seat size and luggage storage exceed what is offered in the current market. A volume of 4.5 ft<sup>3</sup> is available for electronics and battery storage. The fuselage also allows room for ballast and/or any additional equipment to be placed in front of or behind the passenger compartment. A drawing of the fuselage is seen in Figure 5.7.

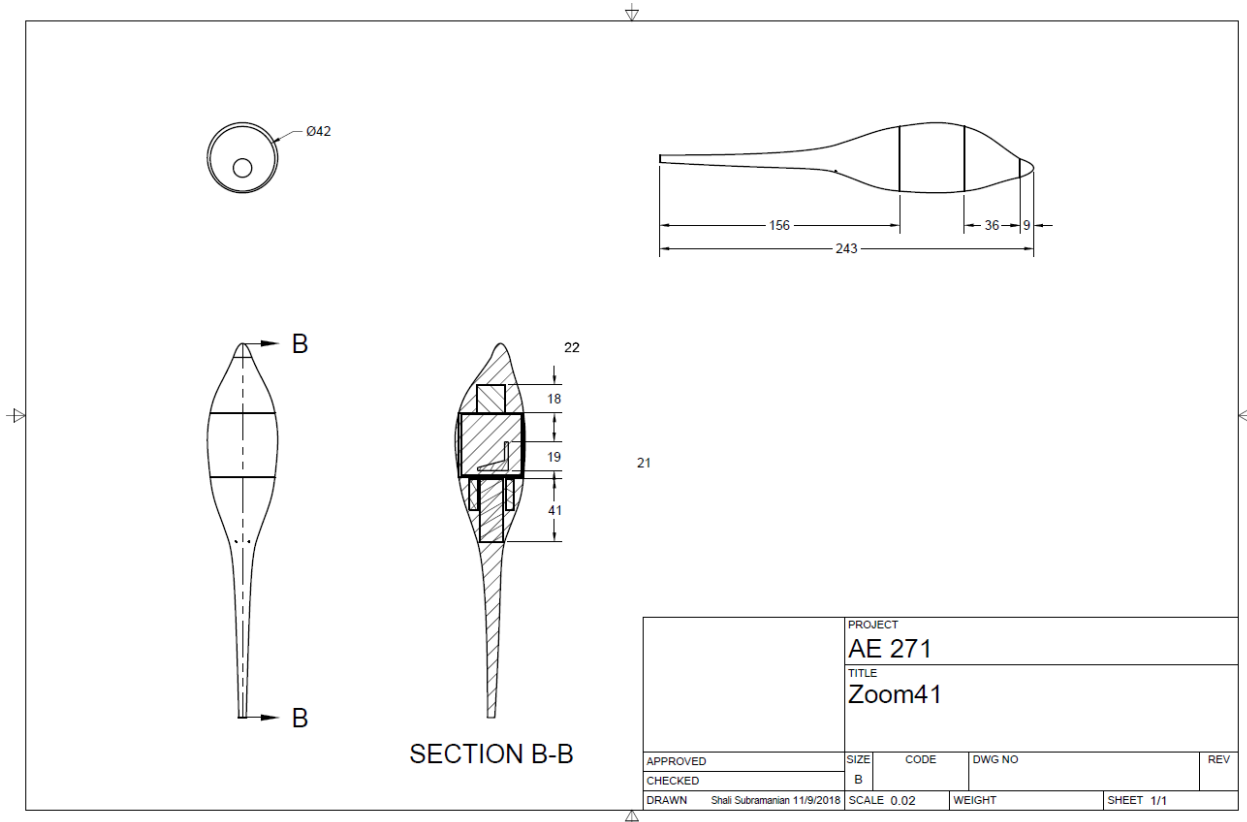


**Figure 5.7: Dimensions of current design (inches)**

## 6.0 WING AND LATERAL CONTROLS DESIGN

This chapter will explore the planform wing design, airfoil selection, and control surface design decisions. The airfoil NLF-0416 characteristics will be studied using XFLR5 simulation and available experimental wind tunnel data. Calculated 3D wing design values will be entered in XFLR to further analyze the design. Control surfaces will be designed to assure the aircraft meets aerodynamic requirements. A drawing encompassing all design features will be presented at the end of the report.

### 6.1 WING PLANFORM DESIGN

Taper ratio and dihedral will be selected in this section. Taper ratio can be used to reduce the weight of the wing structure, reduce bending moment, increase the volume inside the wing, and provide a thicker wing root. A taper ratio of 0.45 produces a lift distribution that is close to the elliptical ideal and will be used for the Zoom41 [27].

The taper ratio can be used to calculate the chord length for wing root and tip. From Chapter 4, the determined wing area of 120 ft<sup>2</sup> and an aspect ratio of 18 will be used for calculations. Utilized equation 6.1 and equation 6.2 to calculate the root chord length of 3.56 ft and wingtip chord length of 1.6 ft.

$$C_{root} = \frac{2*S}{b*(1+\lambda)} \quad 6.1$$

$$C_{tip} = \lambda * C_{root} \quad 6.2$$

The dihedral angle contributes to roll stability. A dihedral effect is already in play for a high-mounted wing and additional dihedral could put the aircraft in a “Dutch roll” mode [27]. Dihedral will be set at 0 degrees for Zoom41 to avoid this problem. Most aircraft in the homebuilt and single-engine category in Roskam also have close to 0 degrees of dihedral. Guidelines provided from Raymer shown in [Figure 6.1](#) also confirm dihedral selection for Zoom41 is valid. Further stability and control analysis may require a negative dihedral to counteract the roll stability provided by the high wing.

	Wing position		
	Low	Mid	High
Unswept (civil)	5 to 7	2 to 4	0 to 2
Subsonic swept wing	3 to 7	-2 to 2	-5 to -2
Supersonic swept wing	0 to 5	-5 to 0	-5 to 0

**Figure 6.1: Dihedral guidelines [27]**

## 6.2 SWEEP ANGLE – THICKNESS RATIO

Sweep is required to prevent wave drag in supersonic flow. In subsonic flow, sweep reduces lift and can contribute to the wing root stalling before the wingtip. The Zoom41 will fly at subsonic speeds, so it will not require leading-edge sweep.

The thickness of the airfoil affects multiple variables such as the type of stall. Three types of stall are illustrated in [Figure 6.2](#). A thicker airfoil with a  $t/c$  greater than 15% stalls from the trailing edge, and has a smooth and continuous increase in separation with angle-of-attack [28]. If the separation begins at the leading edge, then the separation is more abrupt and discontinuous [28]. Although adding a twist and leading-edge devices to the airfoil can aid in eliminating violent stall characteristics of thin airfoils, it would be simpler, safer and more cost-effective to increase the thickness of the airfoil instead. A wing with a large aspect ratio, such as the Zoom41, can benefit from a thicker airfoil because it will produce an increase in maximum lift coefficient and stall angle [27]. The weight varies inversely with the square root of the thickness ratio, which is an additional benefit of thicker airfoils [27].

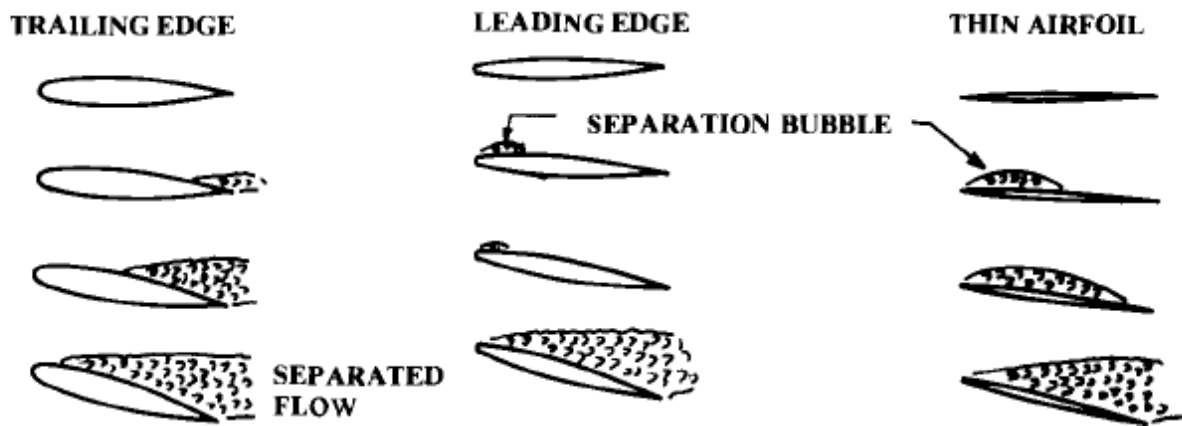


Figure 6.2: Flow separation on varying thickness [27]

Figures below illustrate the relationship between thickness,  $C_{l, \max}$ , and  $C_d$ . As thickness increases the airfoil is able to produce more lift, achieve higher angles of attack, and stall more gradually. The shortcoming of a thick airfoil is the increase in drag.

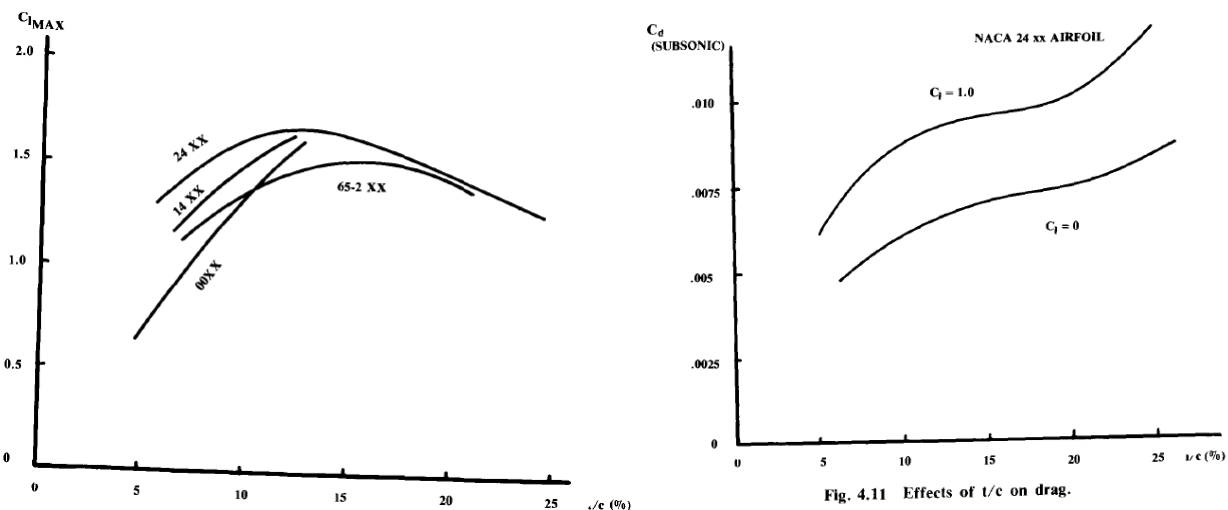


Figure 6.3: Effect of thickness on  $C_l$  and  $C_d$  [27]

Historically the range of thickness ratio is between 12% and 18% for design Mach numbers below 1.0 as seen in Figure 6.4. The Zoom41 will be flying at 0.16 Mach and its thickness ratio should fall in between this historical range. An airfoil thickness ratio of 0.16 was selected for the Zoom41 after considering the properties of thicker airfoils and historical trends.

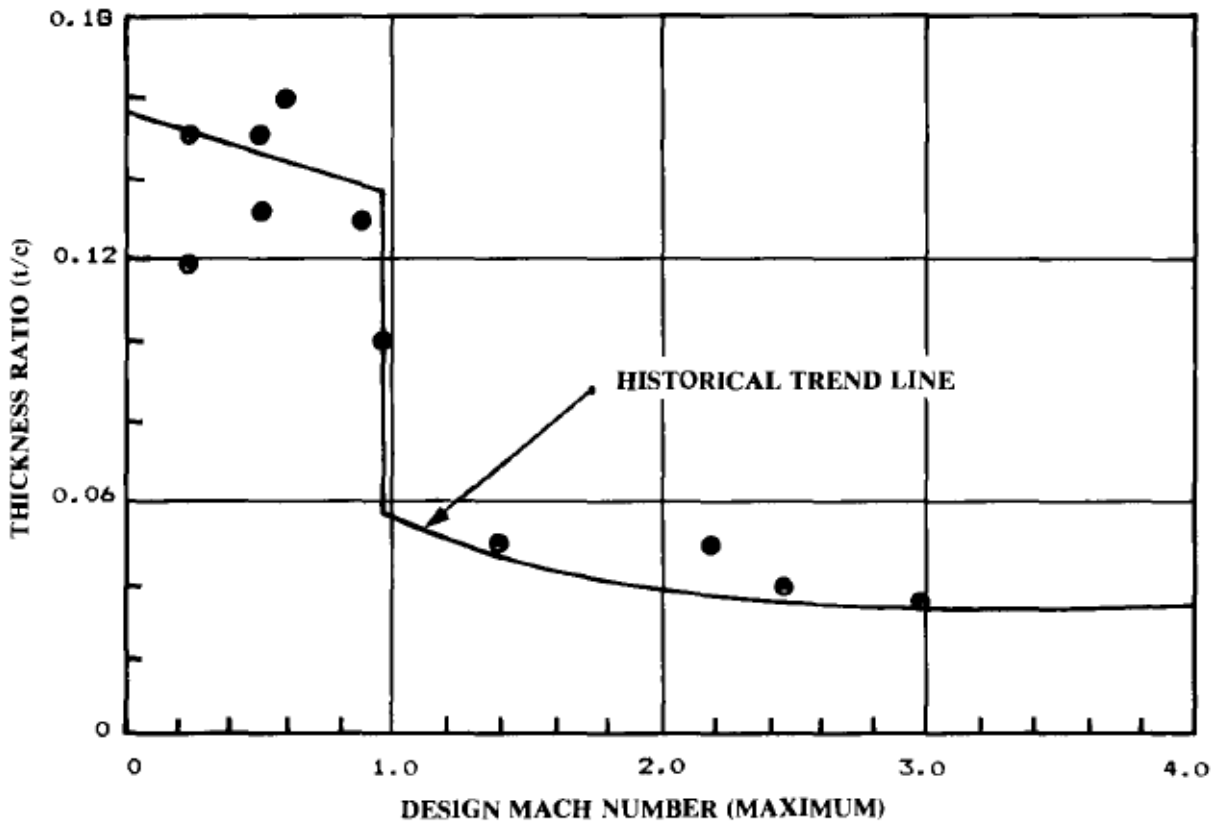


Figure 6.4: Thickness ratio and Mach number [27]

### 6.3 AIRFOIL SELECTION

Multiple airfoil designs were considered for the Zoom41. Only airfoils with experimental data available were included in the selection process to ensure that the stall characteristics can be assessed. Also, selecting an existing airfoil eliminates research and development costs. Natural-laminar-flow airfoils are good candidates for the Zoom41 because NASA succeeded in incorporating the low-drag characteristics of the NACA 6-series airfoils with the high-lift characteristics of NASA's low-speed airfoils [29]. The NLF (1)-0416 airfoil designed for general aviation applications was selected for Zoom41 wing root and chord. The profile of the selected airfoil is shown in the figure below. It is the only airfoil in the NLF series which provides the desired thickness and coefficient of lift. The maximum thickness of 16% occurs at 30% chord and maximum camber at 35% chord [30].

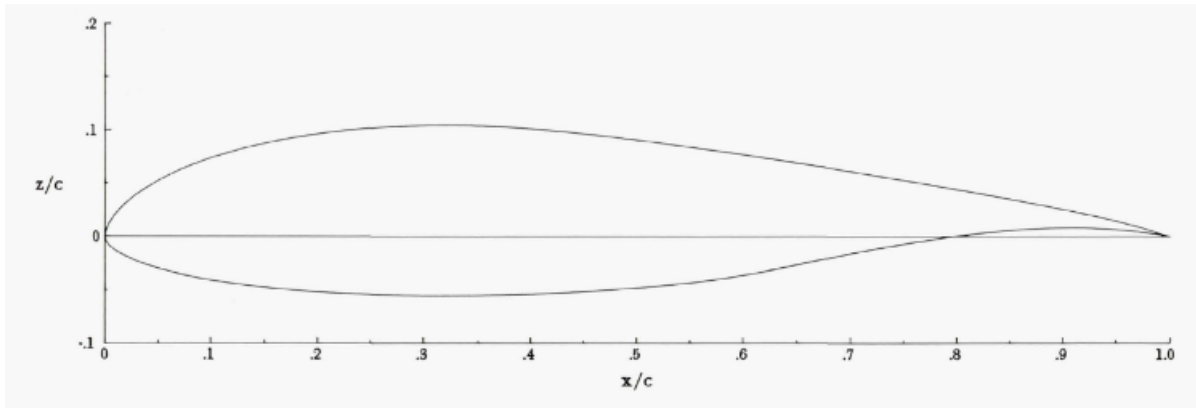


Figure 6.5: Profile of NLF 0416 [30]

### 6.3.1 Reynold's Number

Calculating Reynold's number for operating conditions is a crucial step in assessing the selecting an airfoil. The behavior of airfoil changes with Reynold's number, so it is necessary to evaluate the airfoil for the conditions it will experience during Zoom41's mission.

$$Re = \frac{\rho V l}{\mu} \quad 6.3$$

Equation 6.3 was used to calculate Reynold's number at Zoom41's flight conditions displayed in [Table 6.1](#). The average density for a climb between 0 ft and 1500 ft was used.

Table 6.1: Reynold's number

Phase	Altitude (ft)	Density (slugs/ft <sup>3</sup> )	Dynamic viscosity for air (lb*s/ft <sup>2</sup> )	Velocity (ft/s)	Chord width (16% of chord, ft)	Calculated Reynold's Number
Climb root	0	0.002325	0.3736x10 <sup>-6</sup>	80	0.576	286,810
Climb tip	0	0.002325	0.3736x10 <sup>-6</sup>	80	0.2592	129,064
Cruise root	1,500	0.002274	0.5684x10 <sup>-6</sup>	183	0.576	421,706
Cruise tip	1,500	0.002274	0.5684x10 <sup>-6</sup>	183	0.2592	189,768

Climb and cruise conditions were used as benchmarks for the low and high-speed ranges of the Zoom41 mission. It is seen that the lowest Reynold's number of 130, 000 is experienced at the tip during the climb phase, and highest is at 420, 000 at the root during the cruise phase. These parameters will be used to further analyze the properties of the NLF-0416 airfoil.

## 6.3.2 Airfoil Properties

### 6.3.2.1 Theoretical Results

XFLR5 was used to generate the following graphs at the design cruise Mach number of 0.164 for inviscid flow. The  $C_{l,max}$  increases as Reynold's number increases. A  $C_{l,max}$  of 1.52 at 12.5 degrees of AOA at Reynold's number of 425,000 can be seen in [Figure 6.6](#). Zero lift occurs at an AOA of -3.8 degrees. Lift at zero degrees AOA is 0.42. The stall characteristics cannot be predicted using this software.

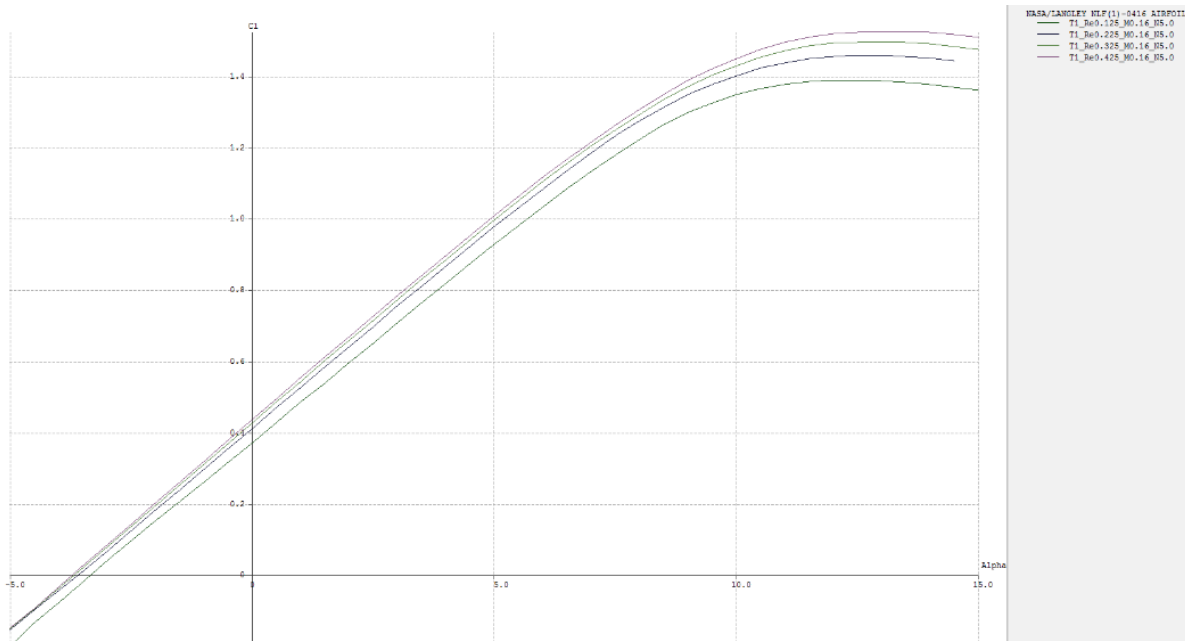


**Figure 6.6: Theoretical lift-curve**

Drag polar was plotted next. The best L/D is at approximately  $C_l$  of 1.31 and  $C_d$  of 0.015. The variation of the drag coefficient is minimal and will not be a major issue for Zoom41.

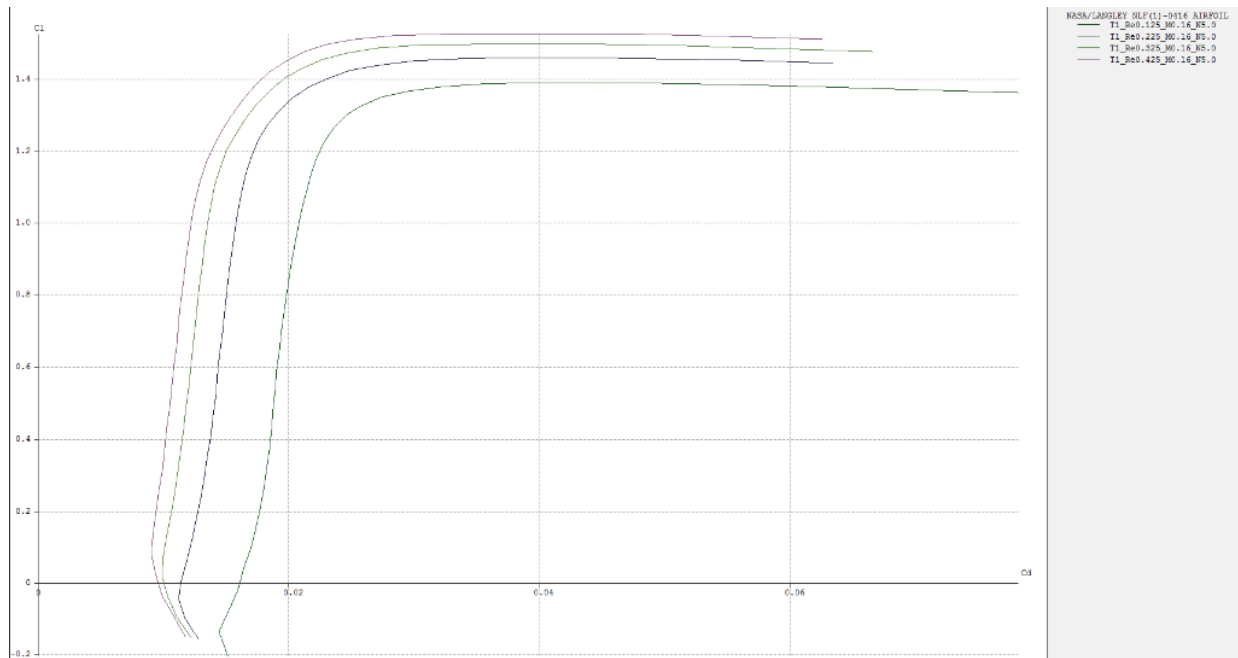


**Figure 6.7: Theoretical drag polar**

### 6.3.2.2 Experimental Results

Experimental data closely matches XFLR5 analysis. The curves in [Figure 6.8](#) are from wind tunnel tests completed by NASA. They present the lift, drag, and pitching moment coefficients at Mach 0.1 for Reynold's numbers between 100,000, and 300,000. At Reynold's number of 100,000 the airfoil is capable of providing a  $C_{l, \max}$  of approximately 1.6 at 12 degrees AOA. This meets the required  $C_l$  determined in [Chapter 4: Performance Sizing](#) for the climb and cruise phases of flight. At zero lift the AOA lies at approximately -3.8 degrees. A lift of 0.42 is produced at zero degrees AOA. The pitching moment lies at -0.09 at zero lift.

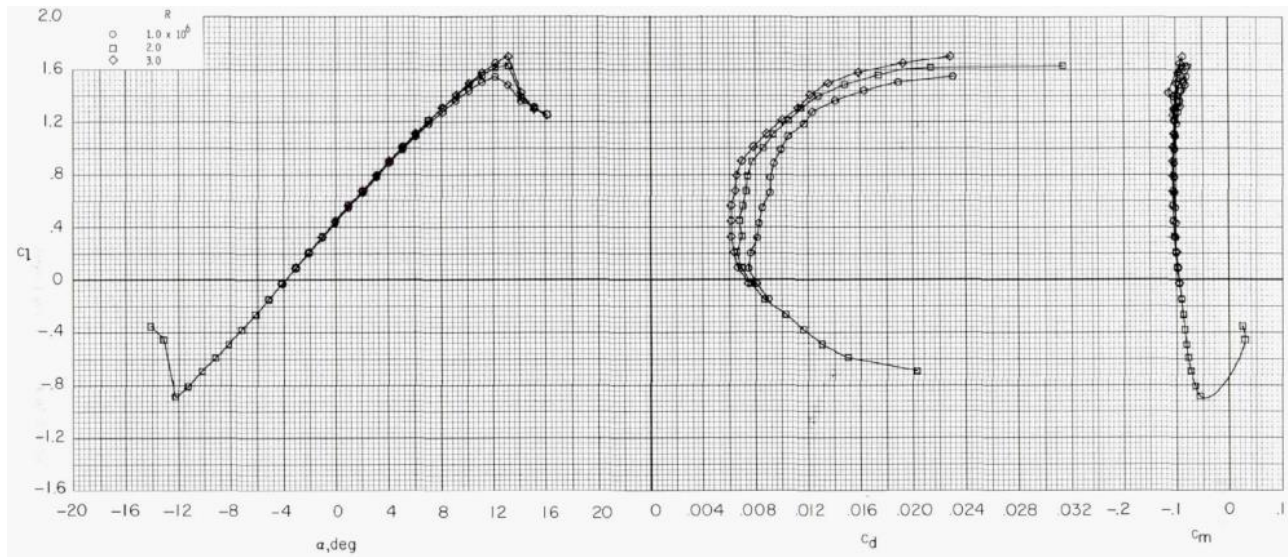


**Figure 6.8: Effect of Re on NLF-0416 [31]**

Experimental data also shows the gentle stall characteristics of this airfoil at low Reynold's numbers. Although a large increase in Reynold's number sharpens the lift curve peak and stall becomes more sudden. There is a steady decrease in drag as Reynold's number and lift coefficient increases. The pitching moment coefficient is insensitive to Reynold's number.

The pressure distribution over the airfoil at Reynold's number of 400,000, Mach 0.1, and AOA of 12 degrees is shown in Figure 6.9. Upper surface pressure decreases rapidly from the stagnation point, then gradually rises at the given angle of attack. This is typical for an airfoil with camber at a high AOA.

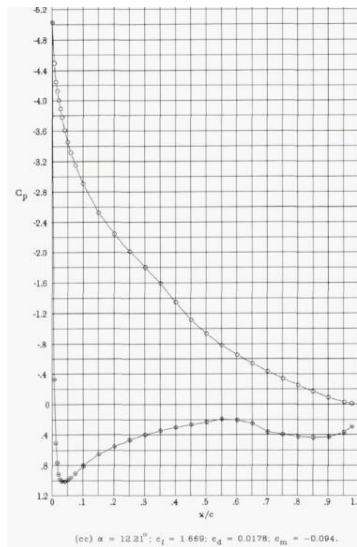


**Figure 6.9: Pressure distribution at  $\alpha = 12$  deg [31]**

## 6.4 AERODYNAMIC TWIST AND INCIDENCE ANGLE

The aerodynamic twist can be used to prevent stall at the wingtips and provide an elliptical lift distribution. A geometric twist angle of four degrees will be used as confirmed by historical data in Roskam and suggested by Raymer. The incidence angle is selected to minimize drag at cruise and will vary from root to tip if the wing is twisted. Incidence angle for aircraft in this category is approximately two degrees while historical data in Roskam presents aircraft with an incidence of up to four degrees. Zoom41 incidence angle will be set at two degrees.

## 6.5 WING DESIGN EVALUATION

### 6.5.1 AAA Wing Geometry Evaluation

AAA was used to reproduce the geometry of the wing as shown in [Figure 6.10](#). A root chord of 3.56 ft and tip chord of 1.60 ft matches hand calculations. It also provides the MAC of 2.71 ft and the location of the MGC.

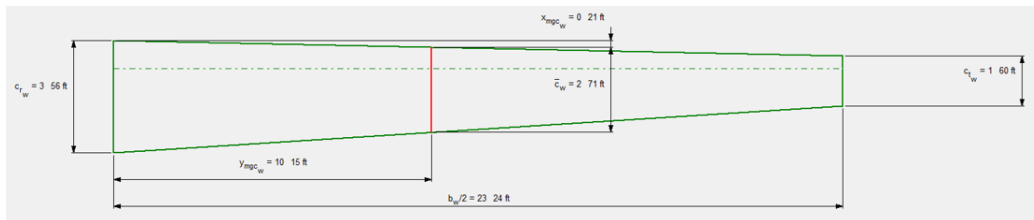


Figure 6.10: AAA Wing Geometry

### 6.5.2 XFLR5 Wing Evaluation

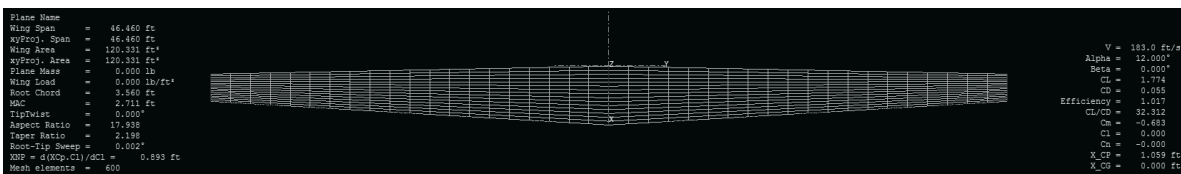
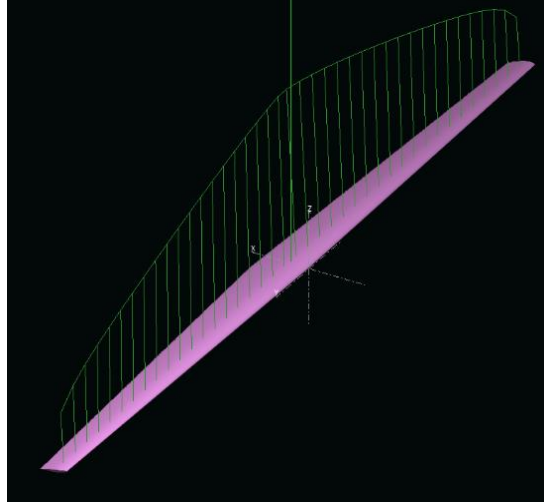


Figure 6.11: Wing geometry

The geometry of the wing was used to create a 3D model of the clean wing in XFLR5 and analysis was completed to retrieve an estimate of the aerodynamic characteristics. The figure above confirms that the mean aerodynamic chord of 2.71 ft calculated by AAA. Analysis at Mach 0.164 showed the  $C_L$  generated at 12 degrees AOA will be 1.77. A  $C_L/C_D$  of 32 is expected at these conditions. The nearly elliptical lift distribution across the tapered wing is shown in [Figure 6.12](#).



**Figure 6.12: Lift distribution**

The following set of figures illustrate the properties of the 3D wing at Reynold's number of 425,000 and Mach 0.16. A  $C_l$  of 0.62 is produced at 0 degrees AOA. An angle of -6.6 degrees is the point where 0 lift is produced. A downward sloping pitching moment graph confirms that the wing is statically stable and is expected to have a positive static margin. A drag of 0.025 occurs at a  $C_l$  of 1.2.

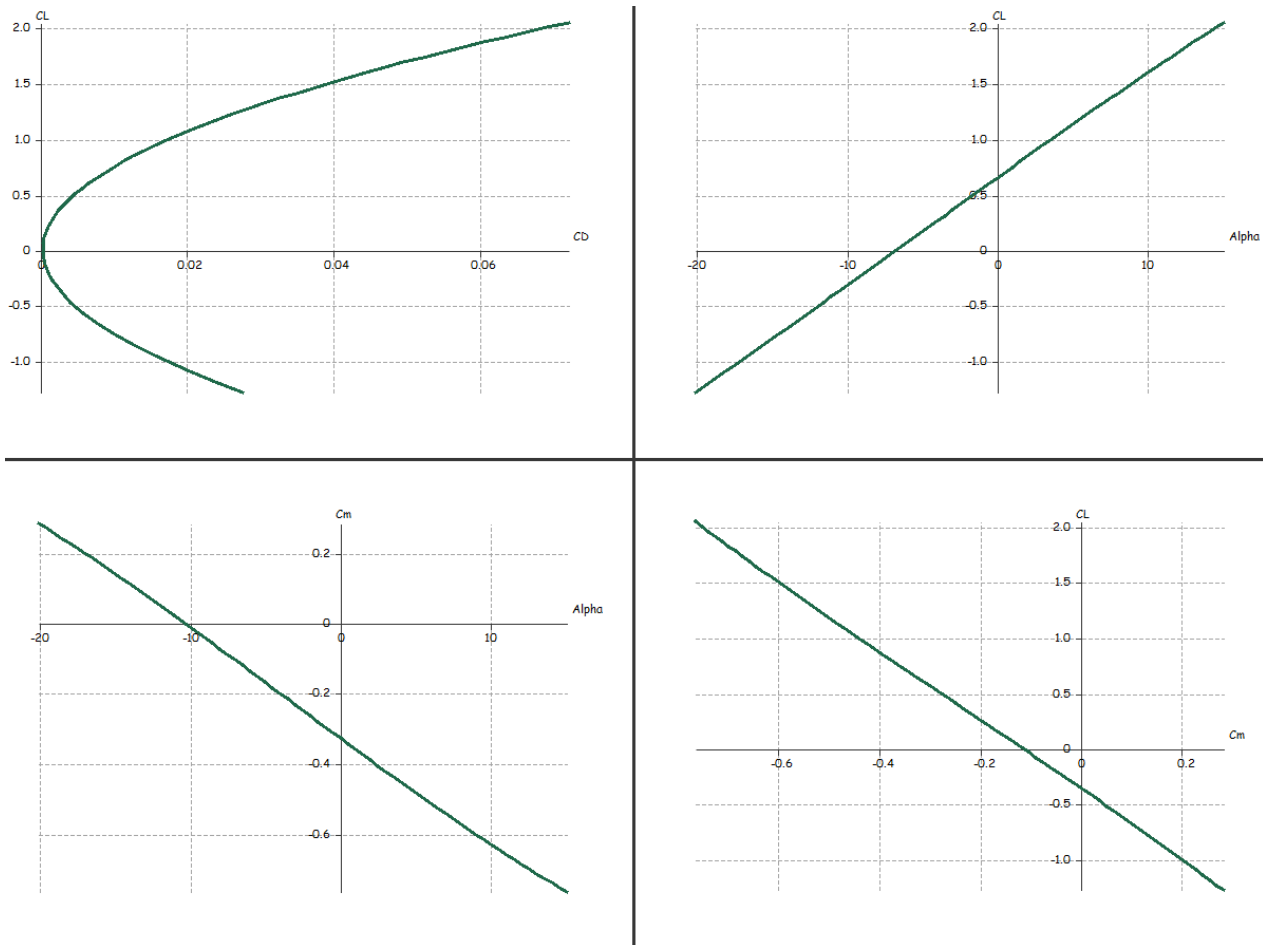


**Figure 6.13: XFLR5 wing analysis**

## 6.6 LATERAL CONTROL SURFACE SIZING

*Chapter 4: Performance Sizing* determined that a  $C_L$  of 2.2 is required for landing, 1.2 for takeoff and 0.87 for a clean wing. This section will evaluate whether the Zoom41’s current wing design will meet these conditions and if control surfaces will be required. The method presented in Roskam Part II will be used for this evaluation. Equation 6.4 defines the relationship used to determine the aircraft type [19]. Distance between the tail and wing of 11 ft was divided by the mean aerodynamic chord of 2.71 ft to produce a value of 4.05. The Zoom41 is a long-coupled aircraft. The wing’s required  $C_L$  will be multiplied by a factor of 1.1 to account for the “tail down-load to trim,” which gives a new  $C_{L, \max}$  requirement of 0.96 [19].

$$l_h/\bar{c} < 3.0, \text{ short - coupled}$$

6.4

$$l_h/\bar{c} > 5.0, \text{ long - coupled}$$

The following approximation can be used to confirm the wing's capability of producing the necessary  $C_{L, \max}$ . Reynold's numbers at the root and tip shown in [Table 6.1](#) were used to approximate  $C_l$ . From XFLR5 analysis, at Mach 0.16, Reynold's number of 200,000 produces a  $C_{l, \max}$  of 1.45 and  $C_{l, \max}$  of 1.52 at 425,000.

$$C_{L, \max, w} = \frac{k_\lambda(C_{l, \max, root} + C_{l, \max, tip})}{2} = \frac{0.95(1.45 + 1.52)}{2} = 1.4 \quad 6.5$$

This confirms that the wing is able to produce lift within 5 percent of the required clean wing  $C_L$  of 0.96 and the takeoff  $C_L$  of 1.2. Notice that this maximum  $C_L$  prediction is lower than the one from XFLR5. This discrepancy may be due to the fact that equation 6.5 does not take into account the wing twist [19].

Flaps will need to be designed because there is an insufficient lift to meet the landing distance requirement. The calculation for the incremental value of maximum lift coefficient for landing is shown below [19].

$$\Delta C_{L, \max, L} = 1.05(C_{L, \max, L} - C_{L, \max}) = 1.05(2.2 - 1.95) = 0.27 \quad 6.6$$

An additional  $C_L$  of 0.27 must be produced by high lift devices. Single plain flaps will suffice since the  $\Delta C_L$  is not very high. Incremental section maximum lift coefficient with flaps down can be calculated using equation 6.7 and equation 6.8 [19].

$$\Delta C_{l, \max} = \Delta C_{L, \max} \left( \frac{S}{S_{wf}} \right) K_\Lambda \quad 6.7$$

$$K_\Lambda = (1 - 0.08 \cos^2 \Lambda_{c/4}) \cos^{3/4} \Lambda_{c/4} \quad 6.8$$

Zero sweep means that the sweep correction factor will be 0.92. Using an arbitrary value of 0.6 for  $S/S_{wf}$  gives a maximum  $\Delta C_l$  of 0.72. Next, the  $\Delta C_l$  for single plain flaps can be computed using equation 6.9 [19].

$$\Delta C_l = C_{l_{\delta_f}} * \delta_f * K' \quad 6.9$$

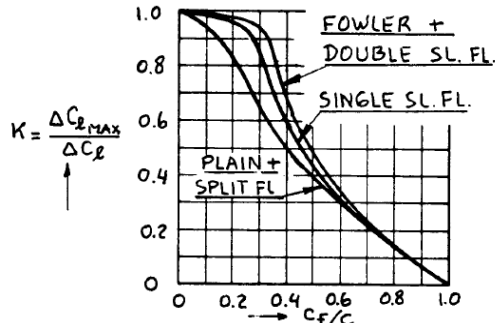


Figure 7.4 Effect of Flap Chord Ratio and Flap Type on  $K = \frac{\Delta C_{L_{max}}}{\Delta C_L}$

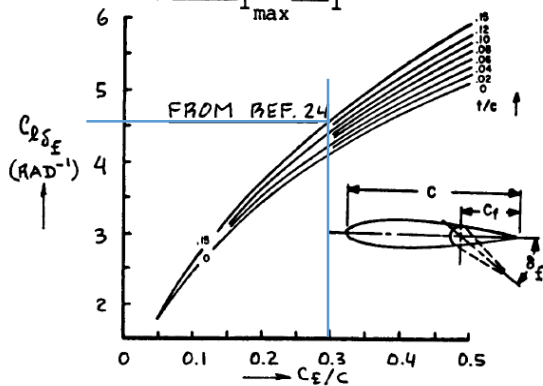
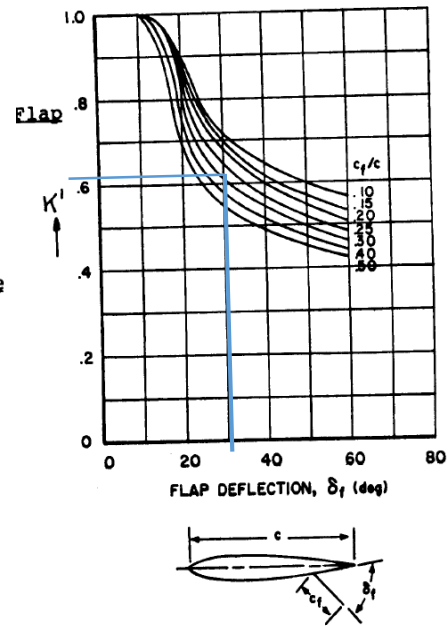


Figure 7.5 Effect of Thickness Ratio and Flap Chord Ratio on  $C_{L\delta_\epsilon}$

Figure 6.14: Flap chord and K [19]

The set of figures above were used to determine the values required for equation 6.9. For a flap chord ratio of 0.3 and flap deflection of 30 degrees, the  $K'$  value is approximately 0.61 and  $C_{L\delta_f}$  is 4.6. A  $\Delta C_L$  of 1.34 was derived. Table 6.2 summarizes the  $\Delta C_L$  for varying flap deflection angles and flap chord ratios.

Table 6.2: Flap deflection

$\delta_f$ (deg)	$K'$	$c_f/c$	$C_{L\delta_f}$ (rad <sup>-1</sup> )	$\Delta C_L$
20	0.78	0.3	4.6	1.14
30	0.61	0.3	4.6	1.34
40	0.55	0.3	4.6	1.61
20	0.86	0.2	3.8	1.14
30	0.68	0.2	3.8	1.35
40	0.62	0.2	3.8	1.64

It is seen that the varying flap chord ratio has little effect on  $\Delta C_L$ . On the other hand, varying flap deflection angle significantly impacts the  $\Delta C_L$ . Next, the spanwise flap stations need to be derived by the use of equation 6.10 [19]. Station  $i$  was determined by dividing the 46 ft wingspan by the 4 ft fuselage diameter, which results in a value of 0.086. With this, the station 0 was found to be located at 0.63.

$$\frac{S_{wf}}{S} = (\eta_o - \eta_i)\{2 - (1 - \lambda)(\eta_i + \eta_o)\}/(1 + \lambda) \quad 6.10$$

## 6.7 DRAWINGS

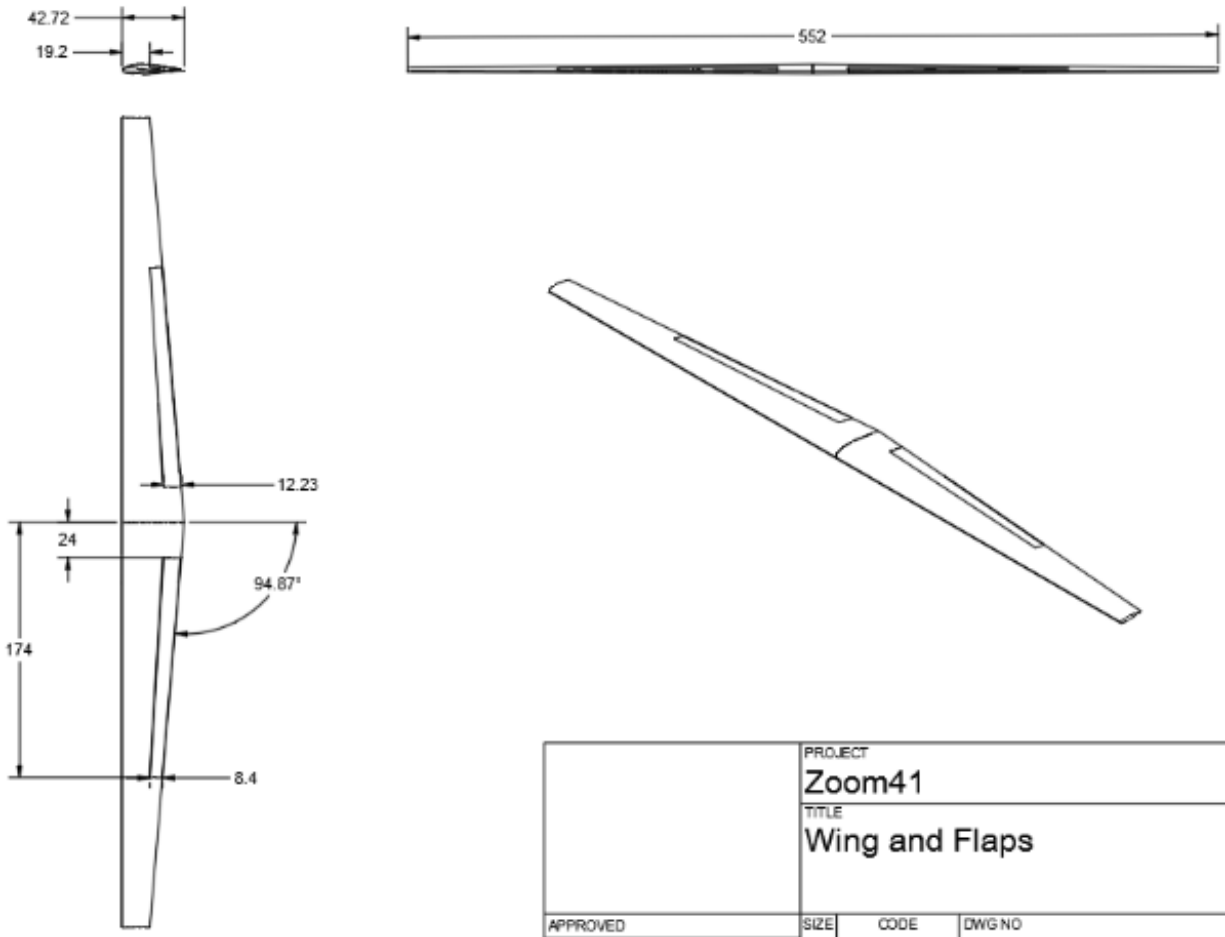


**Figure 6.15: Drawing of wing**

Figure 6.15 displays the overall dimensions of the wing in inches. Location of the flaps is also defined. Trailing edge sweep angle is 4.9 degrees. The wing volume was not calculated, because it will not be used to store batteries/fuel. Table 6.3 presents a summary of the calculated parameters.

**Table 6.3: Summary of wing parameters**

<b>Parameter</b>	<b>Value</b>
Airfoil for root and chord	NFL-0416
Wingspan	46 ft
Wing area	120 ft <sup>2</sup>
Root chord	3.6 ft
Tip chord	1.6 ft
MAC	2.7 ft
MGC	2.6 ft
LE sweep	0 deg
TE sweep	5 deg
MAC coordinates	(0, 10.2) ft
Flap station $\eta_i$	2 ft
$\eta_i$ station flap chord	1 ft
Flap station $\eta_o$	14.5 ft
$\eta_o$ station flap chord	0.7 ft

## 6.8 DISCUSSION, CONCLUSION, AND RECOMMENDATIONS

The wing planform design began by taking the wing area and aspect ratio from Chapter 4: Performance Sizing. Next, the sweep angle of 0 degrees was chosen due to the subsonic speed of Zoom41. The aerodynamic twist of 4 degrees, dihedral of 0 degrees, and incidence angle of 2 degrees were selected based on historical data. Although a range of thicknesses was explored, a thickness of 16% was determined the best fit for the speed and stall characteristics preferred for Zoom41.

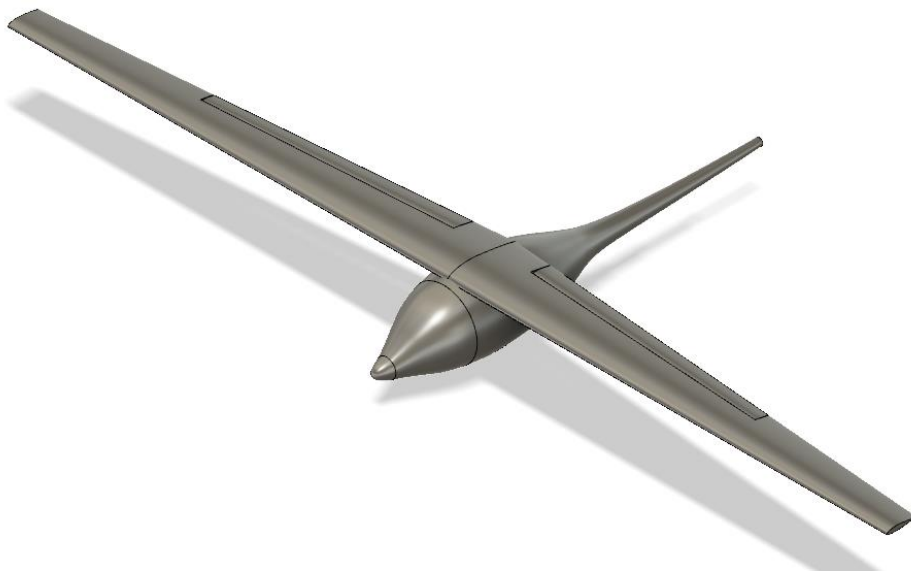


**Figure 6.16: Complete model to date**

The wing root and tip chords were calculated. Then, these values were used to determine Reynold's number for the root and tip. Using Reynold's numbers, an airfoil was selected by considering various aerodynamic characteristics. Both theoretical and experimental analysis was used to confirm the characteristics expected at Reynold's numbers that will be encountered during the mission. Lateral control surface geometry was calculated using the procedure presented in Roskam. Finally, the current 3D aircraft model was updated and is presented in Figure 6.16.

## 7.0 EMPENNAGE DESIGN

This section, *Chapter 7: Design of the Empennage and the Longitudinal and Directional Controls*, will review the overall empennage configuration and design for the Zoom41. The location of the horizontal stabilizer and vertical stabilizer will be established. Finally, the fully assembled empennage and the current version of the aircraft will be presented.

### 7.1 OVERALL EMPENNAGE DESIGN

A conventional T-tail configuration was selected in *Chapter 2*. This decision was made to avoid prop wash from the engine and downwash from the wing. It will allow for reliable spin recovery due to the rudder clearance. Also, a T-tail configuration for a single-engine propeller aircraft will cause a pitch up moment due to prop wash hitting the vertical stabilizer. This may aid in balancing the pitch down moment from the high wing configuration.

The location of the empennage must be positioned to allow for the greatest possible moment arm because it reduces the weight and area of the tail [19]. Raymer states that the tail arm should be located at approximately 65% of the fuselage length for a front-mounted engine configuration [27]. This will place the moment arm at 13.7 ft. Also, the tail volume coefficients can be reduced by 5% when the configuration calls for a T-tail [27]. The average tail volume coefficient for single-engine aircraft for the horizontal is 0.67 and 0.04 for the vertical [32]. A 5% reduction gives 0.665 for the horizontal and 0.038 for the vertical tail volume coefficient. The horizontal stabilizer area of 16 ft<sup>2</sup> and vertical stabilizer area of 15.5 ft<sup>2</sup> was derived using equation 7.1 and equation 7.2.

$$S_h = \frac{\bar{V}_h S \bar{c}}{x_h} \quad 7.1$$

$$S_v = \frac{\bar{V}_v S b}{x_v} \quad 7.2$$

These values can be further compared to the aircraft database of electric aircraft shown in [Table 7.1](#) [17]. Zoom41 areas are slightly larger than the average of the sample shown in the table below. The larger wing area of the Zoom41 than those of the aircraft in [Table 7.1](#) could be an explanation for this discrepancy.

Table 7.1: Aircraft database tail area

Aircraft	Horizontal Area (ft <sup>2</sup> )	Vertical Area (ft <sup>2</sup> )
Alpha Electro	11.6	11.8
Taurus Electro	14.6	-
Alpha Trainer	11.6	11.8
Virus SW	11.6	11.6
Sinus	17.6	11.8

## 7.2 HORIZONTAL STABILIZER DESIGN

### 7.2.1 Horizontal Stabilizer Planform Design

The horizontal stabilizer can be used to generate a moment arm around the lateral axis and controls pitch [27]. Historical data presented in Roskam for single-engine propeller-driven aircraft, shown in [Figure 7.1](#), was used to select the parameters required for the horizontal stabilizer planform design. A 0-degree dihedral and incidence angle were selected for design simplicity. This selection is confirmed as seen below.

Table 8.13 Planform Design Parameters for Horizontal Tails

Type	Dihedral Angle, $\Gamma_h$ deg.	Incidence Angle, $i_h$ deg.	Aspect Ratio, $A_h$	Sweep Angle, $\Delta_c/4_h$ deg.	Taper Ratio, $\lambda_h$
Homebuilts	+5 - -10	0 fixed to variable	1.8 - 4.5	0 - 20	0.29 - 1.0
Single Engine Prop. Driven	0	-5 - 0 or variable	4.0 - 6.3	0 - 10	0.45 - 1.0
Twin Engine Prop Driven	0 - +12	0 fixed to variable	3.7 - 7.7	0 - 17	0.48 - 1.0

Figure 7.1: Historical data for horizontal stabilizer [19]

The aspect ratio for a tail should be approximately half of the wing's aspect ratio, so an aspect ratio of 9 will be used for Zoom41 [27]. Although this value is higher than the historical data presented in Roskam, it agrees with Raymer's suggestion for aircraft with large aspect ratio wings presented in [Figure 7.2](#). The taper ratio of 0.4 was selected based on the average presented in [Figure 7.2](#), which also agrees with [Figure 7.1](#). A tail typically has a 5-degree increase in sweep compared to the wing [19]. Since the Zoom41 wing sweep angle is 0 degrees, the tail will have the sweep of 5 degrees.

	Horizontal tail		Vertical tail	
	<i>A</i>	$\lambda$	<i>A</i>	$\lambda$
Fighter	3-4	0.2-0.4	0.6-1.4	0.2-0.4
Sail plane	6-10	0.3-0.5	1.5-2.0	0.4-0.6
Others	3-5	0.3-0.6	1.3-2.0	0.3-0.6
T-Tail	-	-	0.7-1.2	0.6-1.0

**Figure 7.2: Recommendations of aspect ratio and taper ratio for the tail [27]**

Using the aspect ratio and vertical tail area the tail span of 12 ft was calculated. The root and tip chord were derived by applying equation 7.3 and equation 7.4 [19]. A root chord of 1.9 ft and a tip chord of 0.8 was derived.

$$c_{root} = \frac{2*S}{b*(1+\lambda)} \quad 7.3$$

$$c_{tip} = \lambda * c_{root} \quad 7.4$$

It has been observed that most horizontal and vertical tail airfoils are symmetrical [31]. NACA 0009 and NACA 0012 are the most common airfoils chosen for vertical tails [27]. The NACA 0012 was selected for Zoom41.

### 7.2.2 Elevator Design

Elevators begin at the fuselage and encompass 90% of the tail span, and the elevator chord is typically between 25% and 40% of the tail chord [27]. An elevator span of 10.8 ft was computed. An elevator root chord of 0.57 ft and elevator tip chord of 0.23 ft were derived by selecting a 0.3 horizontal chord to elevator chord ratio. Elevators are deflected downwards of up to 25 degrees and upward of up to 35 degrees [27].

## 7.3 VERTICAL STABILIZER DESIGN

### 7.3.1 Vertical Stabilizer Planform Design

The vertical tailplane creates a moment around the vertical axis and is used to control yaw [27]. Historical data of the parameters for the planform design of the fin is presented in [Figure 7.3](#) [31]. A dihedral of 90 degrees is expected for a vertical stabilizer and will be selected for Zoom41. The incidence angle of 0 degrees was chosen based on data and for simplicity. An aspect ratio of 0.9 and a taper ratio of 0.8 was selected based on the average values for T-tail planes presented in [Figure 7.2](#). These values are in agreement with the historical data below. A sweep of no more than 20 degrees is suggested for the vertical tail and will be used for Zoom41 [19].

**Table 8.14 Planform Design Parameters for Vertical Tails**

Type	Dihedral Angle, $\Gamma_v$ deg.	Incidence Angle, $i_v$ deg.	Aspect Ratio, $\lambda_v$	Sweep Angle, $\Delta_c/4_v$ deg.	Taper Ratio, $\lambda_v$
Homebuilts	90	0	0.4 - 1.4	0 - 47	0.26 - 0.71
Single Engine Prop. Driven	90	0	0.9 - 2.2	12 - 42	0.32 - 0.58
Twin Engine	90	0	0.7 - 1.8	18 - 45	0.33 - 0.74

Figure 7.3: Historical data for the vertical tail from Roskam

These selected values were used to compute the vertical tailplane span of 3.7 ft. Using equation 7.3 and equation 7.4, a root chord of 4.6 ft and tip chord of 3.7ft were estimated.

### 7.3.2 Rudder Design

The rudder, similar to the elevator, will begin at the fuselage and cover up to 90% of the fin span. It will also have a chord of 25% to 40% of the fin chord [27]. A rudder span of 3.4 ft was determined. Vertical stabilizer chord to rudder chord ratio of 0.3 was used to retrieve a rudder root chord of 1.38 ft and rudder tip chord of 1.1 ft. Rudders are deflected upwards and downwards of a maximum of 35 degrees [27].

## 7.4 EMPENNAGE DESIGN EVALUATION

The following images were produced using AAA and used to verify the geometry of the vertical and horizontal tail.

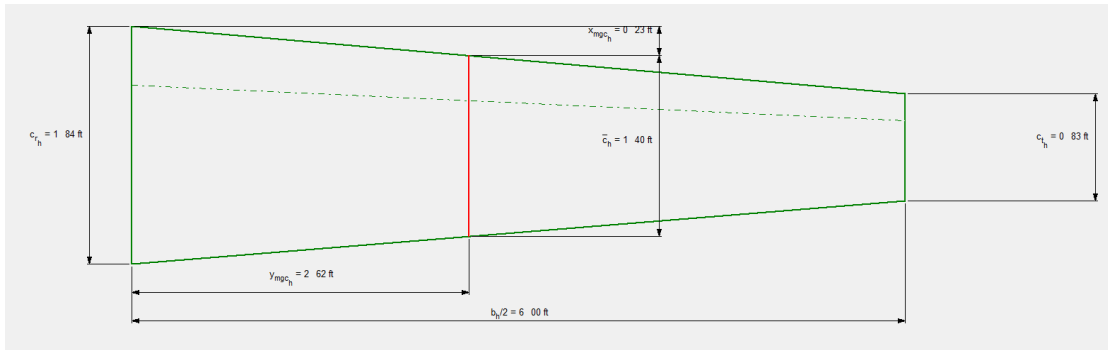


**Figure 7.4: Horizontal stabilizer**

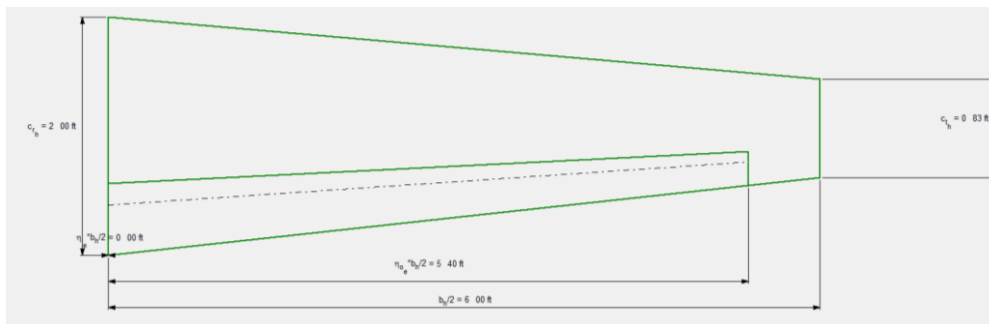


**Figure 7.5: Elevator**

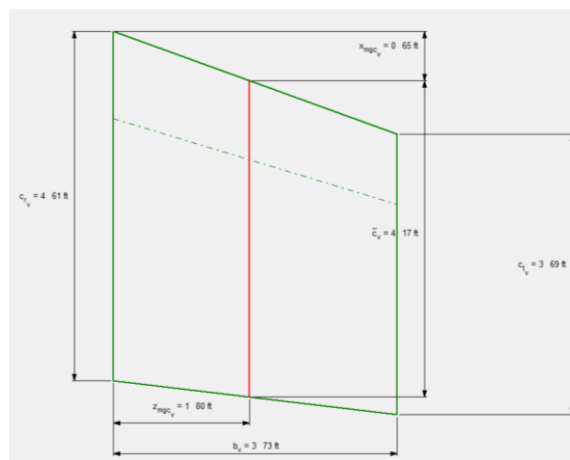


**Figure 7.6: Vertical stabilizer**

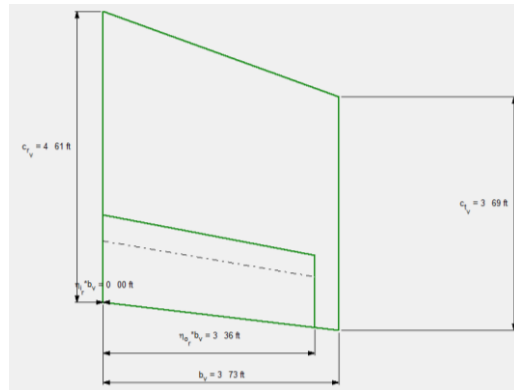


Figure 7.7: Rudder

## 7.5 DRAWING OF TAIL

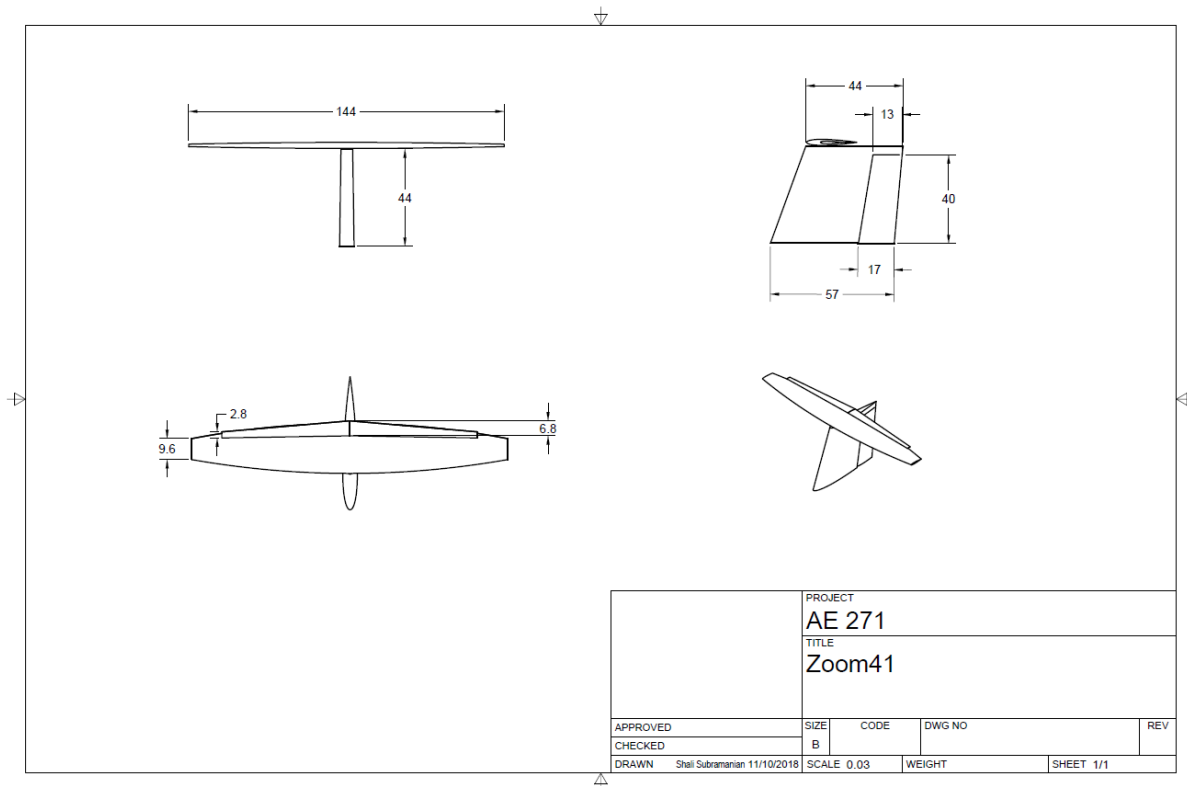


Figure 7.8: Drawing of Zoom41 tail

## 7.6 DISCUSSION AND CONCLUSION

The planform design of the horizontal and vertical stabilizers was completed in this section by the use of historical data. Wingspan largely influenced the sizing of the tail. Horizontal tail area of 16 ft<sup>2</sup> and vertical tail area of 15.5 ft<sup>2</sup> were calculated and compared to the compiled aircraft database.

It was concluded that the Zoom4's tail areas are on the larger end of the scale when weighed against the other aircraft. Some parameters selected for the geometry were based on historical data and Raymer's suggestions for T-tail configurations. Airfoils for the tail seem to be limited, and the NACA 0012 was selected over the NACA 0009. Sizing of the elevator and rudder was also based on historical data. Figure 7.9 illustrates the current aircraft model.



**Figure 7.9: Zoom41 model to date**

## 8.0 LANDING GEAR DESIGN

In *Chapter 8: Landing Gear Design and Weight & Balance Analysis* the CG of the aircraft will be determined for various loading scenarios. The landing gear will be designed according to the calculated CG. The final model of Zoom41 will be presented at the end of the report.

### 8.1 ESTIMATION OF CG LOCATION FOR THE AIRPLANE

#### 8.1.1 Component Weight Estimation

Weight of the components must be estimated before the center of gravity can be found. Empty weight is given by equation 8.1 [19].

$$W_E = W_{struct} + W_{pwr} + W_{feq} \quad 8.1$$

The structural, powerplant and fixed equipment weight can be estimated by using weight fractions from historical data. Weight of each component was presented as a fraction of the gross weight in Roskam and shown in [Appendix C](#). Cessna 150, Cessna 172, and BD5B had gross weights similar to Zoom41 and were averaged for the initial estimation. Calculated takeoff weight, of 800 lb from *Chapter 3: Weight Sizing*, was used to estimate the weight of each component of Zoom41. The historical data represents 100% conventional aluminum alloy construction and was adjusted to represent a 100% composite construction for each component. This weight reduction data for composite construction is also included in [Appendix C](#) [19]

**Table 8.1: Estimated empty weight (lb)**

	Cessna 150	Cessna 172	Bede BD5B	Avg. metal	Avg. composite	Avg. electric composite
Wing Group	115	82	66	88	66	66
Empennage Group	19	21	13	18	13	13
Fuselage Group	123	128	68	106	90	90
Landing Gear	55	40	24	40	40	40
Structure	325	282	171	259	209	209
Powerplant	142	126	144	137	137	243
Electric Motor	-	-	-	-	-	70
Battery	-	-	-	-	-	173
Fixed Equipment	54	58	95	69	69	69
Empty Weight	505	452	410	456	416	521

This estimation does not take into account the heavier powerplant required for an electric aircraft. So, the battery and electric motor weight estimation from *Chapter 3: Weight Sizing* will be used. The final row presents the adjusted weight estimates for the Zoom41.

### 8.1.2 Component Center of Gravity

Table 8.2 summarizes the component breakdown of the aircraft. The x, y, and z coordinates of each component were determined by letting the nose of the aircraft be the origin and is shown below.

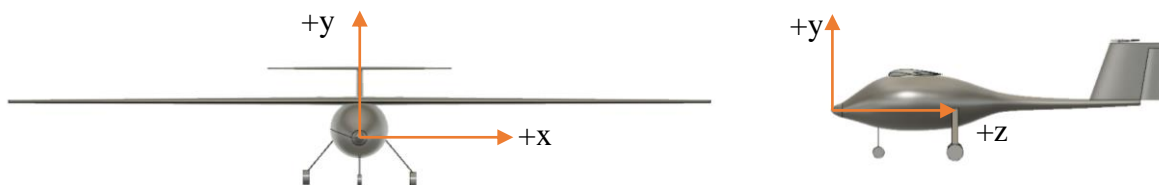


**Figure 8.1: Coordinate System**

Wing and empennage groups include the respective control surfaces. The only factor that affects the CG location is the presence of the passenger because everything else stays constant throughout a typical mission. A thorough breakdown of the estimation of each component will be presented in a later section of this report.

**Table 8.2: Aircraft CG location estimate**

	<b>W<sub>i</sub></b>	<b>x<sub>i</sub></b>	<b>y<sub>i</sub></b>	<b>z<sub>i</sub></b>	<b>W<sub>i</sub>x<sub>i</sub></b>	<b>W<sub>i</sub>y<sub>i</sub></b>	<b>W<sub>i</sub>z<sub>i</sub></b>
	lb	ft	lb*ft	ft	lb*ft	ft	lb*ft
Wing group	66	0	2.1	4.7	0	141	311
Empennage group	13	0	3.4	19	0	45	251
Fuselage	90	0	0.0	5.6	0	0	502
Landing gear	40	0	-0.8	4.8	0	-30	189
Electric motor	70	0	0.3	1.5	0	20	103
Battery	173	0	0.3	8.3	0	47	1429
Passenger	220	0	-0.1	5.7	0	-24	1252
Fixed equipment	70	0	0.2	7.4	0	17	518
Aircraft CG Location at TO w/Passenger					0	0.29	6.1
Aircraft CG Location at TO w/o Passenger					0.00	0.46	6.3

The difference between the most aft and most forward CG location is 0.2 ft or 2.4 inches. Which is lower than the average for homebuilt/single-engine aircraft [19]. This discrepancy is because the Zoom41 is an all-electric aircraft without a changing fuel weight, which translates to a smaller CG range.

## 8.2 LANDING GEAR DESIGN

Design of the fixed tricycle landing gear will be presented in this section. Tricycle landing gear allows for a level aircraft during the boarding of the passenger. Another advantage is the increased control in ground maneuvering with the nose wheel. The tip-over criteria for tricycle gear state, “main landing gear must be behind the aft C.G. location” [19]. It is shown that a 15-degree angle should be formed from the CG and main gear as shown in Figure 8.2 [19].

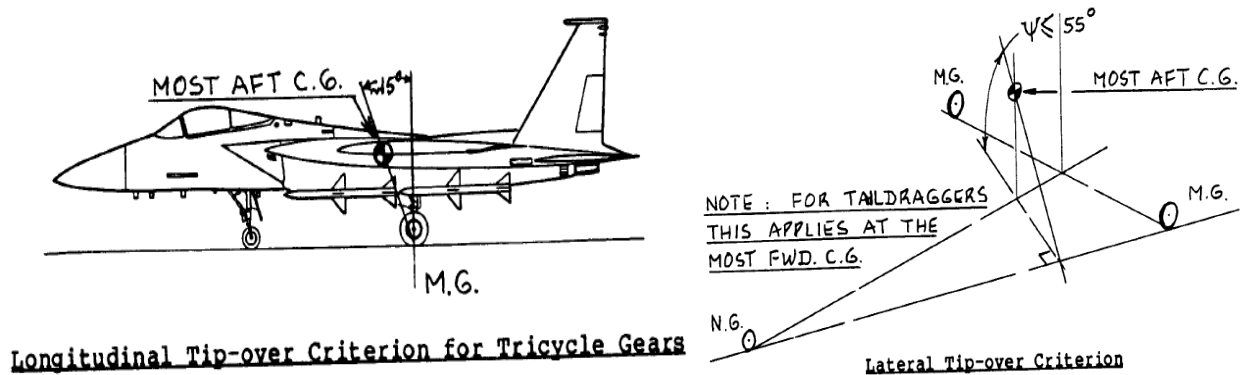


**Figure 8.2: Landing gear tip-over criteria [19].**

The landing gear must be placed 1.05 ft aft of the CG to meet the longitudinal tip-over criterion. Next, the turnover angle must be equal to or less than 55 degrees [19]. Equation 8.2 and equation 8.3 were used to determine the turnover angle [32].

$$\psi = \tan^{-1}\left(\frac{h_{cg}}{l_n \sin \delta}\right) \tag{8.2}$$

$$\delta = \tan^{-1}\left(\frac{t}{2(l_m + l_n)}\right) \tag{8.3}$$

To satisfy this criterion, the nose gear must be placed 5 ft in front of the main gears. Main gears must be placed 7 ft apart. Height from the ground line to the CG will be 4.1 ft. A turnover angle of exactly 55 degrees was determined using these parameters. The figures below illustrate the tip-over criterion for the Zoom41.

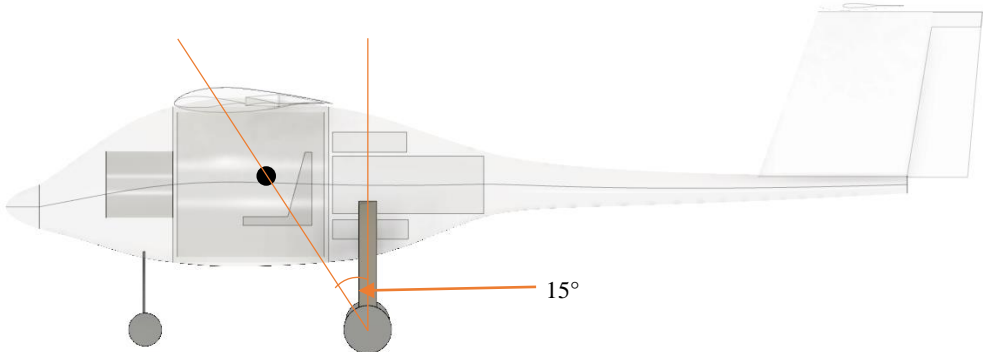


**Figure 8.3: Longitudinal tip-over criterion**

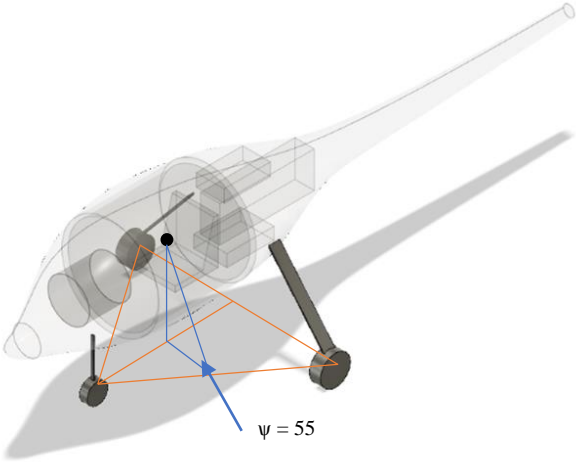


**Figure 8.4: Lateral tip-over criterion**

Next, the ground clearance criteria must be fulfilled. Ground clearance for the tricycle landing gear is illustrated in [Figure 8.5](#) [19].

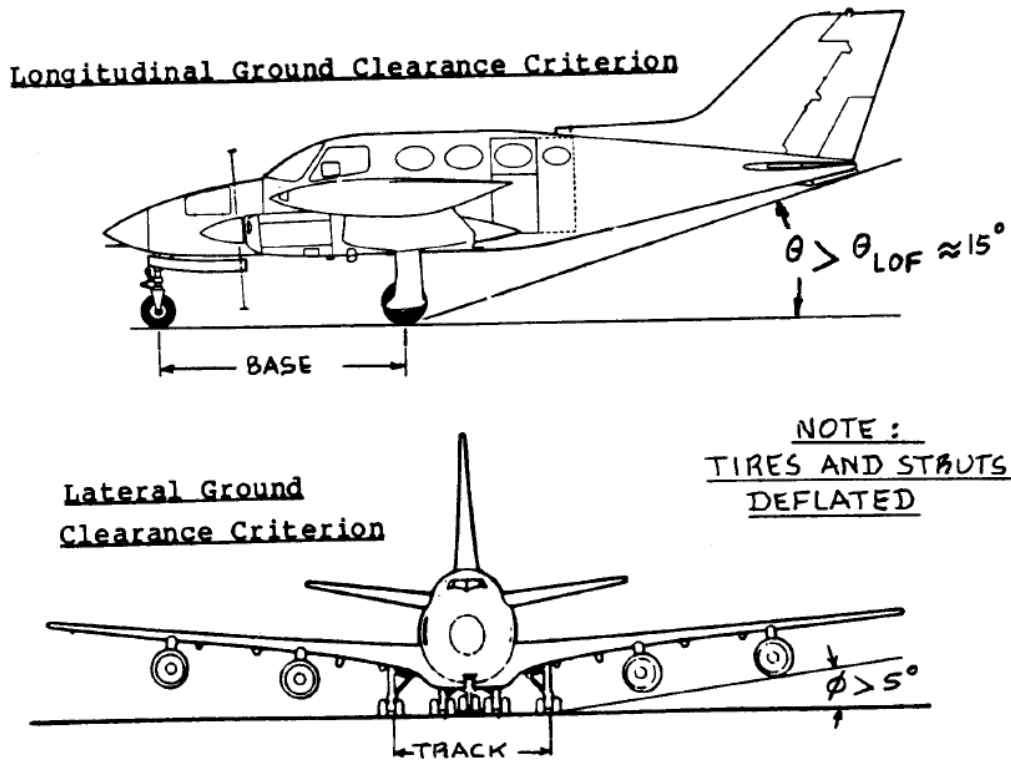


Figure 8.5: Landing gear ground clearance criterion [19]

This will define the length of the struts. The only location for the landing gear struts is under the fuselage due to the high wing configuration. The nose gear strut will be 1.8 ft in length. Each one of the two main gear struts will be 3 ft long and angled at 40 degrees to meet the distance required between the two main gears. The figures below confirm the Zoom41 meets the ground clearance criteria: a longitudinal clearance of 15 degrees and lateral clearance greater than 5 degrees.

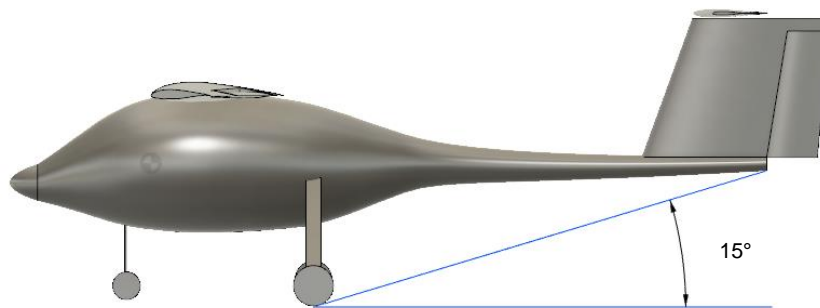


Figure 8.6: Longitudinal ground clearance



**Figure 8.7: Lateral ground clearance**

The maximum static load can be calculated using equation 8.4 and equation 8.5 [19].

$$P_n = \frac{W_{TO} l_m}{l_m + l_n} \quad 8.4$$

$$P_m = \frac{W_{TO} l_n}{n_s(l_m + l_n)} \quad 8.5$$

Maximum load for the nose wheel strut is 133 lb and 333 lb for the main gear strut. The  $P_n/W_{TO}$  is 0.17 and  $n_s P_m/W_{TO}$  is 0.83. These ratios are used to approximate the tire size by comparing them to historical data from Roskam. A diameter of 1.08 ft and a tire width of 0.41 ft will be used for each main gear wheel. The nose wheel diameter will be 0.75 ft with a width of 0.28 ft. A drawing of the final landing gear is shown below.

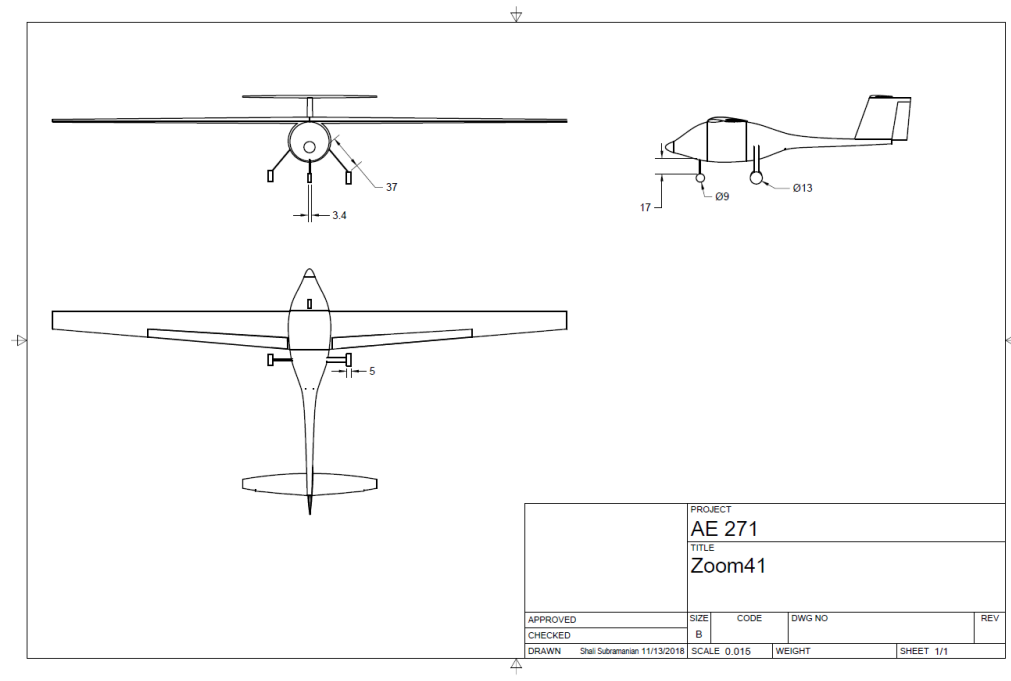


**Figure 8.8: Drawing of landing gear (inches)**

# 8.3 WEIGHT AND BALANCE

## 8.3.1 CG Location Drawings

Figure 8.8 and Figure 8.9 shows the fuselage group and major component CG locations.

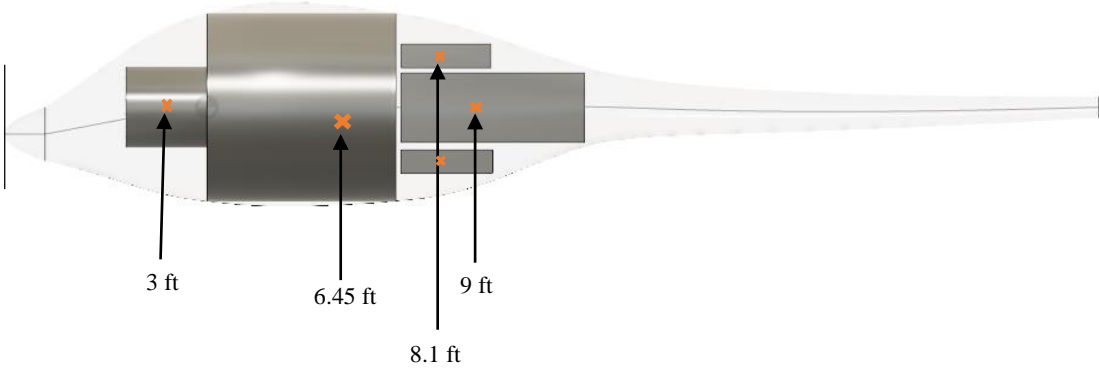


Figure 8.9: Fuselage group CG drawing

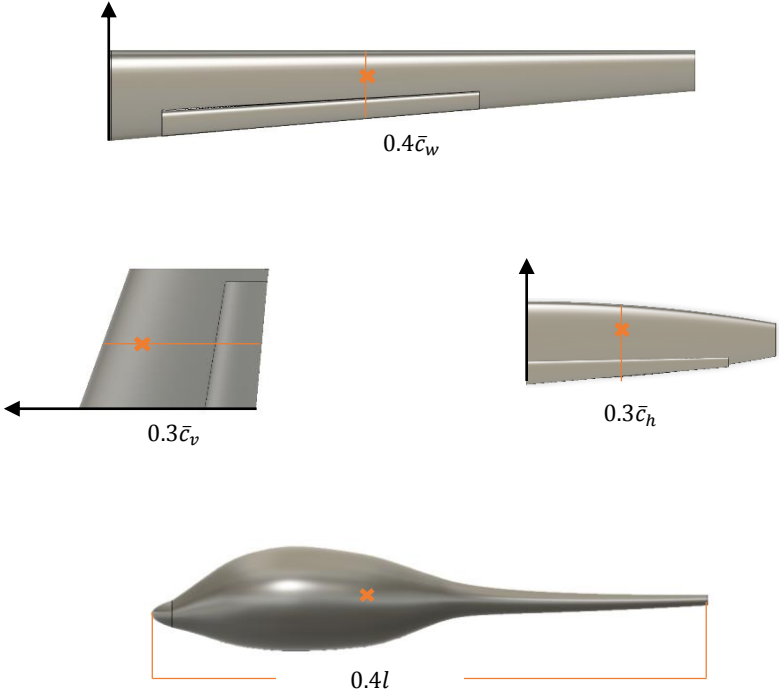


Figure 8.10: CG of major components

### 8.3.2 CG Excursion Diagram

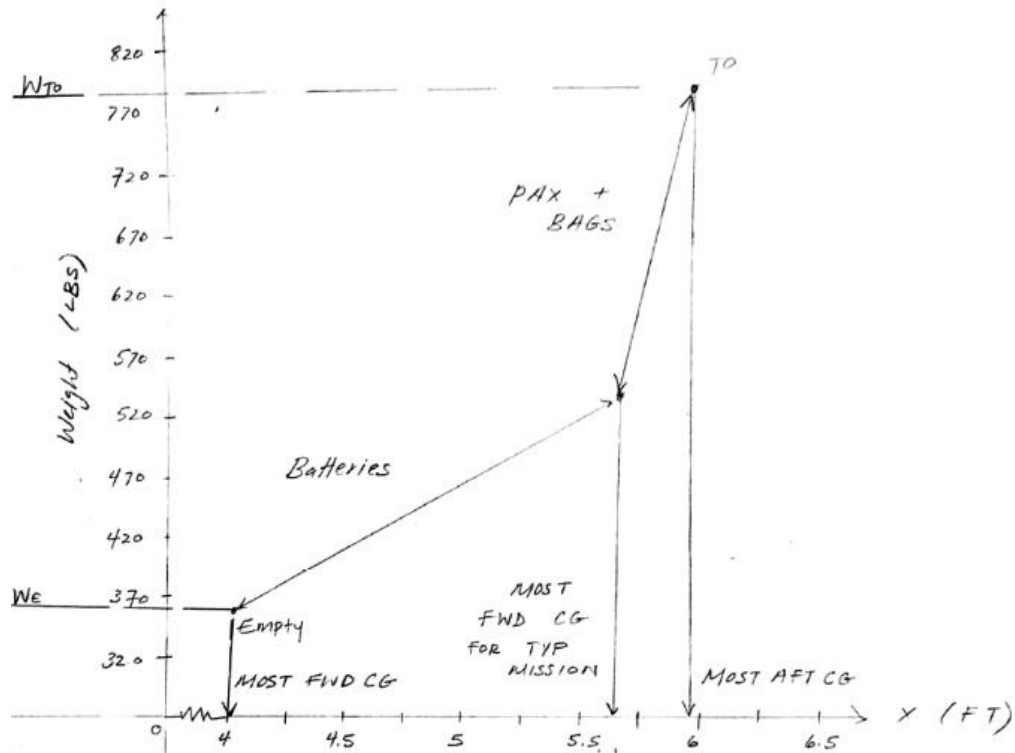


Figure 8.11: Excursion diagram

The weight and balance table was updated to represent the new landing gear placement shown in [Table 8.3](#). Difference between the most aft and most forward location during a typical mission of the CG is 0.11 ft or 1.32 inches. It is 4% of the wing's chord and is on the lower end for aircraft in this category [19]. A typical mission for Zoom41 will only have the onboarding and disembarking of the passenger and their baggage. During maintenance, when the batteries may need to be replaced, the difference between the most aft and most forward is 1.83 ft or 22 inches. So, precautions may need to be taken to keep the aircraft stable during the loading and unloading of batteries.

**Table 8.3: Updated CG location**

	<b>Wi</b>	<b>xi</b>	<b>yi</b>	<b>zi</b>	<b>Wixi</b>	<b>Wiyi</b>	<b>Wizi</b>
	lb	ft	lb*ft	ft	lb*ft	ft	lb*ft
Wing group	66	0	2.1	4.7	0	141	311
Empennage group	13	0	3.4	19	0	45	251
Fuselage structure	90	0	0	5.6	0	0	502
Landing gear	40	0	-2.82	1.2	0	-112	47
Electric motor	70	0	0.3	1.5	0	20	103
Battery	173	0	0.3	8.3	0	47	1429
Passenger	220	0	-0.1	5.7	0	-24	1252
Fixed equipment	70	0	0.2	7.4	0	17	518
Takeoff CG					0	0.18	5.9
Takeoff CG –PAX/BAG					0	0.30	5.6
Empty CG					0	0.32	4.0

## 8.4 DISCUSSION AND CONCLUSION

Component weights were estimated using weight fractions and was adjusted to reflect a composite structure. The battery weight estimated through this method was replaced by the calculated battery weight retrieved from *Chapter 3: Weight Sizing*. CG of the aircraft was determined by breaking it down to major components. The tricycle landing gear was designed according to the CG estimation. It was confirmed that the landing gear will satisfy the tip-over and ground clearance criteria. Final landing gear placement called for a recalculation of the aircraft CG and creating a CG excursion diagram to determine the range of CG. This diagram displayed the CG range for a typical mission, with the onboarding and offboarding of the passenger, and the CG location when batteries are removed. Determining the CG will allow a thorough stability and controls analysis in the following chapter.

## 9.0 STABILITY AND CONTROLS ANALYSIS

*Chapter 9: Stability and Control Analysis* will be focused on checking the longitudinal and directional stability of the aircraft. The Zoom41 will require inherent stability and will implement any changes required by the static stability analysis. Previous requirements that will be affected due to a change in the empennage size will prompt a rechecking of the weight and balance, landing gear, and stability and control check.

### 9.1 STATIC LONGITUDINAL STABILITY

The longitudinal x-plot was derived using the method described in Roskam Part II [19]. The equation used to find the  $x_{ac}$  leg of the x-plot was retrieved from Chapter 11 and is described in Figure 9.1. Values used for each term is explained in Appendix D.

$$\bar{x}_{acA} = [\bar{x}_{acwb} + \{C_{L_{a_h}} (1 - d\epsilon_h/d\alpha) (S_h/S) \bar{x}_{ac_h} - C_{L_{a_c}} (1 + d\epsilon_c/d\alpha) \bar{x}_{ac_c} (S_c/S)\} / C_{L_{a_{wb}}} ] / F, \quad (11.1)$$

where:

$$F = [1 + \{C_{L_{a_h}} (1 - d\epsilon_h/d\alpha) (S_h/S) + C_{L_{a_c}} (1 + d\epsilon_c/d\alpha) (S_c/S)\} / C_{L_{a_{wb}}} ] \quad (11.2)$$

*↳ Camard upwash due to wing change in  $\alpha$   
 $\frac{d\epsilon_c}{d\alpha} \approx 0$  para  $x_{ac_c} = \bar{x}_{ac_{cuer}}$*

Figure 9.1: Aerodynamic center leg of x-plot [19]

The  $x_{cg}$  leg was plotted by utilizing the CG calculations completed in *Chapter 8* for weight and balance. Modifying the vertical tail area altered the weight of the vertical tail resulting in a change in overall CG location. The CG legs for flight with the passenger on board and without the passenger was plotted. Zoom41 x-plot is shown in [Figure 9.2](#).

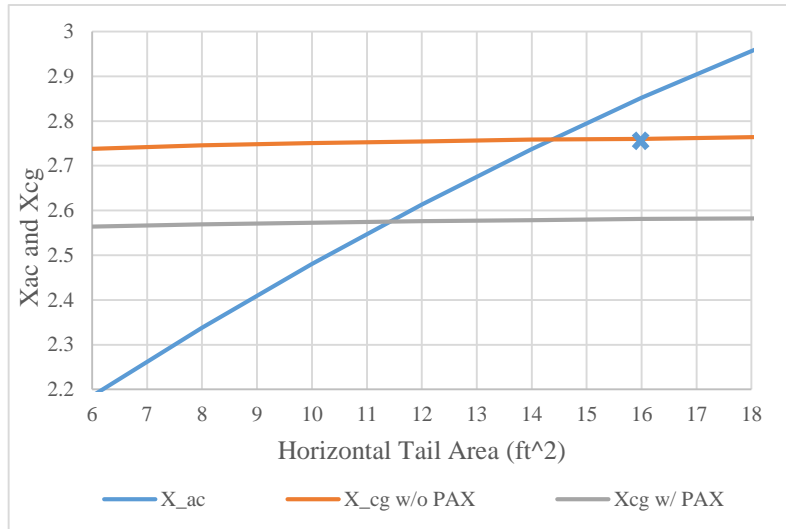


**Figure 9.1: Static longitudinal stability x-plot**

The most aft CG is given by the scenario of the aircraft flying without a passenger and will be used to derive the required tail area. Static margin is an indicator of stability based on the location of the aircraft AC and CG as described in equation 9.1 [19]. Notice that both terms in the equation represent a fraction of the wing mean aerodynamic chord length. Originally calculated horizontal tail area from *Chapter 7* was 16 ft<sup>2</sup>, which gives a static margin of 0.092.

$$SM = \bar{X}_{ac} - \bar{X}_{cg} = -0.10 \quad 9.1$$

This positive number indicates that the CG location is behind the AC, which is not ideal for a stable aircraft. A horizontal tail area of 12.5 ft<sup>2</sup> will provide a static margin of -0.1, which places the CG at a more desirable location, and also meets the 10% static margin recommendation by Roskam for aircraft in this category.

## 9.2 STATIC DIRECTIONAL STABILITY

Directional stability x-plot requires using the equation 11.8 from Roskam Part II shown below and by varying the vertical tail area [19]. The derivation of the values used for this equation is detailed in [Appendix E](#).

$$C_{n\beta} = \dot{C}_{n\beta_{wb}} + C_{L\alpha_v} (S_v/S) (x_v/b)$$

Figure 9.3: Directional stability x-plot equation [19]

The vertical tail area acquired from *Chapter 7* was 15.5 ft<sup>2</sup>, and was used for calculations in this section. A  $C_{n\beta}$  of 0.001 per degree is the overall directional stability requirement, and represents the yawing moment due to sideslip. The figure shown on the following page illustrates Zoom41’s directional stability x-plot.

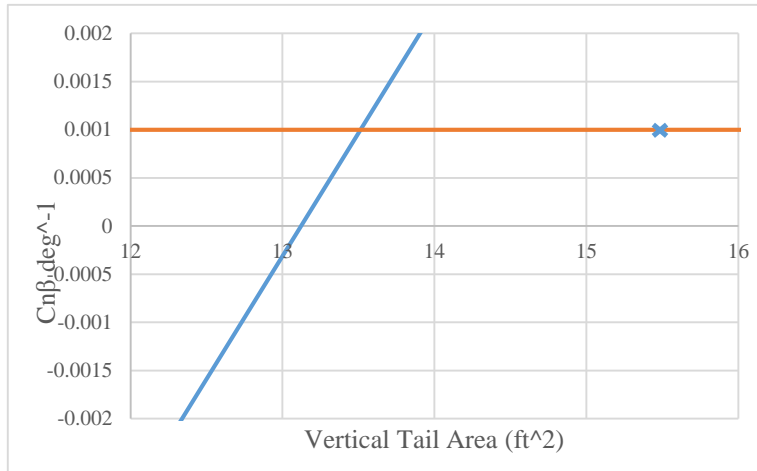


Figure 9.4: Static directional stability

The graph has been zoomed in so that the intersection can be clearly spotted. The vertical tail area can also be reduced according to the plot above. A tail area of 13.5 ft<sup>2</sup> would provide the optimal directional stability. There is no control speed requirement since the Zoom41 because it is a single engine aircraft.

### 9.3 REQUIREMENTS CHECK

Requirements must be reevaluated due to the reduction of both the horizontal and vertical tails. Weight and balance was reworked using the updated tail surface areas and is shown in [Table 9.1](#). The difference in CG is 0.4 ft or 4.8 in., and is 14% of the wing chord. This is a typical value for aircraft in this category.

**Table 9.1: Weight and balance**

	<b>Wi</b>	<b>xi</b>	<b>yi</b>	<b>zi</b>	<b>Wixi</b>	<b>Wiyi</b>	<b>Wizi</b>
	lb	ft	lb*ft	ft	lb*ft	ft	lb*ft
Wing group	66	0	2.1	4.7	0	141	311
Empennage group	70	0	3.4	19	0	242	1333
Fuselage structure	90	0	0	5.6	0	0	502
Landing gear	40	0	-2.82	1.2	0	-112	47
Electric motor	70	0	0.3	1.5	0	20	103
Battery	173	0	0.3	8.3	0	47	1429
Passenger	220	0	-0.1	5.7	0	-24	1252
Fixed equipment	70	0	0.2	7.4	0	17	518
Takeoff CG					0	0.41	<b>6.8</b>
Takeoff CG -PAX					0	0.61	<b>7.3</b>

Next, the longitudinal and lateral tip-over criterion were reviewed. The landing gear must be shifted back 0.8 ft to meet the longitudinal tip over criteria. Sufficient clearance for the landing gear is met since the height of the CG does not change. Finally, the static stability is rechecked.

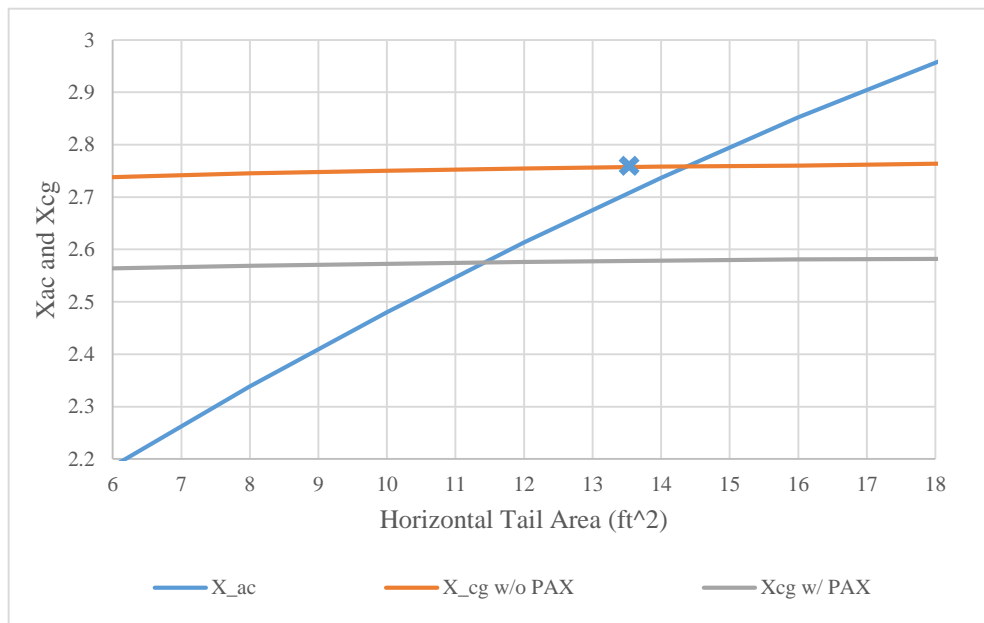


**Figure 9.5: Updated longitudinal stability**

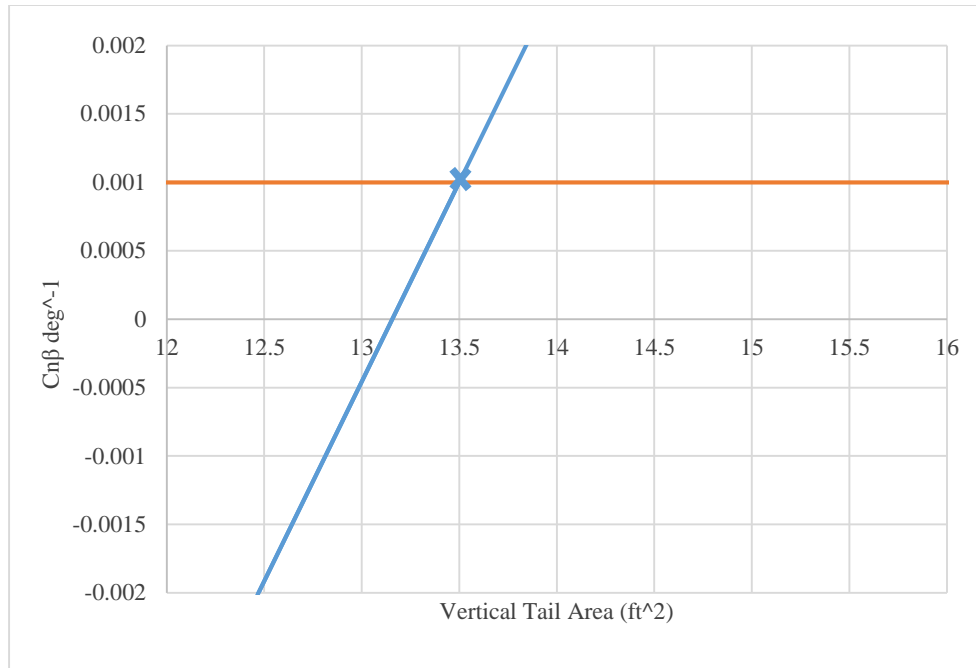


**Figure 9.6: Updated directional stability**

Figure 9.5 and Figure 9.5 display the stability analysis, and show that this updated design meets the criterion for a stable aircraft.

## 9.4 DISCUSSION AND CONCLUSION

The stability control analysis allowed the static stability of the aircraft to be evaluated and resulted in a reduction of the horizontal and vertical tail area. This positive outcome has reduced the weight of the overall structural weight of the aircraft. It is recommended that the performance report is reviewed to assist in trading this weight reduction for an increase in range, baggage limit, or another performance enhancing factor.

## 10.0 DRAG POLARS

*Chapter 10: Drag Polar Estimation* outlines the procedure used to derive the equations needed to estimate the lift-to-drag plot for the aircraft. The aircraft zero lift is adjusted for various flight phases and compressibility in subsonic flight. Final values are presented along with the graphs for each configuration.

### 10.1 AIRCRAFT ZERO LIFT

The following table summarizes the wetted area of Zoom41, the perimeter of the aircraft from nose to tail, obtained from the CAD drawing.

**Table 10.2: Wetted area for Zoom41**

<b>Component</b>	<b>S<sub>wet</sub></b>
Fuselage	74.6 ft <sup>2</sup>
Wing	200 ft <sup>2</sup>
Aileron	44 ft <sup>2</sup>
Horizontal Tail	37.7
Vertical Tail	23.4 ft <sup>2</sup>
Rudder	9.7 ft <sup>2</sup>
Nose Gear	2 ft <sup>2</sup>
Main Gear	12 ft <sup>2</sup>
<b>Total</b>	<b>403 ft<sup>2</sup></b>

Equivalent parasite area of 2.82 ft<sup>2</sup> was derived using the calculated wetted area and Figure 3.21b in Roskam, Part I [19]. A high  $c_f$  value of 0.007 was assumed to obtain the parasite area. This

parasite area value was double checked using equation 10.2 [19]. The clean zero lift drag coefficient for the aircraft is 0.0250, obtained using equation 10.1 [19].

$$C_{D_0} = f/S \quad 10.1$$

$$\log_{10} f = a + b \log_{10} S_{wet} \quad 10.2$$

This matches the estimation completed for weight sizing in *Chapter 3*. So, the weight sizing will not need to be adjusted for the current wetted area of the aircraft.

## 10.2 LOW SPEED DRAG INCREMENTS

The aircraft drag polars using equation 10.3 were derived for various flap configurations and shown below [19]. Although all configurations are shown, Zoom41 will have a fixed landing gear and only need to utilize landing flaps.

$$C_D = C_{D_0} + C_L^2/\pi Ae \quad 10.3$$

The takeoff flaps increment is 0.02, landing gear increment is 0.015, and landing flaps increment is 0.075.

**Table 10.2: Drag polars**

$\Delta C_{D_0}$ due to:	$\Delta C_{D_0}$	e	Drag Polars
Clean	0	0.85	$C_D = 0.025 + 0.0208C_L^2$
Takeoff flaps, gear down	0.025	0.80	$C_D = 0.050 + 0.022C_L^2$
Takeoff flaps, gear up	0.02	0.80	$C_D = 0.045 + 0.022C_L^2$
Landing flaps, gear down	0.09	0.75	$C_D = 0.115 + 0.0236C_L^2$
Landing flaps, gear up	0.075	0.75	$C_D = 0.100 + 0.0236C_L^2$

## 10.3 COMPRESSIBILITY DRAG

The wing drag coefficient is affected by the velocity which the aircraft operates at. Zoom41 is a subsonic aircraft, and will have to take into account compressibility effects. These effects can be

predicted using equation 4.5 in Roskam Part VI, which sums the wing zero-lift drag coefficient and the wing drag coefficient due to lift [19].

$$C_{D_{0w}} = (R_{wf})(R_{LS})(C_{fw})\{1 + L'(t/c) + 100(t/c)^4\}S_{wet,w}/S \quad (4.6)$$

Figure 10.1: Wing zero-lift drag coefficient equation from Roskam VI [19]

The calculated wing zero-lift drag coefficient is 0.00568, which was obtained by using equation described by [Figure 10.1](#).

Table 10.3: Wing zero-lift drag coefficient

Parameter	Value	Source
$R_{wf}$	1	Roskam Part VI, Figure 4.1
$R_{LS}$	1.8	Roskam Part VI, Figure 4.2
$C_{fw}$	0.003	Roskam Part VI, Figure 4.3
$R_{Nw}$	11,344,901	Roskam Part VI, Equation 4.7
$L'$	1.2	Roskam Part VI, Figure 4.4
$t/c$	0.43 ft	Geometry
$S_{wet,w}$	120 ft <sup>2</sup>	Geometry
$S$	120 ft <sup>2</sup>	Geometry

Next, the wing drag coefficient due to lift must be calculated, which can be completed by using the equation described in [Figure 10.2](#).

$$C_{D_{Lw}} = (C_{Lw})^2/\pi Ae + 2\pi C_{Lw} \epsilon_t v + 4\pi^2 (\epsilon_t)^2 w$$

Figure 10.2: Wing drag coefficient due to lift equation from Roskam VI [19]

The values used to calculate this drag coefficient is shown in the table below. Calculated value for the wing drag coefficient due to lift is 0.00097. Adding both calculated drag parameters results in a subsonic wing drag coefficient of 0.00653.

**Table 10.4: Wing drag coefficient due to lift**

Parameter	Value	Source
$C_L$	0.175	Roskam Part VI, Equation 4.10
$e$	0.592	Roskam Part VI, Equation 4.12
$C_{L_w}$	0.184	Roskam Part VI, Equation 4.11
$\varepsilon_t$	-4 deg	Roskam Part VI, Geometry
$v$	-0.0001	Roskam Part VI, Figure 4.9
$w$	0.00212	Roskam Part VI, Figure 4.10
AR	18	Geometry

## 10.4 AIRCRAFT DRAG POLARS

Drag polar equations have been adjusted for compressibility and shown in [Table 10.5](#).

**Table 10.5: Updated Drag Polars**

$\Delta C_{D_0}$ due to:	Drag Polars
Clean	$C_D = 0.0315 + 0.0208C_L^2$
Takeoff flaps, gear down	$C_D = 0.056 + 0.022C_L^2$
Takeoff flaps, gear up	$C_D = 0.052 + 0.022C_L^2$
Landing flaps, gear down	$C_D = 0.122 + 0.0236C_L^2$
Landing flaps, gear up	$C_D = 0.107 + 0.0236C_L^2$

Each drag polar was plotted for varying lift coefficients and displayed in Figure 10.3.

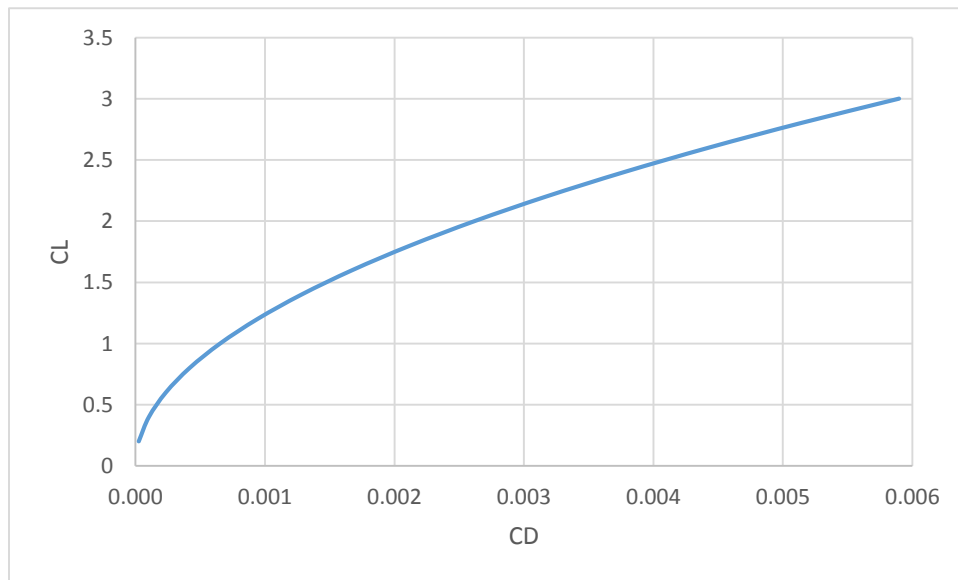


**Figure 10.3: Clean configuration L/D**

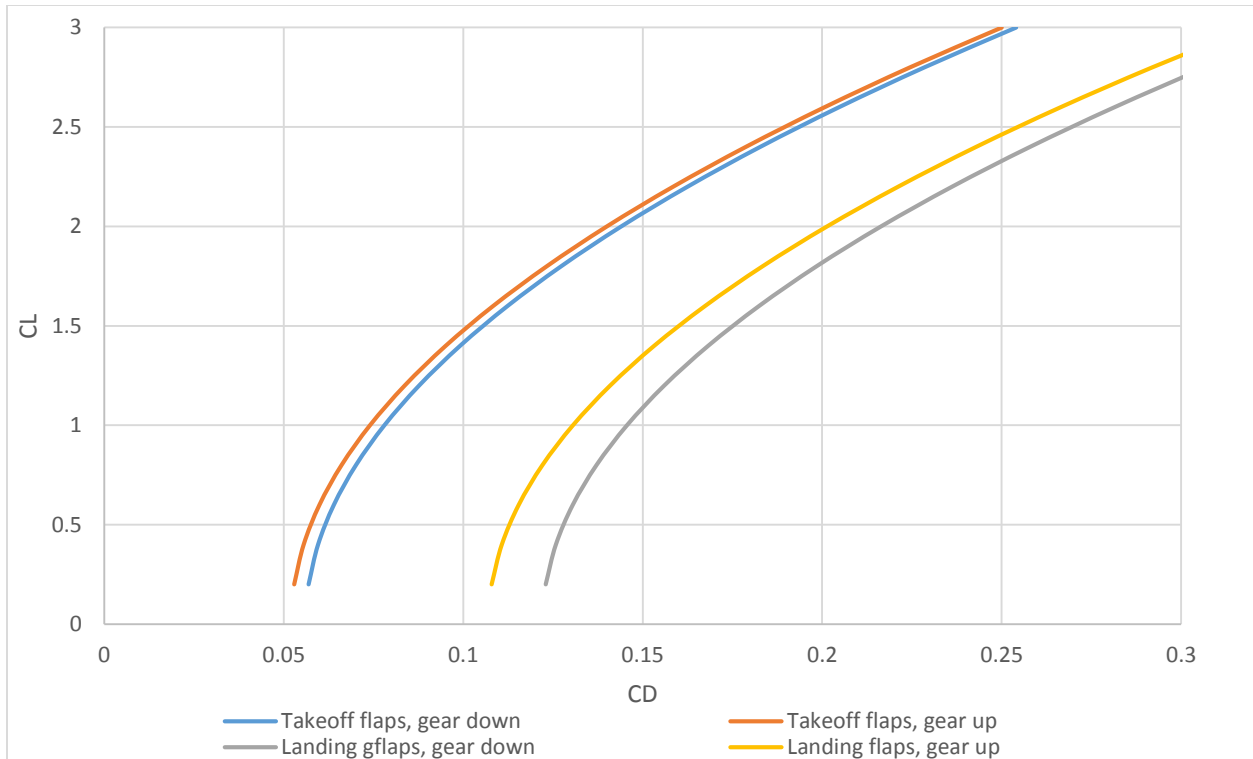


**Figure 10.4: L/D for all configurations**

## 10.5 DISCUSSION AND CONCLUSION

The aircraft zero lift has been derived for various flight phases in subsonic flight conditions. Equivalent parasite area of  $2.82 \text{ ft}^2$  was derived using the calculated wetted area. Next, a clean zero lift drag coefficient for the aircraft is 0.0250 was retrieved. The takeoff flaps increment is 0.02, landing gear increment is 0.015, and landing flaps increment is 0.075. Calculated wing zero-lift drag coefficient is 0.00568, the wing drag coefficient due to lift is 0.00097. Adding both calculated parameters results in a subsonic wing drag coefficient of 0.00653. This allowed the L/D plots for each phase of flight to be obtained.

## REFERENCES

- [1] Gately, K. C., Hutyra, R. L., Peterson, S., and Wing, S. I., “Urban Emissions Hotspots: Quantifying Vehicle Congestion and Air Pollution Using Mobile Phone GPS Data,” *Journal of Environmental Pollution*, Vol. 229, October 2017, pp. 496-504. doi: 10.1016/j.envpol.2017.05.091
- [2] Vegh, J. M., “Sizing Methodologies for Aircraft with Multiple Energy Systems,” Ph.D. Dissertation, Aeronautics and Astronautics Dept., Stanford University, Stanford, CA, June 2018.
- [3] Hepperle, M., “Electric Flight—Potential and Limitations,” *Applied Vehicle Technology 209 Workshop on Energy Efficient Technologies and Concept Operation Proceedings*, STO-MP-AVT-209, NATO, 2012.
- [4] Intwala, A., and Parikh, Y., “A Review on Vertical Take Off and Landing Vehicles,” *International Journal of Innovative Research in Advanced Engineering*, Vol. 2, Issue 2, pp 186-191.
- [5] Hader, M., “Passenger Drones Ready for Take-Off,” *Roland Berger Focus* [online], Roland Berger GMBH, November 2018, URL: <https://www.rolandberger.com/en/Publications/Passenger-drones-ready-for-take-off.html>.
- [6] Lindenbaum, B., “V/STOL Concepts and Developed Aircraft. Volume 1. A Historical Report (1940-1986),” Universal Energy Systems, Inc., Report Number A973571, Dayton, Ohio, June 1986.
- [7] Courtin, C., Burton, M., Yu, A., Butler, P., Vascik, P., and Hansman, R., “Feasibility Study of Short Takeoff and Landing Urban Air Mobility Vehicles Using Geometric Programming,” *18th AIAA Aviation Technology, Integration, and Operations Conference* [online], AIAA, June 2018, doi: 10.2514/6.2018-4151.
- [8] Ma, Z., Yuan, X., Li, L., Ma, Z., Wilkinson, D., Zhang, L. and Zhang, J., “A Review of Cathode Materials and Structures for Rechargeable Lithium–Air Batteries,” *Energy & Environmental Science* [online], Issue 8, pp. 2144-2198, 2015, doi: 10.1039/C5EE00838G.
- [9] Umeshbabu, E., Zheng, B., and Yang, Y., “Recent Progress in All-Solid-State Lithium–Sulfur Batteries Using High Li-Ion Conductive Solid Electrolytes,” *Electrochemical Energy Reviews* [online], February 2019, doi: 10.1007/s41918-019-00029-3.
- [10] Bowler, T., “Why the age of electric flight is finally upon us,” BBC News [online article], Le Bourget, Paris, July 2019, URL: <https://www.bbc.com/news/business-48630656>.
- [11] “Aircraft Electrical Propulsion - The Next Chapter of Aviation? It Is Not a Question of If, But When,” *Think: Act* [online], Roland Berger LTD, September 2017.
- [12] “Autonomy Research for Civil Aviation: Toward a New Era of Flight,” National Research Council, The National Academies Press, Washington, DC, 2014, doi: 10.17226/18815.
- [13] “Fast-Forwarding to a Future of On-Demand Urban Air Transportation,” Uber Elevate [online whitepaper], October 2016, URL: <https://www.uber.com/us/en/elevate/vision/>
- [14] “SAE International Releases Updated Visual Chart for Its “Levels of Driving Automation” Standard for Self-Driving Vehicles,” Society of Automotive Engineers [online article], Warrendale, PA, December 2018, URL: <https://www.sae.org/news/press-room/2018/12/sae-international-releases-updated-visual-chart-for-its-%E2%80%9Clevels-of-driving-automation%E2%80%9D-standard-for-self-driving-vehicles.>
- [15] Thippavong, D., Apaza, R., Barmore, B., Battiste, V., Burian, B., Dao, Q., Feary, M., Go, S., Goodrich, K., Homola, J., Idris, H., Kopardekar, P., Lachter, J., Neogi, N., Ng, H., Oseguera-Lohr, R., Patterson, M. and Verma, S., “Urban Air Mobility Airspace Integration Concepts and Considerations,” *Aviation Technology, Integration, and Operations Conference Proceeding*, AIAA, Atlanta, GA, June 2018, doi: 10.2514/6.2018-3676.
- [16] Riboldi, C., and Gualdoni, F., “An integrated approach to the preliminary weight sizing of small electric aircraft,” *Aerospace Science and Technology*, Vol. 58, November 2016, pp 134-149, doi: 10.1016/j.ast.2016.07.014.
- [17] Jane’s, IHS Markit [online database], URL: <https://janes-ihs-com.libaccess.silibrary.org/> [Accessed June 2019].

- [18] “Alpha Electro,” *Pipistrel* [online], URL: <https://www.pipistrel.si/plane/alpha-electro/technical-data> [Accessed July 2019].
- [19] Roskam, J., *Airplane Design*, DARcorporation.
- [20] “Induced Drag Coefficient,” NASA [online], May 2015, URL: <https://www.grc.nasa.gov/www/k-12/airplane/induced.html>.
- [21] Hunt, T., “Understanding and Choosing Propellers for Electric Flight,” *Chapter 4 – Propeller Terminology* [online PowerPoint slides], Mercury Marine, 2004.
- [22] “Propeller Tip Speed Calculator,” *Warp Drive*, URL: <http://www.warpdriveprops.com/propspd2.html> [Accessed October 13, 2018].
- [23] Pipistrel [online webpage], URL: <https://www.pipistrel-aircraft.com/>.
- [24] “Skylane - Pilots Operating Handbook and Maintenance Manual,” *AirLony* [online], URL: <https://www.airlony.cz> [Retrieved September 11, 2018].
- [25] “STOL CH 701 Performance and Specifications: Real Short Take-off and Landing Performance,” *ZenithAir* [online], URL: <http://www.zenithair.com/stolch701/7-perf.html> [Retrieved September 11, 2018].
- [26] Paul, K., “Why Your Airline Seat May Shrink Even More under New Government Regulations,” *Market Watch* [online], October 2018, URL: <https://www.marketwatch.com/story/why-your-airline-seat-may-shrink-even-more-under-new-regulations>.
- [27] Raymer, D. P., *Aircraft design: A conceptual approach*, 2<sup>nd</sup> ed., American Institute of Aeronautics and Astronautics, 1992.
- [28] McCullough, G. B., and Gault, D. E., “Examples of Three Representative Types of Airfoil-Section Stall at Low Speed,” NACA, Technical Note 2502, 1951.
- [29] Somers, D. M., “Airfoil Design,” *Airfoils, Inc.* [online], URL: <http://www.airfoils.com/index.htm> [Accessed October 2018].
- [30] “NASA/LANGLEY Natural Laminar Flow (1)-0416 Airfoil,” *Airfoil Tools* [online], URL: <http://airfoiltools.com/airfoil/details?airfoil=nlf416-il#polars> [Accessed October 2018].
- [31] Somers, D. M., “Design and Experimental Results for a Natural-Laminar-Flow Airfoil for General Aviation Applications,” NASA, Technical Paper 1861, 1981.
- [32] Scholz, D., Flitta, J., and Pflaum, E., “Aircraft Design,” *Hamburg Open Online University* [Online], May 2017, URL: <http://www.fzt.haw-hamburg.de/pers/Scholz/HOOU/>.
- [33] Chai, S.T., Mason W.H., “Landing Gear Integration in Aircraft Conceptual Design,” Multidisciplinary Analysis and Design Center for Advanced Vehicles Report [online], MAD 96-09-01, September 1996, URL: [http://www.dept.aoe.vt.edu/~mason/Mason\\_f/M96SC.html](http://www.dept.aoe.vt.edu/~mason/Mason_f/M96SC.html).

## APPENDIX A: ROSKAM REGRESSION COEFFICIENTS

The only difference between the two methods used to obtain regression coefficients is that the axis is switched. Thus, the regression value obtained for coefficient A is -1.27 and B is 1.33.

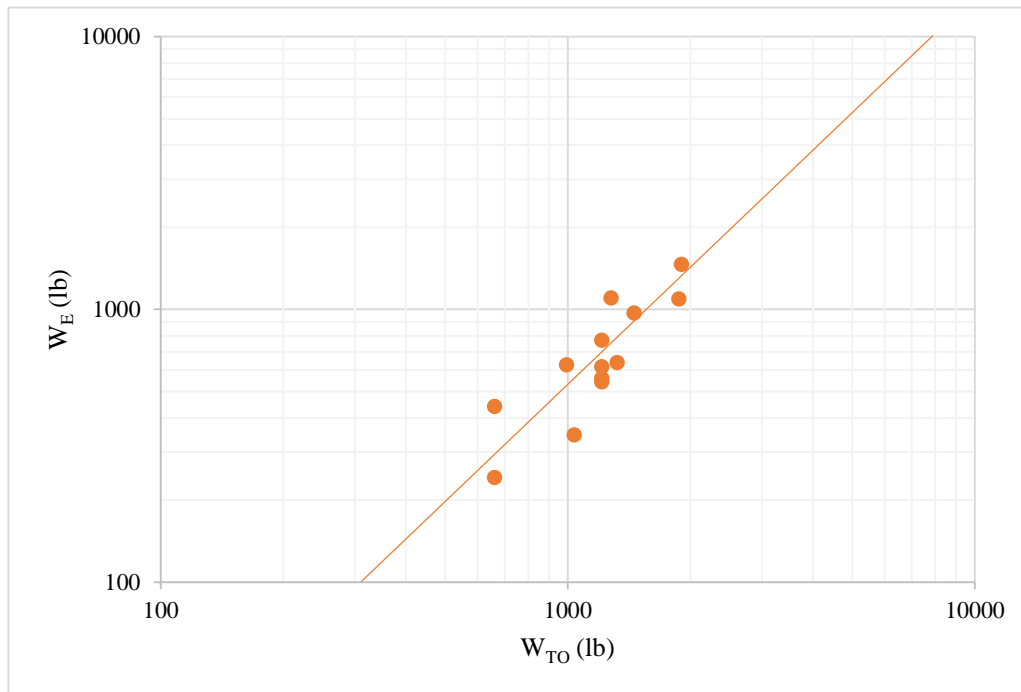


**Figure A.1: Takeoff weight vs empty weight**

There is a difference between the derived coefficients and those found in Roskam. Coefficient A of -0.144 and coefficient B of 1.12 for single-engine propeller-driven aircraft have been tabulated. This significant disparity is likely due to the technological advances that have occurred, e.g. lighter material or increased engine efficiency, since the publishing of Roskam.

## APPENDIX B: WEIGHT CALCULATION ASSUMPTIONS

Table B.1: Parameters used to calculate mission weights

Parameter	Symbol	Value	Units	Assumptions/Notes
Weight Sizing Coefficient	A	1.53		
Weight Sizing Coefficient	B	0.547		
Weight Sizing Coefficient	C	0.972		
Weight Sizing Coefficient	D	0.011		
Battery Energy Density	e	0.693	hp*hr/lbm	Projected using Riboldi [1]
Battery Power Density	p	0.596	hp/lbm	Current state of the art [4]
<b>Takeoff Weight</b>	<b>Wto</b>	<b>800</b>	<b>lb</b>	Estimated using aircraft study
<b>Empty Weight</b>	<b>We</b>	<b>318</b>	<b>lb</b>	Estimation from Regression
Empty Weight Check 1	We	320	lb	Coefficients [1]
Percent Difference We		0.50	%	Within 0.5% of predicted weight check
<b>Motor Weight</b>	<b>Wm</b>	<b>69.9</b>	<b>lb</b>	Estimation from Regression
<b>Battery Weight</b>	<b>Wb</b>	<b>192</b>	<b>lb</b>	Coefficients [1]
<b>Payload Weight</b>	<b>Wpl</b>	<b>220</b>	<b>lb</b>	3 takeoff and landing Accounted for using Riboldi [1]
Power of Motor	Pm	80	hp	One Passenger (200) and baggage(20)*
Max E, P		4.5	slugs	Estimated using aircraft study
Prop Efficiency	$\eta_p$	0.8		Riboldi [1]
<b>CLIMB</b>				
<b>Power Required</b>	<b>P req, cl</b>	<b>48.94</b>	<b>hp</b>	<b>Riboldi [1]</b>
<b>Energy Required</b>	<b>E req, cl</b>	<b>3.671</b>	<b>hp*hr</b>	<b>Riboldi [1]</b>
Rate of Climb	ROC	16.7	ft/s	Estimated using aircraft study
Density	$\rho, cl$	0.00232	slug/ft <sup>3</sup>	Average density from SL to 1500 ft
Velocity	V, cl	100	ft/s	
Wing Area	S	100	ft <sup>2</sup>	Estimated using aircraft study
Coefficient of Drag	CD, cl	0.1169		Roskam [3]
Drag Polar	CD0	0.0350		Roskam [3]
K Value	K	0.0253		Roskam [3]
Aspect Ratio	AR	18		Estimated using aircraft study
Oswald's Efficiency	e	0.7		For rectangular wings [6]
Coefficient of Lift	Cl, cl	1.800		Riboldi [1]
Best time to climb	TTC	270.0	sec	For 3 climb phases. Riboldi [1]
Cruise Altitude	hcr	1500	ft	Mission requirement

**Table B.1: Parameters used to calculate mission weights continued**

<b>Parameter</b>	<b>Symbol</b>	<b>Value</b>	<b>Units</b>	<b>Assumptions/Notes</b>
<b>CRUISE</b>				
<b>Power Required</b>	<b>P req, cr</b>	<b>75.34</b>	<b>hp</b>	<b>Riboldi [1]</b>
<b>Energy Required</b>	<b>E req, cr</b>	<b>50.22</b>	<b>hp*hr</b>	<b>Riboldi [1]</b>
Rate of Climb	ROC	20.3	ft/s	Estimated using aircraft study
Density	$\rho$ , cr	0.00227	slug/ft <sup>3</sup>	Average density from SL to 1500 ft
Velocity	V, cr	183	ft/s	
Wing Area	S	100	ft <sup>2</sup>	Estimated using aircraft study
Coefficient of Drag	CD, cr	0.0361		Roskam [3]
Drag Polar	CD0	0.0350		Roskam [3]
	K	0.0253		Roskam [3]
Aspect Ratio	AR	18		Estimated using aircraft study
Oswald's Efficiency	e	0.7		For rectangular wings [6]
Coefficient of Lift	Cl, cl	0.21		Riboldi [1]
Cruise Time	t, cr	2400.0	sec	Total cruise time of 45 minutes
Cruise Altitude	hcr	1500	ft	Mission requirement
<b>LOITER</b>				
<b>Power Required</b>	<b>P req, lo</b>	<b>63.70</b>	<b>hp</b>	<b>Riboldi [1]</b>
<b>Energy Required</b>	<b>E req, lo</b>	<b>15.93</b>	<b>hp*hr</b>	<b>Riboldi [1]</b>
Rate of Climb	ROC	0.002291	ft/s	Estimated using aircraft study
Density	$\rho$ , lo	164.7	slug/ft <sup>3</sup>	Average density from SL to 1500 ft
Velocity	V, lo	100	ft/s	
Wing Area	S	0.0367	ft <sup>2</sup>	Estimated using aircraft study
Coefficient of Drag	CD, lo	0.0350		Roskam [3]
Drag Polar	CD0	0.0253		Roskam [3]
	K	18		Roskam [3]
Aspect Ratio	AR	0.7		Estimated using aircraft study
Oswald's Efficiency	e	0.26		For rectangular wings [6]
Coefficient of Lift	Cl, lo	900.0		Riboldi [1]
Loiter Time	t, lo	1300.0	sec	Total loiter time of 15 min
Loiter Altitude	h, lo	0.002291	ft	Minimum altitude according to FAA regulations

## APPENDIX C: HISTORICAL DATA FOR COMPONENT WEIGHTS

This appendix displays the historical data used to estimate component weight in *Chapter 8*.

Type	Bede BD5B	At the time of printing no other data were available
Flight Design		
Gross Weight, GW, lbs	1,051	
Structure/GW	0.214	
Power Plant/GW	0.180	
Fixed Equipm't/GW	0.119	
Empty Weight/GW	0.513	
Wing Group/GW	0.083	
Empenn. Group/GW	0.016	
Fuselage Group/GW	0.085	
Nacelle Group/GW	0.000	
Land. Gear Group/GW	0.030	
Take-off Gross Wht, $W_{TO}$ , lbs	1,051	
Empty Weight, $W_E$ , lbs	539	
Wing Group/S, psf	1.8	
Emp. Grp/ $S_{emp}$ , psf	1.1	
Ultimate Load Factor, g's	5.7 assumed	
Surface Areas, $ft^2$		
Wing, $S$	47.4	
Horiz. Tail, $S_h$	10.5	
Vert. Tail, $S_v$	5.0	
Empenn. Area, $S_{emp}$	15.5	

Figure C.1: Historical data

Table A2.1b Group Weight Data for Single Engine Propeller  
Driven Airplanes

Type	Cessna					
	150	172	175	180 **	182	L-19A* **
Flight Design						
Gross Weight, GW, lbs	1,500	2,200	2,350	2,650	2,650	2,100
Structure/GW	0.406	0.352	0.330	0.319	0.326	0.327
Power Plant/GW	0.178	0.157	0.177	0.206	0.206	0.262
Fixed Equipm't/GW	0.068	0.072	0.068	0.065	0.065	0.136
Empty Weight/GW	0.631	0.565	0.561	0.576	0.583	0.727
Wing Group/GW	0.144	0.103	0.097	0.089	0.089	0.113
Empenn. Group/GW	0.024	0.026	0.024	0.023	0.023	0.030
Fuselage Group/GW	0.154	0.160	0.149	0.152	0.151	0.103
Nacelle Group/GW	0.015	0.012	0.013	0.012	0.013	0.016
Land. Gear Group/GW	0.069	0.050	0.047	0.042	0.050	0.064
Take-off Gross Wht, $W_{TO}$ , lbs	1,500	2,200	2,350	2,650	2,650	2,100
Empty Weight, $W_E$ , lbs	946	1,243	1,319	1,526	1,545	1,527
Wing Group/S, psf	1.4	1.4	1.3	1.3	1.3	1.4
Emp. Grp/S <sub>emp</sub> , psf	0.85	1.1	1.1	1.2	1.2	1.2
Ultimate Load Factor, g's	5.7	5.7	5.7	5.7	5.7	5.7
Surface Areas, ft <sup>2</sup>						
Wing, S	160	175	175	175	175	174
Horiz. Tail, S <sub>h</sub>	28.5	34.6	34.6	34.6	34.1	35.2
Vert. Tail, S <sub>v</sub>	14.1	18.4	18.4	18.4	18.4	18.4
Empenn. Area, S <sub>emp</sub>	42.6	53.0	53.0	53.0	52.5	53.6

\*Military observation airplane  
\*\*Taildragger

Figure C.1: continued

Table 2.16 Weight Reduction Data for Composite  
Construction

Structural Component	$W_{comp}/W_{metal}$
<u>Primary Structure</u>	
Fuselage	0.85
Wing, Vertical Tail, Canard or Horizontal Tail	0.75
Landing Gear	0.88
<u>Secondary Structure</u>	
Flaps, Slats, Access Panels, Fairings	0.60
Interior Furnishings	0.50
Air Induction System	0.70 - 0.80

Notes: 1) These weight reduction factors should be used with great caution. They are intended to apply when changing from 100% conventional aluminum alloys to 100% composite construction.

Figure C.2: Composite weight data

## APPENDIX D: LONGITUDINAL STABILITY CALCULATIONS

The values used for the equation presented in [Figure 9.1](#) is presented in the two tables below. All other values not mentioned were obtained directly from the geometry of the aircraft.

**Table D.1: Equation 11.2 values**

Parameter	Value	Description
$\overline{X_{acwb}}$	1.70	Roskam Part VI, Equation 8.83
$\overline{X_{acw}}$	1.72	Roskam Part VI, Equation 8.84
$\Delta \overline{X}_p$	-0.021	Roskam Part VI, Equation 8.85
$-dM/d\alpha$	1544	Roskam Part VI, Equation 8.86
$C_{L\alpha_w}$	5.83	Roskam Part VI, Equation 8.22
$-(\overline{d\varepsilon}/d\alpha)_i$		Values shown for each fuselage section shown in Table A.2
$K_{AR}$	0.048	Roskam Part VI, Equation 8.46
$K_\lambda$	1.26	Roskam Part VI, Equation 8.47
$K_h$	0.12	Roskam Part VI, Equation 8.48
$\eta_h$		Roskam Part VI, Equation 8.41
$(S_h)_{stip}$	10.6 ft <sup>2</sup>	Obtained in ft using geometry and propeller dimensions specified in <i>Chapter 4</i>
$\overline{X_{ach}}$	13.45	Roskam Part VI, Equation 8.84
$C_{L\alpha_h}$	5.26	Roskam Part VI, Equation 8.22
$C_{L\alpha_A}$	6.57	Roskam Part VI, Equation 8.42
F	1.09	Roskam Part VI, Equation 8.81

**Table D.2: Munk's method breakdown**

Section	wfi (ft)	$\Delta x_i$	$d\varepsilon/d\alpha$
1	0.76	0.98	1.45
2	0.76	1.69	1.45
3	0.76	2.45	1.45
4	0.76	3.13	1.45
5	0.76	3.51	2.35
6	1.78	3.77	0.16
7	1.78	3.46	0.16
8	2.44	2.09	0.16
9	2.44	1.01	0.16
10	2.44	0.73	0.16
11	2.44	0.58	0.16
12	2.44	0.45	0.16
13	2.44	0.01	0.16

## APPENDIX E: DIRECTIONAL STABILITY CALCULATIONS

The values used for calculating the equation in [Figure 9.3](#) is shown below. All other values were obtained from the geometry of the aircraft.

**Table E.1: Directional Stability Parameters**

<b>Parameter</b>	<b>Value</b>	<b>Description</b>
$C_{n_{\beta_w}}$	0	Roskam Part VI, Equation 10.41
$C_{n_{\beta_f}}$	-0.038	Roskam Part VI, Equation 10.42
$K_N$	0.003	Roskam Part VI, Figure 10.28
$K_{Rl}$	1.6	Roskam Part VI, Figure 10.29
$S_{f_s}$	74 ft <sup>2</sup>	Roskam Part VI, Figure 10.28
$C_{L_{\alpha_v}}$	0.996	Roskam Part VI, Equation 8.22